STRUCTURAL, MORPHOLOGICAL AND MAGNETIC STUDIES OF TRANSITION METAL DOPED *Mg-Zn* FERRITES

Thesis submitted in fulfillment for the requirement of the Degree of

Doctor of Philosophy

by

ROHIT SHARMA

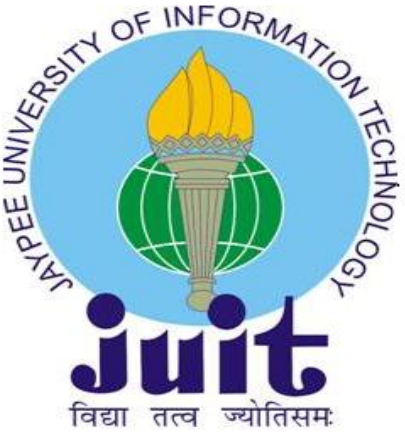

DEPARTMENT OF PHYSICS AND MATERIALS SCIENCE

JAYPEE UNIVERSITY OF INFORMATION TECHNOLOGY
WAKNAGHAT, SOLAN, H.P., INDIA

OCTOBER 2018

CONTENTS

Cover page		**i**
Copyright		**ii**
Table of contents		**iii-vi**
Declaration by the Scholar		**vii**
Supervisor's Certificate		**viii**
Acknowledgement		**x**
Abstract		**xi**
List of Abbreviations		**xii**
List of Symbols		**xiii**
List of Figures		**xiv-xv**
List of Tables		**xvi**
List of Publications		**xvii-xviii**
CHAPTER 1	**INTRODUCTION**	**1-24**
	1.1 History of ferrites 1.2 Ferrites 1.3 Classification of ferrites 1.3.1 Magnetic behaviour (Soft and Hard ferrites) 1.3.2 Crystal structure 1.3.2.1 Spinel ferrite 1.3.2.2 Hexagonal ferrite 1.3.2.3 Rare earth garnet ferrite 1.3.3 Types of spinel ferrites	

	1.3.3.1 Normal spinel 1.3.3.2 Inverse spinel 1.3.3.3 Mixed spinel 1.4 Some important spinel ferrites 1.4.1 Zinc ferrite 1.4.2 Lithium ferrite 1.4.3 Nickel ferrite 1.4.4 Magnesium ferrite 1.4.5 Cobalt ferrite 1.4.6 Manganese ferrite 1.4.7 Nickel-Zinc ferrite 1.4.8 Manganese-Zinc ferrite 1.4.9 Magnesium-Zinc ferrite 1.5 Role of transition metal doping 1.6 General applications of spinel ferrites 1.6.1 Magnetic recording 1.6.2 Microwave devices 1.6.3 Entertainment applications 1.6.4 Power applications 1.6.5 Sensing 1.6.6 Photocatalytic dye degradation 1.6.7 Biomedical applications 1.6.8 Other applications 1.7 Motive and motif of the present work 1.8 Outline of the thesis	
CHAPTER 2	**EXPERIMENTAL AND CHARACTERIZATION TECHNIQUES**	**25-42**
	2.1 Nanoparticles 2.2 Synthesis techniques	

	2.2.1 Physical methods 2.2.1.1 Ball milling 2.2.1.2 Sputtering 2.2.2 Chemical methods 2.2.2.1 Sol-gel 2.2.2.2 Hydrothermal 2.2.2.3 Polyol process 2.2.2.4 Micro-emulsion 2.2.2.5 Co-precipitation 2.3 Reaction mechanism 2.4 Characterization techniques 2.4.1 X-ray diffraction 2.4.2 Energy dispersive X-ray spectroscopy 2.4.3 Field emission scanning electron microscope 2.4.4 Fourier transform infrared spectroscopy 2.4.5 Vibrating sample magnetometer	
CHAPTER 3	**STRUCTURAL, MORPHOLOGICAL AND ELEMENTAL STUDIES OF TRANSITION METAL DOPED *Mg-Zn* FERRITES**	**43-62**
	3.1 Introduction 3.2 Experimental details 3.3 Results and discussion 3.3.1 Structural, morphological and elemental properties of $Mg_{0.5}Zn_{0.5-x}Co_xFe_2O_4$ ferrites 3.3.2 Structural, morphological and elemental properties of $Mg_{0.5}Zn_{0.5-x}Ni_xFe_2O_4$ ferrites 3.3.3 Structural, morphological and elemental properties of $Mg_{0.5}Zn_{0.5-x}Mn_xFe_2O_4$ ferrites 3.4 Conclusion	

CHAPTER 4	**CATION DISTRIBUTION FOR TRANSITION METAL DOPED *Mg-Zn* FERRITES**	**63-76**
	4.1 Introduction 4.2 Cation distribution for $Mg_{0.5}Zn_{0.5-x}Co_xFe_2O_4$ ferrites 4.3 Cation distribution for $Mg_{0.5}Zn_{0.5-x}Ni_xFe_2O_4$ ferrites 4.4 Cation distribution for $Mg_{0.5}Zn_{0.5-x}Mn_xFe_2O_4$ ferrites 4.5 Conclusion	
CHAPTER 5	**MAGNETIC STUDIES OF TRANSITION METAL DOPED *Mg-Zn* FERRITES**	**77-96**
	5.1 Introduction 5.2 Experimental details 5.3 Results and discussion 5.3.1 Magnetic properties of $Mg_{0.5}Zn_{0.5-x}Co_xFe_2O_4$ ferrites 5.3.2 Magnetic properties of $Mg_{0.5}Zn_{0.5-x}Ni_xFe_2O_4$ ferrites 5.3.3 Magnetic properties of $Mg_{0.5}Zn_{0.5-x}Mn_xFe_2O_4$ ferrites 5.4 Analysis of retentivity and coercivity for transition metal doped *Mg-Zn* ferrites 5.5 Conclusion	
CHAPTER 6	**SUMMARY AND FUTURE SCOPE**	**97-102**
	BIBLIOGRAPHY	**103-132**

JAYPEE UNIVERSITY OF INFORMATION TECHNOLOGY
(Established by H.P. State Legislative vide Act No. 14 of 2002)
Dumehar Bani, Kandaghat, Distt. Solan – 173234 (H.P.) INDIA
Website: www.juit.ac.in
Phone No. (91) 07192-257999 (30 Lines)
Fax: (91) 01792 245362

DECLARATION

I hereby declare that the work reported in Ph.D. thesis entitled **"STRUCTURAL, MORPHOLOGICAL AND MAGNETIC STUDIES OF TRANSITION METAL DOPED *Mg-Zn* FERRITES"** submitted at **Jaypee University of Information Technology, Waknaghat, India** is an authentic record of my work carried out under the supervision of **Dr. Vineet Sharma.** I have not submitted this work elsewhere for any other degree or diploma. I am fully responsible for the contents of my Ph.D. Thesis.

Date:

Rohit Sharma
Enrollment No. 146951
Department of Physics and Materials Science
Jaypee University of Information Technology
Waknaghat, Solan, H.P. India-173234

JAYPEE UNIVERSITY OF INFORMATION TECHNOLOGY
(Established by H.P. State Legislative vide Act No. 14 of 2002)
Dumehar Bani, Kandaghat, Distt. Solan – 173234 (H.P.) INDIA
Website: www.juit.ac.in
Phone No. (91) 07192-257999 (30 Lines)
Fax: (91) 01792 245362

CERTIFICATE

This is to certify that the work reported in the Ph.D. thesis entitled **"STRUCTURAL, MORPHOLOGICAL AND MAGNETIC STUDIES OF TRANSITION METAL DOPED *Mg-Zn* FERRITES"**, submitted by **Rohit Sharma** at **Jaypee University of Information Technology, Waknaghat**, **India** is a bonafide record of his original work carried out under my supervision. This work has not been submitted elsewhere for any other degree or diploma.

Date:

Dr. Vineet Sharma
Supervisor
Associate Professor
Department of Physics and Materials Science
Jaypee University of Information Technology
Waknaghat, Solan, H.P. India-173234

Dedicated
To
My Guru- Dr. Shrimali Ji

ACKNOWLEDGEMENT

Before acknowledging anyone I would like to thank almighty Lord Shiva for his blessings. I thank Dr. Vineet Sharma, my supervisor for giving me the opportunity to do Ph.D under his supervision. I am very thankful to him for his constant support throughout my research work. I would like to thank HOD Department of Physics and Materials Science, Dr. P. B. Barman for his support and encouragement.

I would also like to convey my special thanks to Dr. Pankaj Sharma for his constant support throughout my work. I also convey my thanks to Dr. Ragini Raj Singh, Dr. Surajit Hazra, Dr, Sanjeev Tiwari, Dr. Dheeraj Sharma, Dr. Rajesh Kumar and Dr. Raja S. Durai for their cooperation and valuable suggestions.

I extend my gratitude to founder of Jaypee University of Information Technology Shri Jaiprakash Gaur, Prof. (Dr.) Vinod Kumar (VC, JUIT), Maj. Gen. Rakesh Bassi (Registrar Juit), Prof. (Dr.) Samir Dev Gupta (Director & Academic Head JUIT) for providing me all kinds of facilities to carry out my research work.

I would like to thank Dr. Nagesh Thakur (H.P.U Shimla), Dr. N. S. Negi (H.P.U Shimla) and Dr. Manoj Kumar (JIIT Noida) for providing me necessary experimental facilities for characterization. I also like to acknowledge SAIF (Panjab University), NIT Hamirpur, Himachal Pradesh University and Institute Instrumentation Centre (IIT Roorkee) for providing me facilities for characterization. I would also like to thank our technical staff members Er. Kamlesh Mishra, Mr. Ravendra Tiwari and Mr. Deepak Singh for their cooperation.

I am very thankful to my dear friend Prashant Thakur for his support and motivation during my entire research work. I am thankful to my seniors Dr. Pawan, Dr. Hitanshu, Dr. Bandana, Dr. Rajender, Dr. Rajender Kumar, Dr. Sarita, Dr. Dikshita, Dr. Priyam, Dr. Richa and my colleagues Jonny Dhiman, Neha Kondal, Asha, Subhash, Shikha, Sanjay Kumar, Pooja, Dipti Rawat, Ekta, Rajan, Neha Thakur, Dhruv, Anuradha, Deepak Sharma, Swati, Kanchan, Sampan Attri, Neha, Priyanka, Ritik, Shiv Kumar, Raj Kumar and Achyut Sharma.

I am very thankful to my parents, my grandmother, my brother Umesh, my uncle Mr. Dinesh Sharma and Mr. Hemraj Sharma for their support and motivation.

Thank you all.

Rohit Sharma

ABSTRACT

Spinel ferrites are one of important magnetic materials which are considered to be the foundation of various technological industries. Among different spinel ferrites the Magnesium-Zinc spinel ferrite is considered important due to its remarkable magnetic and electrical properties. But in Magnesium-Zinc ferrite the presence of diamagnetic zinc and magnesium metal ions reduce the magnitude of A-B super-exchange interaction and diminishes magnetic behaviour. In the present work, the diamagnetic zinc ions have been replaced with transition metal ions (Co^{2+}, Ni^{2+} and Mn^{2+}) to enhance the magnetic behavior of magnesium-zinc ferrite. The transition metal doped magnesium-zinc ferrites synthesized using co-precipitation route have been investigated for structural, morphological, elemental and magnetic properties. The brief description of thesis which has been divided into six chapters is given below:

Chapter 1 includes the history of ferrites and various spinel ferrite systems. The role of transition metal doping, some general applications of spinel ferrites and the motive of the present work has been given.

Chapter 2 describes the commonly used synthesis methods for the synthesis of ferrite nanoparticles. The complete reaction mechanism utilized for the synthesis of transition metal doped magnesium-zinc ferrites have been described in detail. The characterization techniques used for the analysis of various physical properties of prepared samples are described.

Chapter 3 describes the structural, morphological and elemental properties of transition metal doped Magnesium-Zinc ferrites. Several structural parameters have been calculated for prepared samples using the *XRD* data. The values of atomic % of cations and anions have also been listed.

Chapter 4 includes the proposed cation distribution for transition metal doped Magnesium-Zinc ferrites. Various structural parameters calculated with the help of proposed cation distribution have been correlated with the obtained *XRD* results.

Chapter 5 describes the variation in magnetic properties of Magnesium-Zinc ferrites on transition metal ion doping. The nature of magnetic exchange interactions investigated with the help of proposed cation distribution and Yafet –Kittel model have been included.

Chapter 6 summarizes the present work. The future scope of the present work has also been given.

LIST OF ABBREVIATIONS

DTGS	Deuterated triglycine sulfate
DC	Direct current
RF	Radio frequency
EDS	Energy dispersive X-ray spectroscopy
FE-SEM	Field effect scanning electron microscopy
FT-IR	Fourier transform infrared spectroscopy
FCC	Face centered cubical
FWHM	Full width at half maximum
HLB	Hydrophilic-Lipophilic balance
KBr	Potassium bromide
pH	Power of Hydrogen
VSM	Vibrating sample magnetometer
XRD	X-Ray diffraction
Y-K	Yafet Kittel

LIST OF SYMBOLS

A	Tetrahedral site
B	Octahedral site
ml	Milliliter
M	Transition metal
K	Kelvin
R	Agreement factor
λ	X-ray wavelength
nm	Nano meter
v_1	Lower frequency band
v_2	Higher frequency band
%	Percentage
δ	Inversion parameter

LIST OF FIGURES

Figure No.	Caption	Page No.
Figure 1.1	Hysteresis loop (a) soft ferrites & (b) hard ferrites	**6**
Figure 1.2	Crystal structure of spinel ferrite	**7**
Figure 1.3	Hexagonal crystal with its lattice parameter a and c	**8**
Figure 2.1	Flow chart for the synthesis of $Mg_{0.5}Zn_{0.5-x}M_xFe_2O_4$ ferrites	**32**
Figure 2.2	Schematic diagram of Bragg's diffraction for a set of lattice planes	**33**
Figure 2.3	Shimadzu (*XRD* 6000) X-Ray diffractometer employed for *XRD* studies	**34**
Figure 2.4	Schematic of emission of X-rays	**36**
Figure 2.5	Schematic of *EDS* spectrophotometer	**37**
Figure 2.6	Ray diagram of *FE-SEM*	**38**
Figure 2.7	Quanta 200 *FEG* Field effect scanning electron microscope	**38**
Figure 2.8	Graphic of *FT-IR* spectrophotometer	**39**
Figure 2.9	*FT-IR* spectrophotometer	**40**
Figure 2.10	Schematic representation of *VSM*	**41**
Figure 2.11	Experimental set up of PAR-155 Vibrating sample magnetometer	**41**
Figure 3.1	*XRD* patterns of Co^{2+} doped *Mg-Zn* ferrites	**47**
Figure 3.2	*FT-IR* spectra of Co^{2+} doped *Mg-Zn* ferrites	**49**
Figure 3.3	*FE-SEM* micrographs for Co^{2+} doped *Mg-Zn* ferrites	**50**
Figure 3.4	*EDS* spectra for Co^{2+} doped *Mg-Zn* ferrites	**51**
Figure 3.5	*XRD* patterns of Ni^{2+} doped *Mg-Zn* ferrites	**52**
Figure 3.6	Shift in position of most prominent (311) X-ray diffraction peak with Ni^{2+} substitution	**53**
Figure 3.7	*FT-IR* spectra of Ni^{2+} doped *Mg-Zn* ferrites	**54**
Figure 3.8	*FE-SEM* micrographs for Ni^{2+} doped *Mg-Zn* ferrites	**55**
Figure 3.9	*EDS* spectra for Ni^{2+} doped *Mg-Zn* ferrites	**56**
Figure 3.10	*XRD* patterns of Mn^{2+} doped *Mg-Zn* ferrites	**57**
Figure 3.11	*FT-IR* spectra of Mn^{2+} doped *Mg-Zn* ferrites	**59**

Figure 3.12	*FE-SEM* micrographs for Mn^{2+} doped *Mg-Zn* ferrites	**60**
Figure 3.13	*EDS* spectra for Mn^{2+} doped *Mg-Zn* ferrites	**60**
Figure 4.1	Variation of mean ionic radii of A and B lattice sites with Co^{2+} substitution	**67**
Figure 4.2	Variation of a_{exp} and a_{th} with Co^{2+} substitution	**68**
Figure 4.3	Variation of oxygen positional parameter *(u)* with Co^{2+} substitution	**69**
Figure 4.4	Variation of r_A and r_B with Ni^{2+} substitution	**71**
Figure 4.5	Variation of oxygen positional parameter *(u)* with Ni^{2+} substitution	**72**
Figure 5.1	M-H curves for $Mg_{0.5}Zn_{0.5-x}Co_xFe_2O_4$ ferrites	**81**
Figure 5.2	Zoomed image of M-H curves for $Mg_{0.5}Zn_{0.5-x}Co_xFe_2O_4$ ferrite samples	**82**
Figure 5.3	Variation of H_c and M_s with cobalt substitution	**83**
Figure 5.4	Neel's collinear and Yafet-Kittel's non-collinear arrangement of spins	**84**
Figure 5.5	The interionic distances and bond angles	**85**
Figure 5.6	M-H curves for $Mg_{0.5}Zn_{0.5-x}Ni_xFe_2O_4$ ferrites	**88**
Figure 5.7	Zoomed image of M-H curves for $Mg_{0.5}Zn_{0.5-x}Ni_xFe_2O_4$ ferrite samples	**89**
Figure 5.8	M-H curves for $Mg_{0.5}Zn_{0.5-x}Mn_xFe_2O_4$ ferrites	**92**
Figure 5.9	Zoomed image of M-H curves for $Mg_{0.5}Zn_{0.5-x}Mn_xFe_2O_4$ ferrite samples	**92**
Figure 5.10	Variation of retentivity & coercivity with Co^{2+}, Ni^{2+} and Mn^{2+}doping	**95**

LIST OF TABLES

Table No.	Caption	Page No.
Table 3.1	Different structural parameters for Co^{2+} doped *Mg-Zn* ferrites	**49**
Table 3.2	Values of atomic % for Co^{2+} doped *Mg-Zn* ferrites	**51**
Table 3.3	Different structural parameters for Ni^{2+} doped *Mg-Zn* ferrites	**54**
Table 3.4	Values of atomic % for Ni^{2+} doped *Mg-Zn* ferrites	**56**
Table 3.5	Different structural parameters for Mn^{2+} doped *Mg-Zn* ferrites	**58**
Table 3.6	Values of atomic % for Mn^{2+} doped *Mg-Zn* ferrites	**61**
Table 4.1	Proposed cation distribution for $Mg_{0.5}Zn_{0.5-x}Co_xFe_2O_4$ ferrites	**66**
Table 4.2	Several structural parameters calculated theoretically using proposed cation distribution	**68**
Table 4.3	Proposed cation distribution for $Mg_{0.5}Zn_{0.5-x}Ni_xFe_2O_4$ ferrites	**70**
Table 4.4	Several structural parameters calculated theoretically using proposed cation distribution	**71**
Table 4.5	Proposed cation distribution for $Mg_{0.5}Zn_{0.5-x}Mn_xFe_2O_4$ ferrites	**73**
Table 4.6	Several structural parameters calculated theoretically using proposed cation distribution	**74**
Table 5.1	Magnetic parameters calculated for $Mg_{0.5}Zn_{0.5-x}Co_xFe_2O_4$ ferrites	**83**
Table 5.2	Net calculated magnetic moment and interionic distances for $Mg_{0.5}Zn_{0.5-x}Co_xFe_2O_4$ ferrites	**86**
Table 5.3	Bond angles and Y-K angles for $Mg_{0.5}Zn_{0.5-x}Co_xFe_2O_4$ ferrites	**87**
Table 5.4	Magnetic parameters calculated for $Mg_{0.5}Zn_{0.5-x}Ni_xFe_2O_4$ ferrites	**90**
Table 5.5	Net calculated magnetic moment and interionic distances for $Mg_{0.5}Zn_{0.5-x}Ni_xFe_2O_4$ ferrites	**90**
Table 5.6	Bond angles and Y-K angles for $Mg_{0.5}Zn_{0.5-x}Ni_xFe_2O_4$ ferrites	**91**
Table 5.7	Magnetic parameters calculated for $Mg_{0.5}Zn_{0.5-x}Mn_xFe_2O_4$ ferrites	**93**
Table 5.8	Net calculated magnetic moment and interionic distances for $Mg_{0.5}Zn_{0.5-x}Mn_xFe_2O_4$ ferrites	**94**
Table 5.9	Bond angles and *Y-K* angles for $Mg_{0.5}Zn_{0.5-x}Mn_xFe_2O_4$ ferrites	**94**

LIST OF PUBLICATIONS

International Journals

1. Sharma R., Thakur P., Kumar M., Thakur N., Negi N. S., Sharma P., Sharma V., "*Improvement in magnetic behaviour of cobalt doped magnesium zinc nano-ferrites via co-precipitation route*", Journal of Alloys and Compounds, vol. 684, pp.569-581, 2016, (WoS, UGC List Serial No. 19077, Scopus Indexed, I.F = 3.779).
2. Sharma R., Thakur P., Sharma P., Sharma V., "*Ferrimagnetic Ni^{2+} doped Mg-Zn spinel ferrite nanoparticles for high density information storage*", Journal of Alloys and Compounds, vol. 704, pp.7-17, 2017 , (WoS, UGC List Serial No. 19077, Scopus Indexed, I.F = 3.779).
3. Sharma R., Thakur P., Kumar M., Barman P. B., Sharma P., Sharma V., "*Enhancement in A-B super-exchange interaction with Mn^{2+} substitution in Mg-Zn ferrites as a heating source in hyperthermia applications*", Ceramics International, vol. 43, pp.13661-13669, 2017, (WoS, UGC List Serial No. 6831, Scopus Indexed, I.F = 3.057).

Conference Proceedings

1. Sharma R., Thakur P., Sharma P., Sharma V., "*Structural and optical analysis of $Mg_{0.625}Zn_{0.375}\ Fe_2O_4$*", International Journal of Scientific Research , vol. 4, pp.187-189, Oct. 2015.

2. Sharma R., Thakur P., Sharma P., Sharma V., " *Structural anlysis of Magneiusm-Zinc ferrite synthesized by co-precipitation route*", International Journal of Basic and Applied Scientific Aspects", vol. 1, pp. 12-14, July 2015.

National / International Conferences/ Workshops

1. International conference on "*Emerging Trends in Basic and Applied Sciences*" May 1-2, 2015 at Maharaza Agar Sen University Baddi Solan.

2. National Conference on "*Recent innovations in Applied Sciences and Humanities*" NCASH-2015 at Rawal Institution Faridabad.
3. National seminar on "*Innovations & Challenges in Basic & Applied Sciences*" at Maharaza Agar Sen University Baddi Solan, March 2017.

4. National level workshop on Characterization tools at NIT Kurukshetra, June, 2015.
5. National level workshop on Technical manuscript preparation with latex at Juit Solan, November, 2015.

CHAPTER 1

INTRODUCTION

Magnetism and magnetic materials have a long and fascinating history. In ancient times, Magnes who lived in Magnesia near Greece mount discovered loadstone. Loadstone is a naturally occurring magnetic material. In middle Ages, Chinese travelers used suspended loadstone as a compass needle for navigation purpose. In 1088, Shen Kuo described the use of magnetic compass needle and the first documented use of compass needle was reported by Zheng He. In modern history, English scientist William Gilbert confirmed observations regarding magnetic poles and conclude that earth is like a magnet. After that magnetism and magnetic materials have been explored by many scientists and research groups across the globe. Several theories have been published by various researchers explaining the magnetic behavior of magnetic materials. Currently magnetism and magnetic materials are playing a crucial role in making human life easy. Magnetic materials are an integral part of most of the technologically important devices. There are different types of magnetic materials present but, among all of them, ferrite are considered to be one of the most important type of magnetic material. It is because there are no other magnetic metal oxides equivalent to them in terms of their magnetic and electrical properties. Snoek in 1936 laid the foundation of physics and technology of ferrites resulting in the establishment of a new technological industry. Ferrites are utilized in broad range of applications ranging from electronic materials to biomedical sciences.

1.1 History of ferrites

The ceramic ferromagnetic materials which are mainly composed of ferric oxide are known as ferrites. The magnetite or the ferrous ferrite (Fe_3O_4) is an example of naturally occurring ferrite [1]. The magnetite was found in magnesia district located in the Asia Minor and therefore, named magnetite. In 1909 Hilpert tried to improvise the magnetic properties of ferrites and successfully prepared several ferrites such as manganese, copper, cobalt, copper and zinc ferrite [2]. In 1928 Forestier prepared various ferrites by precipitation and heat treatment technique and measured their saturation magnetization and curie temperature [3]. Japanese researcher Kato and Takei have studied these magnetic materials exhaustively from 1932 to 1933 [4, 5]. In 1932 Japanese researchers' Kato and Takei discovered that the solid solution of magnetite and cobalt ferrite was strongly magnetized at room temperature and have large number of practical applications. They prepared permanent magnet having a coercive force of about 600 *Oe* [5]. But the role of ferrites in modern technology started with the work of Snoek in 1933 [6]. Vermey, Heilalan and some

other researchers from Philip's research laboratory have also contributed a lot in the development of ferrites for their technological applications [7]. The large scale production of televisions in 1950's was the major reason for the rise of ferrite industry, especially in America and Europe. Ferrites have been used as a special transformer in television sets [8]. Thereafter various ferrites have been synthesized and have been found useful in high frequency applications, permanent magnets and some other fields.

To explain the magnetic behavior of ferrites, some theories have been reported. In this respect the Neel's and Kramer's theory throw a great insight on the magnetic behavior of ferrites [8, 9]. The fundamental interaction among the magnetic ions mediated with the help of oxygen atoms was explained by Anderson [9] This type of interaction among the magnetic ions is recognized as A-B super-exchange interaction. The work by Vermey and Heilalan dealing with the metal cations distribution in crystallographic lattice sites provides a significant help in understanding the physics and chemistry of ferrites [10]. During 1940 to 1950 the use of ferrites was mainly focused on radio and microwave frequency applications. From 1950 onwards ferrites have been utilized in several consumer goods of technological importance [11].

1.2 Ferrites

Ferrites are the mixed metal oxides (*M-Fe*) containing ferric oxide as a major component. Ferrites are usually non-conducting oxides, which are derived from iron oxides such as naturally occurring magnetite (Fe_3O_4) or hematite (Fe_2O_3) [12]. In anti-ferromagnetic materials the magnitude of magnetic moment on the two crystallographic lattice sites which are opposite to each other are equal which results in net cancellation of magnetic moment. But, in case of ferrites the magnetic moment on crystallographic lattice sites which are opposite to each other is not equal in magnitude so complete cancelation of magnetic moment is not possible like anti-ferromagnetic materials. This type of magnetic behaviour is called ferrimagnetism or uncompenstated anti-ferromagnetism. This is because of the presence of different concentration of ions of magnetic element at the two different crystallographic lattice sites which are anti parallel to each other [13]. Ferrites have excellent magnetic and electrical properties, which make them industrially and technologically an important magnetic material [14]. High magnetic permeability, soft magnetic nature, chemical and thermal stability and high electrical resistivity

which prevent loss of energy at high frequency applications are some of the important physical properties of ferrites [15]. These properties of ferrites make them potential candidate in some useful applications such as high density information storage, recording heads, microwave devices, telecommunication systems, transformer cores, antenna rods, ferrite electrodes, magnetic toner for copiers, electromagnetic wave absorption, choke coils, switched power supplies, ferro-fluids, magnetically guided drug delivery, hyperthermia and gas sensors *etc.* [10, 16-18]. Ferrites have different types, which can be distinguished from each other on account of their magnetic behavior and crystal structure. The classification of ferrites on the basis of their magnetic behaviour and crystal structure has been discussed in detail in next section.

1.3 Classification of ferrites

1.3.1 Magnetic behavior (Soft and Hard ferrites)

Ferrites can be classified as Hard and Soft type of ferrites on the account of their magnetic behaviour. The magnetic materials which have large value of M_s the saturation magnetization and low value of H_c the coercivity (H_c < 10A/cm) are known as soft ferrites [19]. Figure 1 (a) shows the hysteresis loop for soft ferrites. Their strength to retain magnetization is very low, so they can be easily magnetized as well as demagnetized. Soft ferrites have low magnetic losses at high applied frequencies [20]. Soft ferrites show application in wide range of applications such as in ac motors, generators, transformer cores, recording equipments and telecommunication systems *etc.* [20]. In soft ferrites the magnetic behavior is due the interaction between magnetic metal ions situated at two different crystallographic lattice sites. Nickel, Zinc, Manganese, Magnesium and Copper ferrite *etc.* are the examples of soft ferrites [21].

On the other hand the magnetic materials having large value of coercivity (H_c >300 A/cm) and low value of saturation magnetization are regarded as hard ferrites. Their strength to retain magnetization is very high as compare to soft ferrites, so it's not easy to demagnetize them [20]. Figure 1 (b) shows the hysteresis loop for hard ferrites.

Hard ferrites are made in isotropic and oriented form. The isotropic hard ferrite is firstly formed in preferred shape, sintered and then magnetized. They mostly find application in cycle dynamos and ring magnets. On the other hand the oriented type hard ferrite is firstly formed into desired shape under the influence of strong magnetic field and then sintered. They find application in

loudspeakers and magnets of automobiles [21]. Most of the permanent magnets belong to oriented type of hard ferrites. Barium and strontium ferrites are the examples of hard ferrite [21].

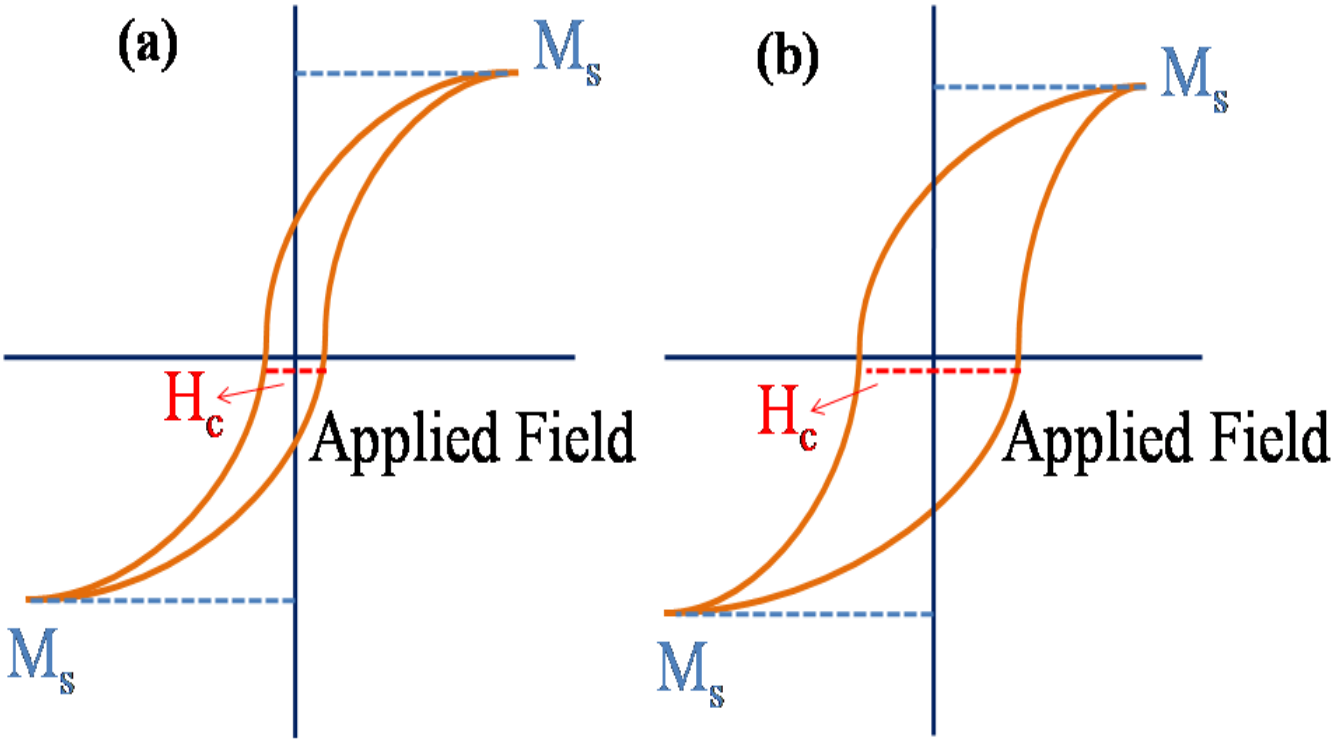

Figure 1.1: Hysteresis loop (a) soft ferrites & (b) hard ferrites

1.3.2 Crystal structure

On the basis of crystal structure, the ferrites can be divided into three different categories as spinel ferrite, hexagonal ferrite and rare earth garnet ferrite.

1.3.2.1 Spinel ferrite

Ferrites crystallizes in the form of spinel structure, the name spinel associated with ferrites is because of the similarity of the structural formula (MFe_2O_4) of ferrites with $Mg\ Al_2O_4$, which is known as spinel [13], where *M* refers to metal ions. The spinel structure belongs to *Fd3m* space group. The spinel structure can be described as face centered cubically closed pack arrangement

of 32 oxygen anions which forms the unit cell. Figure 1.2 shows the crystal structure of spinel ferrite [22].

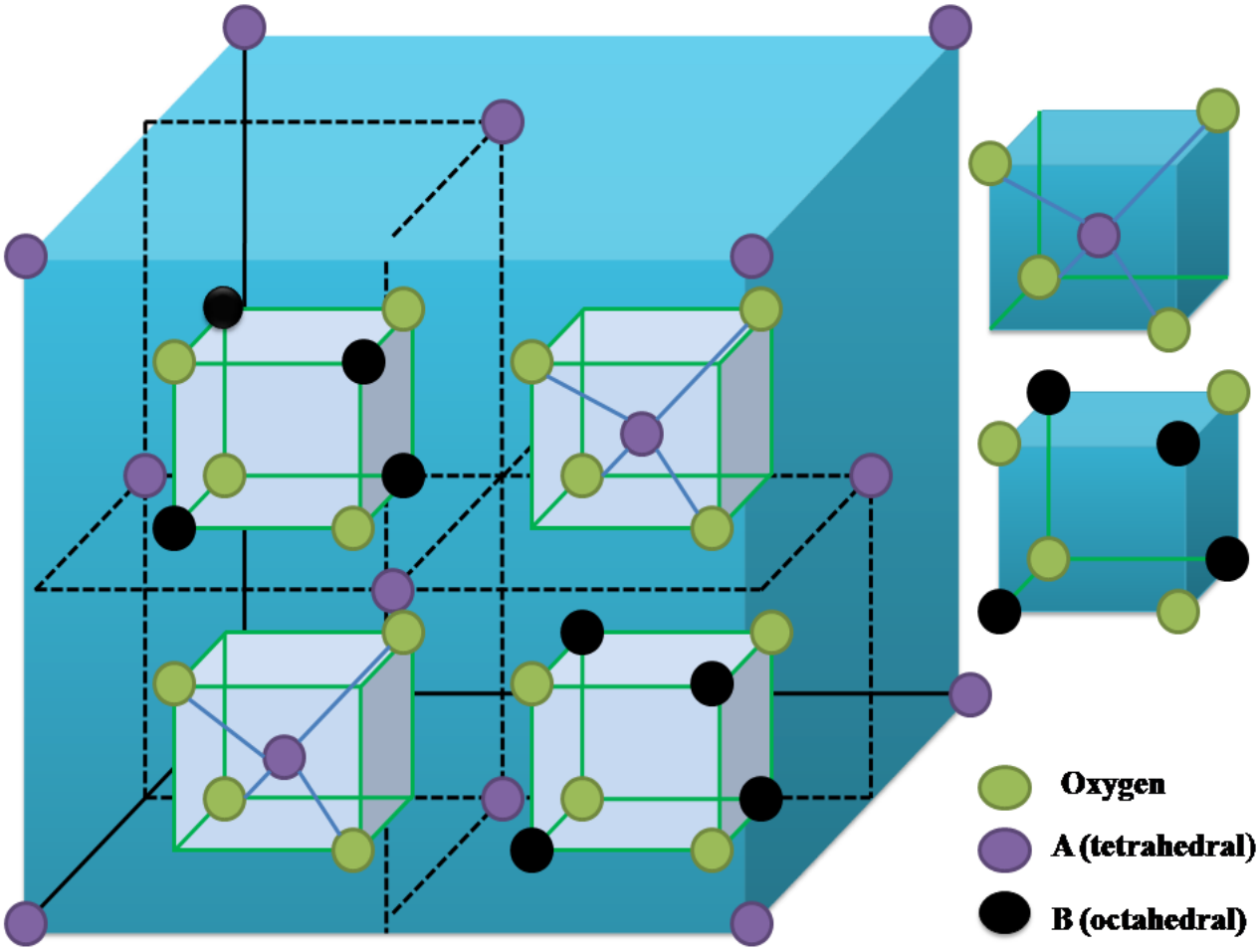

Figure 1.2: Crystal structure of spinel ferrite

The arrangement of these 32 oxygen anions in the unit cell leaves two kinds of crystallographic lattice sites in the unit cell. These lattice sites are known as tetrahedral (A) and octahedral (B) sites [22]. The tetrahedral sites have coordination with four oxygen anions and octahedral sites have coordination with six oxygen anions. In spinel structure, the unit cell which is made up of 32 oxygen anions has 64 A and 32 B sites. The net positive charge will become more in comparison to net negative charge when all the crystallographic lattice sites have been filled with 2^+ or 3^+ metal ions and this will destroy the electrical neutrality of unit cell. So there are only eight A sites and sixteen B sites in a unit cell of spinel ferrite which are filled with 2^+ or 3^+

valency metal ions so that the unit cell remains electrically neutral [13]. Nickel, zinc, magnesium, manganese, lithium and cobalt ferrites are common examples of spinel ferrite.

1.3.2.2 Hexagonal ferrite

The hexagonal ferrite is known as magnetoplumbite. The mineral magnetoplumbite was discovered in 1925 and in 1938 the crystal structure of magnetoplumbite was found to be hexagonal [23]. The c axis is the major preferred axis in hexagonal structured ferrite, and a axis is the minor axis. The length of c and a axis is termed as c and a lattice parameter respectively. These two lattice parameters are required to give the dimensions of a hexagonal crystal [13]. Figure 1.3 shows hexagonal crystal with two of its lattice parameters [23].

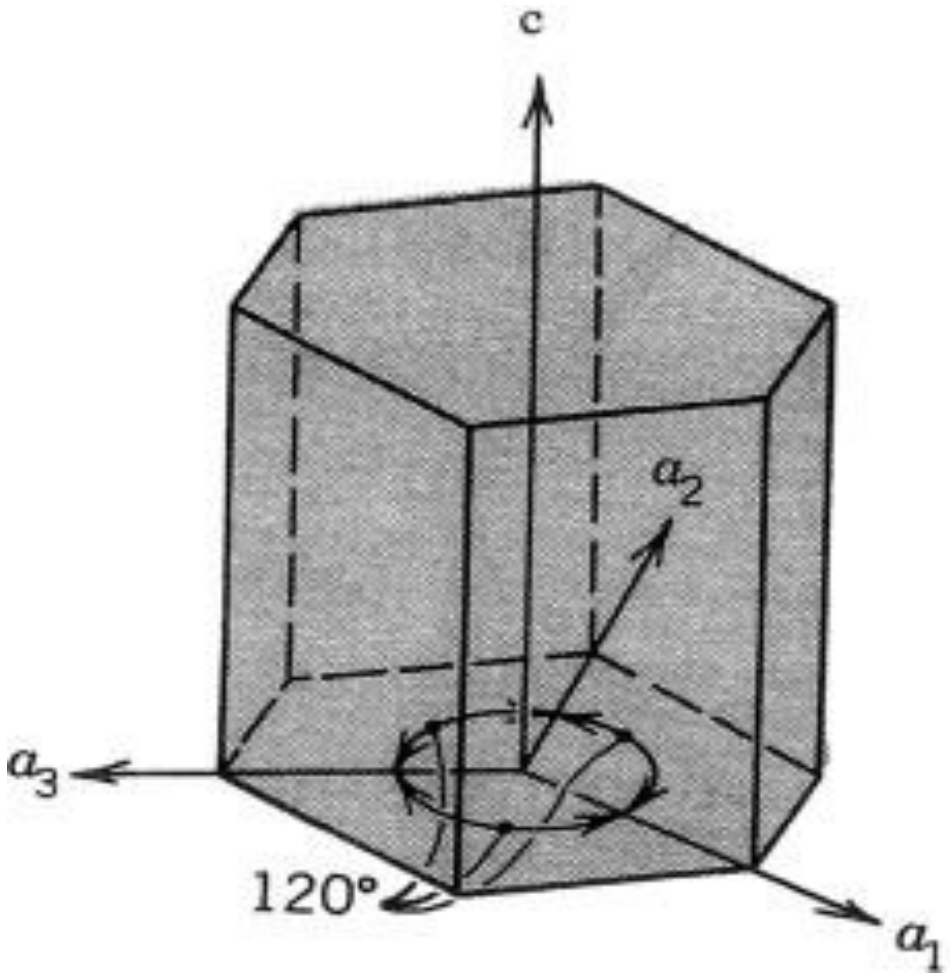

Figure 1.3: Hexagonal crystal with its lattice parameter a and c

The chemical formula for hexagonal ferrites is $M\ Fe_{12}O_{19}$, where M can be barium, strontium or lead. In hexagonal ferrites the oxygen anions show close packing similar to the spinel structure

where some layers of oxygen exist that can accommodate the divalent metal ions of barium, strontium or lead. The ionic radii of barium, strontium or lead are comparable to oxygen anions, so they can replace oxygen anions in the crystal lattice [23]. Several workers at Philips Research Laboratories discovered large number of compounds having hexagonal structure [13]. These compounds were prepared by mixing magnetoplumbite with other spinel compounds in different stoichiometric ratios. There are different types of hexagonal ferrites designated as M, W, X, Z, Y and U ferrites. The hexagonal ferrites have found application in data storage, microwave devices, electromagnetic wave absorption, actuators, sensors, motors, generators, electronic components for mobile and wireless communication and stealth technology [23].

1.3.2.3 Rare earth garnet ferrite

In 1956 Bertaut and Forrat discovered Garnet ferrite and after one year Geller and Gilleo (1957) also invented these garnet ferrites. Geller & Gilleo (1957) have explained the crystal structure of garnet ferrites [13]. Rare earth garnet ferrites crystallize in the 12-sided structure or dodecahedral, resemble to the mineral garnet. Garnet structure is similar to spinel structure except the presence of dodecahedral lattice sites [24]. The rare earth garnets have general formula $M_3Fe_5O_{12}$, where yttrium (Y) is represented by M is or some other rare earth ion. Although Y is not a element belonging to rare earth but it shows behaviour like rare earth. Hence it is placed in the family of rare earth garnets [25]. In garnet ferrites all the meal ions are trivalent in nature. The three different lattice sites in garnet ferrites are octahedral, tetrahedral and dodecahedral. The octahedral, tetrahedral and dodecahedral sites occupy 16 Fe^{3+}, 24 Fe^{3+} and 24 M^{3+} ions respectively [25]. In garnet ferrite, every tetrahedron is interconnected with four octahedrons and every octahedron is connected with six tetrahedrons. The shared corners in this type of structure are distorted and form a series of dodecahedrons. These dodecahedrons sites provide space for rare earth metal cations [26]. The rare earth metal cations align them in a direction opposite to metal cations present at tetrahedral sites and contribute to the magnetization of sublattice. Rare earth garnet ferrites are suitable in several applications such as isolators, circulators, high frequency microwave devices, optical isolator, fiber communication and magnetic recording media etc [27]. $Y_3Fe_5O_{12}$, $Sm_3Fe_5O_{12}$, $Eu_3Fe_5O_{12}$, $Tb_3Fe_5O_{12}$, and $Lu_3Fe_5O_{12}$ are the common examples of rare earth garnet ferrites [13].

1.3.3 Types of spinel ferrites

Spinel ferrites exist in three different types which are normal spinel, inverse spinel and mixed spinel. The type in which spinel ferrite crystallizes is dictated by the distribution of metal cations in A and B crystallographic lattice sites. The various types of spinel ferrite are discussed in detail in the following section.

1.3.3.1 Normal spinel

The spinel structure is said to be normal spinel when divalent metal ions ($M^{2+)}$ prefer to occupy tetrahedral (A) sites. The structural formula for normal spinel ferrite is $[M^{2+}]_A\,[Fe^{3+}]_B O_4^{2-}$ [20]. The preference of metal ions to occupy lattice site depends on ionic radii of metal ions, temperature, size of lattice sites and orbital preference [13]. Zinc and cadmium ferrite are the examples of normal spinel ferrite [28]. In case of zinc and cadmium ferrite, the electronic configuration of Zn^{2+} and Cd^{2+} is favorable for tetrahedral bonding to oxygen anions, so they prefer to occupy tetrahedral lattice sites.

1.3.3.2 Inverse spinel

The spinel structure is said to be inverse spinel when all the divalent metal ions (M^{2+}) occupy A sites and trivalent (Fe^{3+}) metal ions get equally distributed among A and B sites. Barth and Posnak discovered that the trivalent metal cations preferred the A sites and occupied them first [13]. The structural formula for inverse spinel ferrite is $[Fe^{3+}]_A\,[M^{2+}Fe^{3+}]_B\,O_4^{2-}$ [20]. Nickel and cobalt ferrite are the most common examples of inverse spinel ferrite [29-30]. Most of the commercially important ferrites are inverse spinels.

1.3.3.3 Mixed spinel

The divalent and trivalent metal cations in mixed spinel structure get positioned at both the tetrahedral and octahedral lattice sites [20]. For mixed spinel ferrites, the structural formula is $[M_{1-\delta'}{}^{2+}\,Fe_{\delta'}{}^{3+}]_A\,[M_{\delta'}{}^{2+}Fe_{2-\delta'}{}^{3+}]_B\,O_4^{2-}$, where δ' is the degree of inversion [31]. Magnesium-Zinc, Manganese-Zinc, Nickel-Zinc and Cobalt-Zinc ferrites belong to family of mixed spinel ferrites.

1.4 Some important spinel ferrites

1.4.1 Zinc ferrite

Zinc ferrite has a crystal structure of normal spinel ferrite, in which all divalent zinc metal ions are positioned at A lattice sites and trivalent iron metal ions take position at B lattice sites. Zinc ferrite shows anti-ferromagnetic order and zero magnetization below 10 *K* [32]. In ferrites the magnetic ordering is controlled by A-B, B-B and A-A magnetic exchange interactions [32]. In Zinc ferrites, the A-B exchange interaction is not present on account of the presence of non-magnetic Zn^{2+} metal cations at A lattice sites. The presence of Fe^{3+} ions at B lattice sites creates the intra site B-B exchange interaction which is responsible for anti-ferromagnetic ordering in Zinc ferrite. But, in nano-crystalline form the Zinc ferrite nanoparticles have shown ferrimagnetic behaviour due to distribution of some of non-magnetic zinc ions in octahedral lattice sites. Carta *et al.* have reported the distribution of divalent zinc ions in octahedral sites for nano-crystalline Zinc ferrite [33]. The presence of zinc ions in octahedral lattice sites have been confirmed using X-ray absorption spectroscopy [33]. The transfer of non-magnetic zinc ions from sites A to B pushes some of magnetic trivalent ions from sites B to A, which enhances the A-B exchange interaction leading to ferrimagnetism in zinc ferrites. Tanaka *et al.* have reported large magnetization of 32 *emu/gm* for zinc ferrite thin films which indicate the presence of ferrimagnetic behaviour [34].

Zinc ferrite nano-particles exhibit anomalous properties such as soft magnetic nature, spin glass state, super-paramagnetic behaviour at room temperature, low dielectric losses, low toxicity, photocatalytic activity etc. [35, 36]. The interesting properties of zinc ferrite nanoparticles show that they are useful in different applications such as information storage, supercapacitor, high frequency devices, electronic and communication devices, MRI contrast agents, magnetic hyperthermia, degradation of toxic dyes and gas sensing [35-37]. The low toxicity of zinc ferrite nanoparticles make them more promising magnetic resonance imaging agent in comparison to other biocompatible magnetic resonance imaging agents [36]. There are several methods available for the synthesis of zinc ferrites such as microwave assisted combustion, electrophoretic deposition, sol gel, hydrolysis *etc.* [32, 33, 35, 36].

1.4.2 Lithium Ferrite

The exclusive magnetic and electrical properties of lithium ferrite make it an important spinel ferrite. Lithium ferrite generally crystallizes into ordered and disordered ferrite. Ordered lithium ferrite is α-$LiFe_5O_8$ in which A lattice sites are only filled by trivalent iron ions and remaining iron and lithium ions occupy B lattice sites. It is also known as α phase lithium ferrite. In disordered lithium ferrite the lithium ions are randomly distributed over B lattice sites. The disordered lithium ferrite is also called as β lithium ferrite. Lithium ferrite also exists in γ phase but mainly crystallizes into α and β phases [38].

Lithium ferrite has large saturation magnetization, high curie temperature and high electrical resistivity. Lithium ferrite has been regarded as an important candidate for microwave devices, antennas, read and write heads for high disk digital tapes, cathode material for lithium ion batteries, ferro fluid, gas sensing *etc.* [38-40]. There are numerous methods alike solution combustion, sol-gel, co-precipitation, hydrothermal, mechanical alloying *etc.* available for the preparation of lithium ferrite nanoparticles [38, 40].

1.4.3 Nickel ferrite

Nickel ferrite is a soft ferrimagnetic material and has inverse spinel structure. In nickel ferrite, all the divalent nickel ions are situated at B lattice sites and trivalent iron ions occupy both tetrahedral and octahedral lattice sites [22]. But, in few studies, it has been reported that on reducing the grain size to few nano-meters the nickel ferrite becomes mixed spinel ferrite. Chinnasamy *et al*. have reported mixed type of spinel structure for $NiFe_2O_4$ on reducing the grain size to few nano-meters [41].

Nickel ferrite is very important for technological industry due to its notable properties such as high saturation magnetization, soft magnetic character, high permeability, high electrical resistivity, mechanical hardness, chemical stability, low eddy current losses and cost effectiveness [42, 43]. Nickel ferrites have been widely used in various technologically important applications such information storage, inductors cores, magnetic heads, antenna rods, contrast agent in MRI applications, magnetic refrigeration, anti-bacterial activities and hyperthermia [44-46]. Bae *et al.* have observed the nickel ferrites to witness high biocompatibility and appropriate magnetic characteristics required for hyperthermia applications [45]. Golkhatmi *et al.* have observed the nickel ferrite nanoparticles to show good antibacterial activity against gram-negative

pseudomonas syringae, gram-positive bacillus subtilis and phytopathogenic fungi [46]. There are number of synthesis techniques available to prepare $NiFe_2O_4$ nanoparticles such as chemical vapor deposition, thermal decomposition, sol gel, co-precipitation, laser ablation, hydrothermal, ultrasound irradiation, etc. [45, 46].

1.4.4 Magnesium ferrite

Magnesium ferrite crystallizes into normal cubical spinel structure wherein A and B lattice sites are occupied by Mg^{2+} and Fe^{3+} metal ions respectively [13]. Magnesium ferrite is soft magnetic in nature. Magnesium ferrite has been regarded as a crucial ferrite material due to its interesting magnetic and electrical properties such as low saturation magnetization and high resistivity [47]. Apart from magnetic and electrical characteristics, the magnesium ferrite is highly stable, non toxic and cost effective [48].

Kurian *et al.* reported that the magnesium ferrite nanoparticles prepared using solvothermal method have shown desired magnetic properties which make them useful in high density recording applications [49]. Maensiri *et al.* [50] shown that the magnesium ferrite nanostructures prepared using electrospinning method are beneficial in electronic and storage device applications. Jung *et al.* have reported that the magnesium ferrite based magnetic composites have shown potential for removal of phosphates from waste water [48]. Maehara *et al.* have shown that the magnesium ferrite has desired magnetic properties which make it suitable for hyperthermia applications [51]. Tang *et al.* have reported that the superparamagnetic magnesium ferrite nanoparticles can be used as effective nanoadsorbent for removal of arsenic from contaminated water [52].

1.4.5 Cobalt ferrite

Cobalt ferrite has inverse spinel structure in which half of Fe^{3+} metal ions occupy A lattice sites and other half of Fe^{3+} metal ions occupy B lattice sites along with Co^{2+} metal ions. Cobalt ferrite has gained an enormous amount of interest in recent years due to its moderate saturation magnetization, high magneto-crystalline anisotropy, high coercivity, good chemical stability and high mechanical hardness [53]. Recently, Amirthavalli *et al.* have reported a maximum coercivity of 1769.7 *Oe* and saturation magnetization of 69.10 *emu /gm* for cobalt ferrite nano-particles [54]. The high coercivity, saturation magnetization and high chemical and physical stability make cobalt ferrite suitable in high density information storage, ferro-fluid technology, magnetocaloric

refrigeration [55, 56]. Jung *et al.* have described that the functionalization of cobalt ferrite with organic memory devices enhances memory storage [57]. Cobalt ferrite has also been found to be beneficial in different biomedical applications such as drug delivery, contrast agent in magnetic resonance imaging and hyperthermia. Dey *et al.* showed that the $CoFe_2O_4$ nanoparticles are suitable for the drug release applications using hyperthermia technique [58]. Oh *et al.* studied the $CoFe_2O_4$ nanoparticles and suggested their potential use as therapeutic agent for cancer treatment [59].

1.4.6 Manganese ferrite

Manganese ferrite is a mixed type of spinel, where divalent (Mn^{2+}) and trivalent (Fe^{3+}) metal ions may occupy either A or B sites. The bulk manganese ferrites are found to be 20 % inverse spinel and nano manganese ferrites have been reported to have 60 % inverse spinel structure [60]. Manganese ferrite is known for higher saturation magnetization, high magnetic permeability, high curie temperature, low power losses at high frequency and good chemical stability [61]. Manganese ferrites are suitable for different applications such as magnetic recording devices, super capacitors, biosensors, ferro fluids, drug delivery, contrast enhancement agent in MRI the magnetic resonance imaging and hyperthermia applications [62, 63].

The electrodes of manganese ferrite nano-particles are excellent for supercapacitor applications [62]. The manganese ferrite nanoparticles have shown strong antifungal and antibacterial activity against two gram positive and two gram negative bacteria [64]. Singh *et al.* have reported that the enhanced adsorption capacity of manganese ferrite nanoparticles towards harmful dyes make it a suitable material for water purification [65]. The desirable thermal properties and bio-compatibility of manganese spinel ferrites make them beneficial for hyperthermia applications [66].

1.4.7 Nickel-Zinc ferrite

Nickel–Zinc ferrite is one of the most widely studied ferrite material. Nickel –Zinc ferrite has a mixed spinel structure where A lattice sites are filled by Zn^{2+} metal ions and B lattice sites are filled by Ni^{2+} metal ions. The Fe^{3+} metal ions in nickel zinc ferrite are distributed among both the lattice sites [67]. Nickel-Zinc nano-ferrite is mainly known for its application in high frequency microwave devices due its large electrical resistivity, high curie temperature, good chemical

stability and excellent soft magnetic characteristics [68]. Nickel-Zinc ferrites are also found to be practicable in different applications alike memory storage transformer cores, inductors, magneto-optical devices, magnetic resonance imaging and catalysis [69, 70].

The $Ni_{0.5}Zn_{0.5}Fe_2O_4$ ferrite based dielectric resonator antenna is suitable for wireless communication systems at microwave band [71]. The Nickel-Zinc ferrite synthesized by electrospinning technique have proven to be an excellent microwave absorber [72]. Nickel-Zinc ferrites have also shown application in removal of toxic dyes from aqueous solutions and gas sensing. The nickel-zinc ferrite can be used as an efficient adsorbent for the degradation of cationic and well as anionic dyes [73]. The nickel-zinc ferrites can be used for sensing of chlorine gas at room temperature [74].

1.4.8 Manganese-Zinc ferrite

Manganese-Zinc ferrite crystallizes into mixed spinel structure [20]. In Manganese-Zinc ferrites few of the divalent Mn^{2+} metal ions occupy A lattice sites and trivalent Fe^{3+} metal have preference for both of the lattice sites. Manganese-Zinc ferrites are of significant interest due to their high value of permeability, low hysteresis loss, large saturation magnetization, high resistivity and low power losses [75, 76]. Magnesium-Zinc ferrites are widely utilized in various applications such as transformer cores, antenna rods, recording heads, magnetic sensor, high quality filters, radio frequency circuits, electromagnetic wave absorbers, switching devices, medical diagnosis, photocatalysis *etc.* [20, 75, 76].

Manganese-Zinc ferrites synthesized using combustion method are suitable for high frequency electromagnetic device applications [76]. The Manganese-Zinc ferrites having high saturation magnetization and low hysteresis losses are useful in many important technical devices like microwave devices, magnetic recording heads, computer memory chips and transformers [77]. Manganese-Zinc based ferrites having high resistivity, high magnetization and low dielectric losses can be explored as antenna rods, radio frequency circuits, high quality filters, transformer cores and read and write heads for high digital tapes [78]. The manganese-zinc ferrite synthesized by one pot co-precipitation method show high specific capacitance and are suitable for supercapacitor applications [79]. Manganese-Zinc ferrites have also shown potential in biomedical applications. Phong *et al.* have shown that the manganese-zinc ferrites having high intrinsic losses are suitable material for hyperthermia applications [80].

1.4.9 Magnesium-Zinc ferrite

Magnesium-Zinc ferrites represent an important class of magnetic oxides. Magnesium-Zinc ferrite crystallizes into mixed spinel structure. The divalent $Zn^{2+}$and Mg^{2+} metal ions preferably inhabit A and B lattice sites respectively, while Fe^{3+} metal ions can inhabit both A and B lattice sites [13]. Silva *et al.* have confirmed the presence of Zn^{2+}, Fe^{3+} and Mg^{2+} ions in A and B lattice sites respectively in magnesium-zinc ferrite system using Raman spectroscopy [81].

Magnesium-Zinc ferrites are extremely important to technological industry because of their interesting magnetic and electrical properties. Magnesium-zinc ferrites have soft magnetic character, high permeability, high saturation magnetization, high electrical resistivity, high curie temperature, low energy losses at high frequencies, low cost and better environmental stability [31, 82]. The high permeability, high electrical resistivity and low eddy current losses make them favorable soft magnetic material among other ferrite systems [83]. Magnesium-Zinc ferrites are also regarded as a cheap alternative to costly Nickel-Zinc ferrites [84]. Skołyszewska *et al.* have obtained soft magnetic properties for magnesium-zinc ferrites assuring high magnetic permeability and low energy losses [85]. Hajarpour *et al.* have reported enhancement in saturation magnetization for $Mg_{0.6}Zn_{0.4}Fe_2O_4$ sample with increase in glycine to nitrate ion ratio [86]. The enhancement in magnetization for $Mg_{0.5}Zn_{0.5}Fe_2O_4$ ferrite sample prepared at different *pH* values using hydrothermal method have been reported [87]. Barbosa *et al.* have observed enhanced magnetic characteristics for $Mg_{0.6}Zn_{0.4}Fe_2O_4$ nano-ferrite sample synthesized using combustion reaction method [88]. Choodamani *et al.* have shown superparamagnetic character for $Mg_{0.5}Zn_{0.5}Fe_2O_4$ ferrite sample synthesized using combustion method [89]. Singh *et al.* have reported soft magnetic characteristics for Magnesium-Zinc ferrite samples synthesized using co-precipitation route [90]. Rahman *et al.* have also obtained soft magnetic properties for Magnesium-zinc ferrites prepared using co-precipitation route. The maximum value of coercivity has been observed for $Mg_{0.5}Zn_{0.5}Fe_2O_4$ ferrite sample as compared to other stoichiometric compositions of *Mg-Zn* ferrite [91].

Magnesium-Zinc ferrites show use in high density storage devices, high frequency devices, sensing, transformer cores, switched mode power supplies and in biomedical applications [31, 82]. The magnesium-zinc ferrites synthesized by microwave assisted sol-gel combustion method are useful in energy storage and as writing and reading head for memory storage applications [92]. The magnesium-zinc spinel ferrites synthesized using solution combustion technique have

desired magnetic and electrical properties which make them useful in various electromagnetic applications [93].

Magnesium-zinc spinel ferrites have also shown application in biomedical and sensing applications [90, 94]. The super-paramagnetic magnesium-zinc ferrite nanoparticles are suitable for magnetic hyperthermia uses [95]. The magnesium-zinc ferrite based humidity sensors are very fast and reliable [96]. Mukherjee *et al.* have reported that the $Mg_{0.5}Zn_{0.5}Fe_2O_4$ nano-tubes have shown promising sensing response towards hydrogen, carbon monoxide and nitrous oxide [97].

1.5 Role of transition metal doping

The quantum mechanical phenomenon which is known as A-B super-exchange interaction has a strong impact on different physical properties of ferrites. The strength of A-B exchange interaction depends on the metal cations magnetic moment present at lattice sites A and B. Transition metal ions Co^{2+}, Ni^{2+} *etc.* have partially filled *d* orbital which give rise to magnetic moment corresponding to number of unpaired electrons. The spin of unpaired electrons of partially filled *d* orbital is responsible for magnetic moment [98]. The substitution of transition metal is of special importance because transition metal ions substitution increases the value of magnetic moment at lattice sites which result in the enhancement of various physical properties.

There are numerous reports of the substitution of different transition metal ions like copper, cobalt, chromium, zinc *etc.* which enhance the various physical properties in spinel ferrites [99-101]. Abraham *et al.* have shown increase in coercivity and remnant magnetization for cobalt doped magnesium ferrites synthesized using combustion method [102]. Ati *et al.* have also shown enhancement in magnetic properties of cobalt doped nickel ferrite nanoparticles which make them appropriate for memory storage and microwave device applications [103]. The cobalt substituted manganese ferrites synthesized using micro-emulsion route have that desired magnetic characteristics which make them useful in memory recording applications [104].

Padmapriya *et al.* have reported enhancement in magnetic properties of zinc ferrites on nickel substitution. The nickel substitution also enhances the dye degradation efficiency of zinc ferrite nanoparticles [105]. It has been reported that the magnetic properties of nickel doped ferrites are suitable for memory storage device applications [106]. The *Co-Mn* doping enhances the magnetic properties of *Ni-Sn* ferrites and have been found to be useful in high density recording media

[107]. The high permeability and low magnetic losses have been observed for manganese doped zinc ferrites [76]. The manganese doped *La-Ce* ferrites show use in memory recording applications [108]. The manganese substituted magnesium-zinc ferrites synthesized using oxalate precursor method have shown decrease in dielectric losses with increase in frequency which makes them highly desirable for high frequency device applications [109]. The manganese substituted ferrites may be useful in energy storage and other technological applications [110]. Anjana *et al.* have obtained enhanced magnetic properties with copper substitution in nickel ferrites [111]. Yadav *et al.* have found low dielectric losses and increase in dielectric constant for chromium doped manganese ferrites which makes them advantageous in charge storage device applications [112].

The transition metal ion substituted ferrites have also shown potential in environmental and biomedical applications [73, 95, 99]. The substitution of cobalt in zinc spinel ferrites provides a possible candidate for purification of polluted water [113]. Lassoued *et al.* have reported enchaned photo-catalytic dye degradation for nickel doped cobalt-zinc ferrites [114]. Gharibshahian *et al.* have reported that the magnetic properties along with non toxic nature of zinc doped cobalt ferrites are useful in biomedical applications [115]. The copper substituted cobalt ferrites have improved antibacterial activities and are useful as ingredient in creams or lotions for biomedical applications [116]. The reported results confirm that transition metal doping enhances the various physical properties of spinel ferrites and make them suitable for several applications which are of technological, biological and environmental importance.

1.6 General applications of spinel ferrites

1.6.1 Magnetic recording

Magnetic recording is one of the main applications of spinel ferrite nanoparticles. While recording, the magnetic states are impressed on the magnetic media made up of magnetic nanoparticles or magnetic thin films. Since 1947 the fine particles of spinel γ-Fe_2O_3 have been used for memory storage applications. These spinel ferrite magnetic nanoparticles have been used in digital as well as video and audio recordings. The saturation of spinel ferrite in one direction is taken as a digital state 1 and saturation in other direction is taken as digital state 0. For this the material must have some intermediate value of coercivity to sustain digital state, but also do not

have so much coercivity that a large field is required to demagnetize it [13]. The magnetic nanoparticles are also utilized in the hard disks to increase the storage density. For high storage density application, the high coercivity along with high retentivity and appropriate value of saturation magnetization is desired. The γ-Fe_2O_3 used for tape recording has specific saturation magnetization of 74-76 emu/gm [13]. Cobalt, Nickel and Manganese-Zinc ferrites based systems have also been explored for recording purposes. Hu *et al.* have shown that the spinel ferrites are beneficial in memory storage device applications [117]. Gilani *et al.* have described that the $LiCo_{0.5}Pr_xFe_{2-x}O_4$ ferrites are useful in high density memory recording applications [118].

1.6.2 Microwave devices

Spinel ferrites are useful in several microwave device applications. These materials operate near the resonance as microwave absorber or electromagnetic wave shielding materials and above resonance as highly permeable and low loss materials in various devices as isolators, filters, circulators, phase shifters and inductor cores [119]. The ideal materials for high frequency microwave device applications require moderate saturation magnetization, high permeability, high resistivity, low magnetic and dielectric losses [119]. Spinel ferrites are considered as important materials because they possess all these above mentioned properties. In modern microwave systems the ferrite circulator is one of the most frequently used device. In ferrite circulator the ferrite material interacts with the strong electromagnetic wave and provides non-reciprocal behaviour required for operation of circulator. Ahmed *et al.* have shown that the *Ni-Ti* substituted *Mn-Zn* ferrites have shown promising electromagnetic properties which make them useful in various microwave device applications such as high quality filters, transformer cores, rod antennas, power supplies *etc.* [120]. The ferrite based materials have also been used for suppressing unwanted electromagnetic wave signals. Li *et al.* have shown that the nickel-zinc ferrites have potential microwave absorbing properties [121].

1.6.3 Entertainment applications

Soft spinel ferrites are utilized on large scale in entertainment applications. They are particularly useful in radio and television industry. They have been used as television deflection tube yokes, flyback transformers, interstage and pincushion transformers. The television defection yokes made up of ferrites are funnel shaped toroids. The properties such as permeability, saturation, curie temperature, coercivity, loss factor, density and electrical resistivity of ferrites play crucial

role in deciding their application for television deflection tube yokes. Magnesium-Zinc and Manganese-Zinc ferrites are preferred for television deflection tube yokes [13]. The interstage transformers are used in audio and well as video circuits for coupling of different stages of impedance and isolation matching. Ferrites are also utilized as an antenna in radio and television. The electromagnetic waves associated with radio and televisions have quite large wavelengths which require large antennas' for operation. The antennas' made up of ferrite materials which are also smaller in size have the ability to receive that large wavelengths. This factor makes ferrite antennas' important for portable radio and television sets. *Mn-Mg-Zn* ferrites are useful in high definition television deflection yokes respectively [109].

1.6.4 Power applications

Ferrites are very useful in dc power supplies especially in integrated circuits and computers. They are used in circuits where there is a requirement of well regulated DC power supply. In linear and switched power supplies the ferrite materials are used [13]. In linear power supplies the transformer, rectifier and choke made up of ferrite materials are used to reduce the residue ac ripple. In audio frequency applications the transformers, speakers, audio processing instrument and microphones require several components which are made up of ferrite materials. In telecommunication application the channel filters and wide band transformers are made up of ferrite materials. Loading coils made of ferrite are also put in use in transmission lines to enhance the inductance [13, 20].

1.6.5 Sensing

In present time the gas sensing has become one of the important topic of interest in research. Spinel ferrites have been found to be useful as gas sensors for sensing of different gases such as hydrogen sulfide (H_2S), carbon dioxide gas (CO_2), carbon monoxide (CO) *etc.* [122]. The dynamic response is a parameter used to characterize the sensing characteristics of a sensor device. Abu-Hani *et al.* have described that the zinc and copper based ferrite have shown significant sensitivity towards the detection of hydrogen sulfide gas [123]. The zinc ferrites have shown good response towards the detection of carbon dioxide and liquefied petroleum gas [124]. The *Ni-Cu-Zn* ferrites can be explored as a chemical sensor for various toxic vapors such as acetone and ethanol [125]. The cerium substituted cobalt ferrite works as an efficient acetone

sensor [126]. Spinel ferrites have also worked as an efficient electrochemical biosensor due to their sensing accuracy and fast analysis time. Fe_3O_4, γ-Fe_2O_3, $MnFe_2O_4$, $CoFe_2O_4$ and $ZnFe_2O_4$ are some of the examples of electrochemical biosensor [127].

1.6.6 Photocatalytic dye degradation

Spinel ferrites are one of the most promising photocatalyst for the degradation of toxic dyes [128]. Spinel photocatalysts use light energy to carry out the oxidation and reduction reaction mechanism. The light provides energy which excites electron from the valence to conduction band generating a hole with creation of electron hole pairs. When this reaction mechanism proceeds in aqueous solution the hydroxide and water ions react to form hydroxyl radicals which are the primary source of oxidizing agents in dye degradation process [128]. The most important advantage of using spinel ferrites for dye degradation is that they can be reused because they are magnetically separable. In spinel structure there are large number of catalytic reaction sites available which also helps in the enhancement of dye degradation [129]. Spinel ferrites have been used for removal of many toxic dyes like bromophenol blue, methyl orange, methylene blue, rhodamine B, phenol red, eosin yellow *etc.* [129]. The degradation of methylene blue using various $CuFe_2O_4$, $NiFe_2O_4$, $ZnFe_2O_4$ and $CoFe_2O_4$ ferrite photocatalysts has been studied. The maximum dye degradation efficiency has been obtained for $CuFe_2O_4$ ferrite followed by $ZnFe_2O_4$, $NiFe_2O_4$ and $CoFe_2O_4$ ferrites [130]. Lassoued *et al.* have obtained the high dye degradation efficiency for nickel ferrite nanoparticles against methyl orange [114].

1.6.7 Biomedical applications

Spinel ferrite nanoparticles have shown enormous potential for different biomedical applications like magnetic hyperthermia, contrast enhancement, magnetic resonance imaging, tissue repair treatment, targeted and magnetically controlled drug delivery, magnetic carriers in bio-screening *etc.* [127]. The magnetic hyperthermia treatment has attracted the attention as a safe technique for cancer therapy, it includes injection of ferromagnetic / ferrimagnetic nanoparticles into the tumor tissue followed by the irradiation using an alternating applied magnetic field [131]. Jadhav *et al.* have observed the $MnZnFe_2O_4$ ferrite nanoparticles to show the properties necessary for hyperthermia applications [132].The spinel ferrite based nanoparticles has been used clinically as

a T_2 contrast agents since 1990. Ahmad *et al.* have reported that the silica coated manganese nanoparticles act as efficient T_2 contrast agent [133]. The cobalt ferrite based nano-composite can be utilized as an efficient drug delivery system [134].

1.6.8 Other applications

There are other applications of ferrites which include magnetostrictive transducers, delay lines and copier powders. In magnetostrictive transducer applications the high value of magnetostriction is required. Cobalt added to nickel ferrite have high magnetostriction which make them potential candidate in magnetostrictive transducer applications [13]. The magnetic properties of ferrites help to get rid of the carrier powder from the rotating drum.

1.7 Motive and motif of the present work

Spinel ferrites are the materials of present research on account of the interesting magnetic and electrical behaviour. Spinel ferrites are mainly useful in memory storage, microwave device, electrode material, photocatalytic dye degradation, sensing and biomedical applications. There are various spinel ferrite systems such as nickel ferrite, cobalt ferrite, zinc ferrite, manganese-zinc ferrite, magnesium-zinc ferrite *etc* [22, 53, 32, 60, 47, 31]. Among various spinel ferrites, Magnesium-Zinc (*Mg-Zn*) ferrite is an important system due to its remarkable magnetic and electrical properties [75, 76]. Several compositions of *Mg-Zn* ferrites have been studied and investigated for their properties but, $Mg_{0.5}Zn_{0.5}Fe_2O_4$ shows high saturation magnetization, soft magnetic nature, low dielectric losses and enhanced sensing characteristics [89, 91, 93, 97]. Therefore, $Mg_{0.5}Zn_{0.5}Fe_2O_4$ has been chosen for the present study. The preference of Mg^{2+}, Zn^{2+} and Fe^{3+} metal ions for crystallographic lattice sites in $Mg_{0.5}Zn_{0.5}Fe_2O_4$ creates the antiparallel alignment of ferromagnetic Fe^{3+} metal ions observed in case of ferrimagnetism. But, the presence of diamagnetic Mg^{2+} ($0\mu B$) and Zn^{2+} ($0\mu B$) ions at B and A sites respectively in *Mg-Zn* ferrite, reduce the magnitude of most significant A-B super-exchange interaction which lessens magnetic character. This stresses on the need for the addition of magnetic element which may result in the enhancement of magnetic characteristics.

The magnetic behaviour of spinel ferrites show dependence on the allocation of metal cations in crystallographic sites. The replacement of divalent Zn^{2+} metal ions which have strong preference for tetrahedral lattice sites with magnetic metal ions will create antiparallel alignment of metal

ions enhancing the A-B exchange interaction. The transition metal substitution plays a vital part in the modification of magnetic characteristics [102-104]. *Mg-Zn* spinel ferrite system and its properties are very sensitive to the method of preparation. In present study the co-precipitation method has been used for synthesis because its offers inexpensive experimental set up, non toxic nature and most importantly the availability of different parameters which help in controlling the nucleation and growth of nanoparticles [135]. The divalent Zn^{2+} metal ions have been replaced with transition metal (Co^{2+}, Ni^{2+} *and* Mn^{2+}) to enhance the magnetic characteristic of $Mg_{0.5}Zn_{0.5}Fe_2O_4$ ferrite. The transition metal doped *Mg-Zn* ferrites prepared using co-precipitation path have been characterized for their structural, morphological, elemental and magnetic studies. The structural study has been carried out using X-ray diffraction *(XRD)* and Fourier transform infrared spectroscopy *(FT-IR)*. The morphological and elemental studies have been investigated using Field effect scanning electron microscopy *(FE-SEM*) and Energy dispersive X-ray spectroscopy (*EDS)* respectively. The Vibrating sample magnetometer *(VSM)* has been employed to study the magnetic behaviour.

1.8 Outline of the thesis

The thesis is composed of six chapters

Chapter 1 includes the history of ferrites, classification of ferrites on the basis of their magnetic properties and on the basis of their crystal structure. The various types of spinel ferrite systems, role of transition metal doing in modifying the properties of spinel ferrites and some general applications of spinel ferrites have been presented. The aim of the present work and outline of the thesis has been included in the present chapter.

Chapter 2 describes the various methods (sol-gel, micro-emulsion, co-precipitation *etc*.) utilized for the synthesis of spinel ferrites. The co-precipitation method utilized for the synthesis of transition metal doped Magnesium-Zinc ferrites have been discussed in detail. The advantages of co-precipitation method have also been discussed. The experimental techniques (*XRD*, *FE-SEM*, *VSM etc*.) utilized for the characterization of various physical properties have been described in detail.

Chapter 3 explains the structural, morphological and elemental characteristics of transition metal doped Magnesium-Zinc ferrites and presents their analysis. *XRD* and *FT-IR* techniques have been

employed for the investigation of structural properties. *FE-SEM* and *EDS* characterization techniques have been used to investigate the morphological and elemental properties respectively. The structural parameters calculated with the help of *XRD* data have also been analyzed.

Chapter 4 explains the proposed cation distribution for transition metal doped Magnesium-Zinc ferrites. The choice of cations for crystallographic lattice sites and experimental *XRD* results have been taken into account to propose the cation distribution. Various structural parameters calculated with the help of proposed cation distribution have been described.

Chapter 5 describes the change in magnetic properties of Magnesium-Zinc ferrites on transition metal ion substitution. The nature of magnetic exchange interactions investigated with the help of proposed cation distribution using Yafet –Kittel model have been included in the present chapter.

Chapter 6 presents the summary of the present work. The future scope of the present work has also been included.

CHAPTER 2

EXPERIMENTAL AND CHARACTERIZATION TECHNIQUES

This chapter gives the description of synthesis route utilized for preparation of ferrite nano-particles and the experimental techniques utilized for their characterization. The co-precipitation technique, its advantages and reaction mechanism for the synthesis of transition metal ion ($M = Co^{2+}, Ni^{2+}$ *and* Mn^{2+}) doped *Mg-Zn* ferrites have been discussed. The equations used for the calculation of several experimental parameters have been described.

2.1 Nanoparticles

The science associated with different materials is said to be nano-science when these materials have at least one dimension in nano-meter size. Nano-science includes different types of materials such as thin films, nano wires and nano-particles *etc.* Nano-particles have all three dimensions in nano size. Due to their small size, nano-materials exhibit different properties in comparison to their corresponding bulk counter-parts, which make them a vital candidate in various applications. The reduction in particle size leads to increase in surface to volume ratio and also modifies the electronic states due to quantum confinement effect. The increment in surface/volume ratio is an important factor as the surface atoms are different to inner atoms. This is because the surface atoms have less coordination with non saturated bonds and canted spins [1]. In recent years, several researchers have studied spinel nano-ferrites due to their interesting chemical and physical properties [2-4]. The interesting–properties of nano-ferrites make them potential candidate in several technologically important applications such as magnetic recording, telecommunication systems, transformer cores, microwave devices, magnetic fluids, gas sensors, photo-magnetic materials, catalysts, targeted drug delivery, spintronics, bio-sensing *etc.* [5-8]. The *Mn-Mg* spinel nano-particles have high electrical resistivity and ten times smaller *tan* δ losses than their bulk counterparts, which make them beneficial in applications involving high frequencies [9]. The $CoCrFeO_4$ ferrite nano-particles have large value of coercivity in comparison to their bulk counterpart [10]. The interesting properties and diverse applications of ferrite nanoparticles in technological industry have raised the interest of scientific community towards their synthesis.

2.2 Synthesis techniques

The properties of ferrite nano-particles depend on the distribution of cations in lattice sites and their particle size, which are very sensitive to synthesis method [11]. So, to tailor the properties

of ferrite nano-particles the selection of synthesis method is crucial. There are several physical and chemical routes available for the preparation of ferrite nano-particles such as ball milling, ion beam, sputtering, auto-combustion, sol-gel, hydrothermal, co-precipitation, micro-emulsion *etc.* The few of the synthesis methods have been discussed below.

2.2.1 Physical methods

2.2.1.1 Ball milling

Ball milling is an established method for nano-particles synthesis. In this technique, the material suffers from high energy strikes due to ball-to-ball and ball-to-vial wall collisions. The formation of material in nano-crystalline form is due to the regular disintegration and re-welding process of grains [12]. Spinel ferrites synthesized by ball milling method are nano-crystalline in nature, the milling of nano-crystalline ferrites for different time intervals changes the structure of nano-crystalline ferrites from normal spinel to inverse spinel structure [12].

2.2.1.2 Sputtering

In this technique the atoms or ions of very high energy strikes on a solid surface and eject atoms, molecules or clusters and will deposit them on surrounding. It is widely used for the preparation of thin films for microelectronic applications. Sputtering can be divided onto four different classes *i.e* DC, RF, Magnetron and reactive. In DC or direct current sputtering the source is direct current, the sputtering is under high pressure ranging from 1 to 100 m Torr. In DC sputtering the positively charged sputtering gas is accelerated towards the target which is negatively charged. In Radio frequency sputtering the source is alternation current. It can be utilized for all type of materials but mainly employed for dielectric target materials. The magnetron sputtering can work with direct current as well as with radio frequency. In magnetron sputtering the powerful magnets are used to confine the plasma to the area which is nearest to the target. This technique maintains a high deposition rate in comparison to other techniques. Magnetron sputtering can also operate at low pressure conditions. In reactive sputtering the target is sputtered in the environment of a gas or mixture different gases. The gaseous mixture reacts with target leading to a different composition in the form of thin film. In most of the cases the main constituent gas is argon. Several authors have reported for the preparation of ferrite thin

films using sputtering technique [13, 14]. The sputtering technique is known for producing ferrite thin films of controllable thickness and crystalline nature [13].

2.2.2 Chemical methods

2.2.2.1 Sol-gel

Sol-gel method is known for generating solid materials from small molecules. For ferrites synthesis using sol gel method, the aqueous solutions of desired metal salts are precipitated using a suitable base and then further treated to form a colloidal solution. The prepared colloidal solution is concentrated to form a gel and fired for desired ferrite nano-particles [15]. There are several studies in which sol-gel method has been used for the synthesis of pure spinel and nano-crystalline ferrites [16, 17]. The formation of pure spinel ferrite nano-particles having narrow particle size distribution for nickel-zinc ferrites synthesized using sol-gel method have been observed [17].

2.2.2.2 Hydrothermal

Hydrothermal synthesis is basically a heterogeneous reaction of aqueous solvents or minerals under elevated temperature and pressure condition in an autoclave to re-crystallize and dissolve the materials which are insoluble under normal conditions of temperature and pressure [18]. The hydrothermal method is a popular technique for the formation of ferrite nanoparticles with highly crystalline nature and narrow particle size distribution [19]. Köseoğlu *et al.* [20] have reported the formation of pure spinel and crystalline nano-particles of manganese doped ferrites synthesized by hydrothermal method.

2.2.2.3 Polyol process

In Polyol process the Polyol word refers to diol, like ethylene glycol and its derivatives. The isomers of propanediol, butanediol, pentanediol, etc. also refer to Polyol. Due to the presence of *OH* groups, the Polyol have high reducing and coordinating properties which help in the preparation and controlling the shape and size of nanoparticles. Highly crystalline nanosphere clusters of cobalt ferrites have been synthesized using polyol process [21].

2.2.2.4 Micro-emulsion

Micro-emulsion is a clear, thermodynamically stable and isotropic liquid. Micro-emulsions are the mixtures of oil, water and surfactant. Micro-emulsion is generally of two types, *i.e.* water in

oil and oil in water micro-emulsions. It depends on ratio of the components used and hydrophilic–lipophilic balance (HLB) value of the used surfactant [22]. In both types of micro-emulsions, the dispersed phase offers close surroundings for the preparation of nano-particles. The dispersed phase has mono-dispersed droplets in the range 2 to 100 *nm* [23]. Pulišová *et al.* [24] have reported that the nickel and cobalt ferrites synthesized by micro-emulsion route are purely spinel and crystalline in nature. Zeng *et al.* [25] have obtained high crystallinity and uniform pore size distribution for nickel based ferrite prepared by micro-emulsion route.

2.2.2.5 Co-precipitation

Co-precipitation is one of the most frequently routes used route for the synthesis of ferrite nano-particles. Several authors have reported that the ferrites synthesized by the co-precipitation method are purely spinel and highly crystalline in nature [26-27]. Erfaninia *et al.* [28] reported that the *Zn*-ferrite synthesized using co-precipitation route is highly crystalline in nature and does not have any single impurity. In this technique, the aqueous solutions of metal salts taken in desired molar ratio are mixed with suitable precipitating agent followed by stirring and agitation of prepared aqueous solution. This results in the formation of precipitates. The precipitating agent plays a crucial role in deciding the pH value, precipitation and growth of ferrite nano-particles [23, 29]. Co-precipitation route has several advantages which makes it advantageous over other synthesis techniques. The following are the advantages of co-precipitation route.

(i) Co-precipitation technique is known for the production of homogenous nano-particles having narrow particle size distribution [26, 30].

(ii) Co-precipitation is a cost effective technique, it does not require any sophisticated instrumentation for the reaction process.

(iii) It does not require high reaction temperatures and hazardous solvents.

(iv) It does not require more time to complete reaction process and easily applicable to industrial level production.

(v) In co-precipitation method there are different parameters such as pH value, synthesis temperature and stirring rate which provides a choice to control the growth and formation of nano-particles.

2.3 Reaction mechanism

The co-precipitation route has been used in the present work for the synthesis of transition metal (*M*) ions doped ($M = Co^{2+}, Ni^{2+}$ *and* Mn^{2+}) doped *Mg-Zn* ferrites. In co-precipitation technique, the chemical co-precipitation of metal salts using suitable base results in the formation of precipitates that contain all components which have been mixed at the ionic level. The following is the proposed chemical equation for the synthesis of $Mg_{0.5}Zn_{0.5-x}M_xFe_2O_4$ (x = 0.125, 0.250, 0.375, 0.500) ferrites:

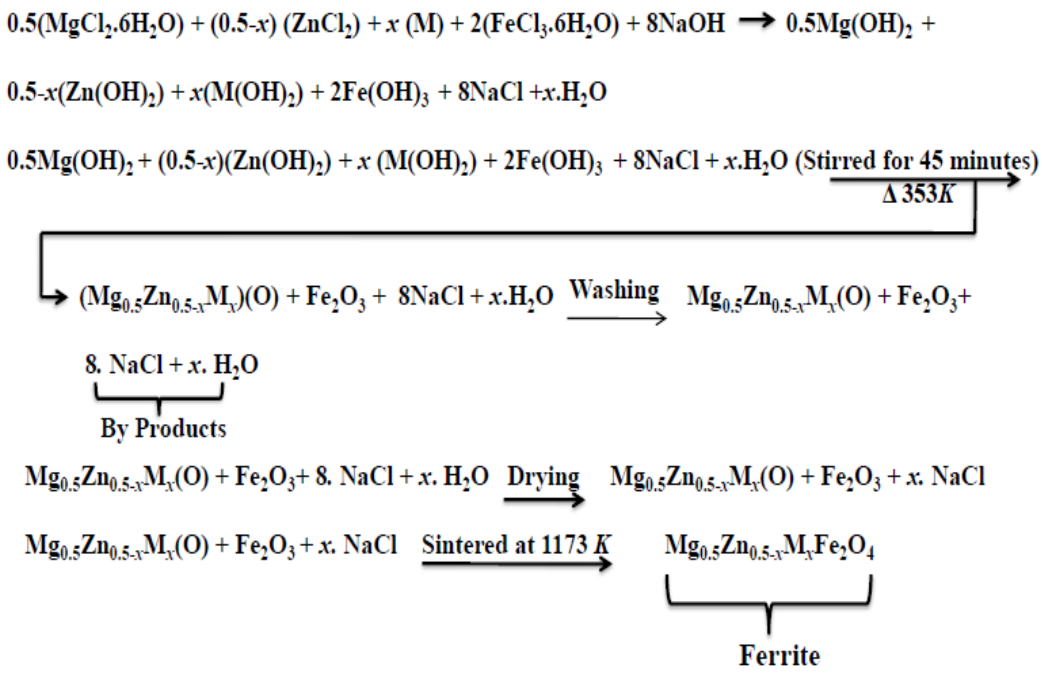

The reaction mechanism and chemicals used for the above synthesis have been discussed below:

$MgCl_2.6H_2O$ the Magnesium (II) chloride hexahydrate, ≥ 98%, $ZnCl_2$ the Zinc (II) chloride ≥ 98%, $FeCl_3.6H_2O$ the Iron (III) chloride hexahydrate ≥ 99%), $MnCl_2.4H_2O$ the Manganese (II) chloride tetrahydrate ≥ 99%) and *NaOH* the sodium hydroxide ≥ 98% purchased from Merck India and $CoCl_2.6H_2O$ the Cobalt (II) chloride hexahydrate ≥ 99%) and $NiCl_2.6H_2O$ the Nickel (II) chloride hexahydrate 98% from Alfa Aesar have been utilized as procured. The stoichiometric amount of salts ($MgCl_2.6H_2O$, $ZnCl_2$, $FeCl_3.6H_2O$, $M = CoCl_2.6H_2O$, $NiCl_2.6H_2O$ and $MnCl_2.4H_2O$), according to their required molar ratio (1:2 of *Mg Zn M: Fe*) in double distilled water (100 ml) have been mixed to synthesize the solution. This is followed by stirring

till the solution becomes clear. The prepared solution has been added with precipitating agent *NaOH* and then stirred for 45 minutes at 353 *K*. The pH value has been maintained in the range 11-12. After the completion of reaction, the precipitates settled down. The double distilled water have been utilized to wash the precipitates. This treatment makes them free from sodium and chloride ions. Oven has been used to dry the precipitates for 12 hrs at 373 *K*. The dried precipitates after collection have been powdered with the help of granite mortar pestle. An automatic muffle furnace has been used to sinter the powdered precipitates at 1173 *K* for 3 hours. There is formation of pure spinel phase for *Mg-Zn* ferrites when sintered at 1173 *K* [31]. Figure 2.1 shows the flow chart for the synthesis of $Mg_{0.5}Zn_{0.5-x}M_xFe_2O_4$ ferrites.

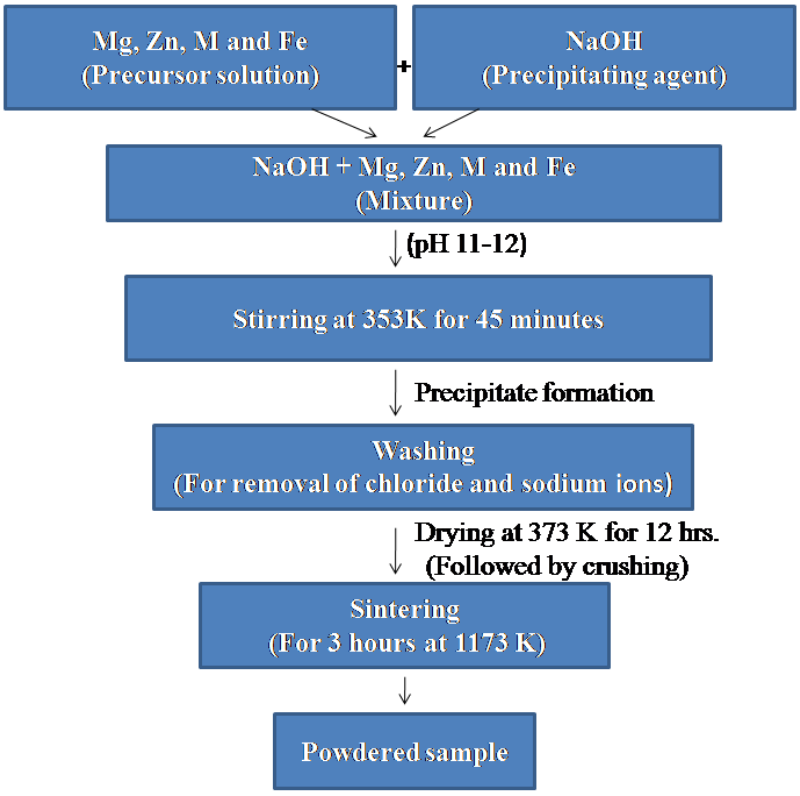

Figure 2.1: Flow chart for the synthesis of $Mg_{0.5}Zn_{0.5-x}M_xFe_2O_4$ ferrites

2.4 Characterization techniques

The structural, elemental, morphological, magnetic characteristics of prepared transition metal (*M*) ions doped ferrite samples have been studied. *XRD* (X-ray diffraction) and *FT-IR* (Fourier transform infrared spectroscopy) have been utilized for the structural confirmation of prepared

samples. Elemental and morphological investigation of prepared samples have been carried out using *EDS* (Energy dispersive X-ray spectroscopy) and *FE-SEM* (Field emission scanning electron microscopy) respectively. To investigate the magnetic characteristics of prepared samples the *VSM* (Vibrating sample magnetometer) has been used. The experimental tools used for the investigation of above mentioned properties have been described in detail in the following subsection.

2.4.1 X-ray diffraction (*XRD*)

XRD is a technique employed to identify crystallographic structure of material samples. The diffraction pattern observed in X-ray diffraction technique gives information about the structural properties of materials. It works on the principle of constructive interference of X-rays diffracted from a crystalline sample. When X-rays fall on sample it gets diffracted in all possible directions and an intense diffraction pattern as a result of constructive interference from various planes is detected by the detector of X-ray diffractometer. The condition of X-ray diffraction according to Bragg's law is [32]

$$2d_{hkl}\sin\theta = n\lambda \tag{2.1}$$

where n = 1, 2, 3…., d is inter-planar distance between adjacent planes and h, k, l are Miller indices relevant to the respective planes, θ is the diffraction angle and λ is the X-ray wavelength . The schematic representation of Bragg's diffraction for a set of lattice planes is displayed in Figure 2.2.

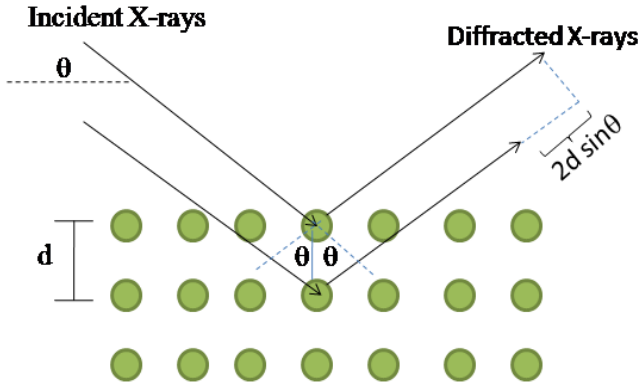

Figure 2.2: Schematic diagram of Bragg's diffraction for a set of lattice planes

The diffraction of X-rays due to crystallites in sample that are randomly orientated get detected by scanning across diffraction angle range (2θ). In the present work Shimadzu X-ray diffractometer (XRD 6000, JIIT Noida) has been employed for the *XRD* studies. *Cu* K_α radiation with wavelength of 1.5406 *Å* has been used in the X-ray diffractometer. The angular range of 10°-80° at a scan speed of 2°/minute has been used to acquire data at operating parameters 40 kV and 30 mA.

Figure 2.3: Shimadzu (*XRD* 6000) X-Ray diffractometer employed for *XRD* studies

The following equations have been used to calculate some structural parameters using experimental X-ray diffraction data:

(i) Crystallite size (*D*)

Scherrer's equation has been employed to calculate the crystallite size for prepared samples:

$$D = 0.9\lambda / \beta \cos\theta \tag{2.2}$$

where β represents the FWHM (full width at half maximum), λ represents the X-ray wavelength and θ represents the Bragg's diffraction angle.

(ii) Inter-planar spacing (d_{hkl})

Bragg's equation has been used to calculate the inter-planar spacing.

$$d_{hkl} = n\lambda / 2\sin\theta \tag{2.3}$$

where *h, k, l* correspond to the miller indices of the respective planes.

(iii) Lattice constant (*a*)

The lattice constant for the samples has been calculated using equation:

$$a = d_{hkl}(h^2 + k^2 + l^2)^{1/2} \tag{2.4}$$

(iv) Packing factor (*p*)

It signifies the existence of atomic layers in crystalline domains. The value of *p* the packing factor for prepared samples has been determined using equation [33]:

$$p = D / d \tag{2.5}$$

(v) Strain (ε_u) (Compressive and Tensile)

The presence of strain type has been determined using equation [34]:

$$\varepsilon_u = c(d_f - d_i) / d_i = c\Delta d / d_i \tag{2.6}$$

where *c* is a constant that depends on the material, Δd represents inter-planar spacing difference between pure (d_i) and doped samples (d_f).

2.4.2 Energy dispersive X-ray spectroscopy (*EDS*)

The stoichiometric investigation of prepared samples has been carried out using *EDS*. It is a qualitative and quantitative technique used for the elemental analysis. It also provides information about the chemical composition. In this technique the beam of highly energetic electrons is allowed to fall on the sample resulting in emission of X-rays. The nature of the X-ray emitted from the sample gives information about the elements and their relative atomic % present in the sample. The X-rays energy emitted is equivalent to characteristic difference of energy b/w two shells and depends on the constituent element atomic structure [34]. Figure 2.4 shows the schematic of emission of X-rays.

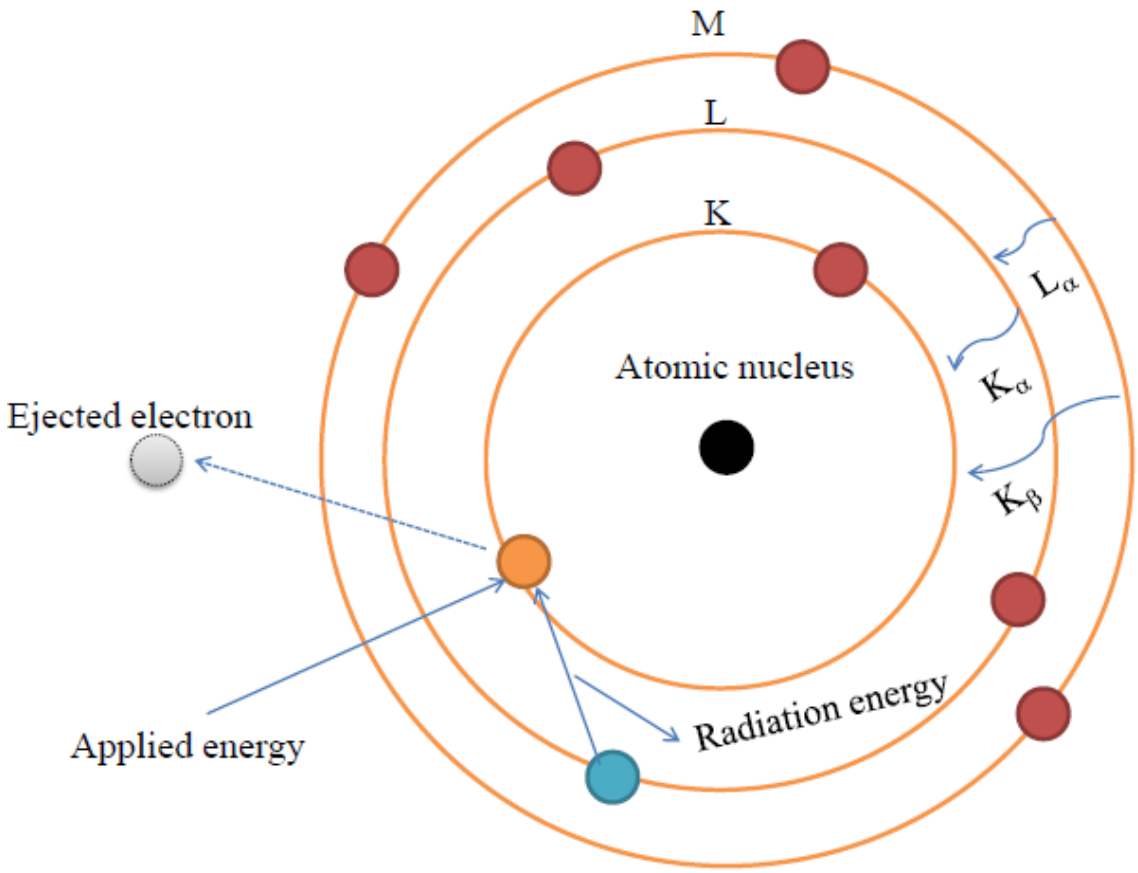

Figure 2.4: Schematic of emission of X-rays

The energy of X-rays emitted from sample is measured by *EDS* spectrophotometer. In the present work the elemental characterization has been performed using Oxford Instruments *EDS*, IIT Roorkee. Figure 2.5 shows the schematic diagram of *EDS* spectrophotometer.

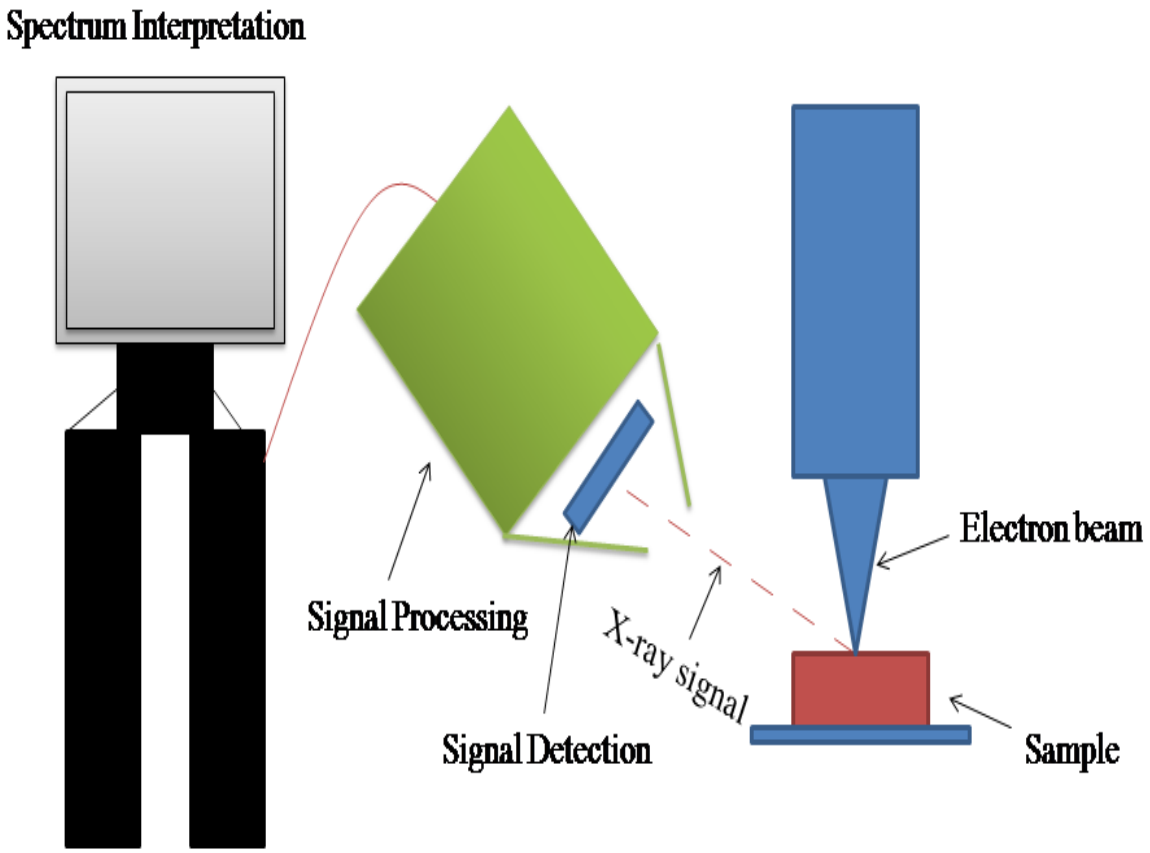

Figure 2.5: Schematic of *EDS* spectrophotometer

2.4.3 Field emission scanning electron microscope (*FE-SEM*)

FE-SEM is a high resolution microscope which employs electrons to investigate the topographic and morphological details of the sample. In *FE-SEM* the electrons are liberated from a source and then accelerated in a high electric field. The accelerated electrons are focused and deflected using lenses to produce a narrow incident beam striking the sample. The secondary electrons are emitted from the sample where the electron beam is incident on the sample. The velocity and angle of the secondary electrons depend on the surface morphology of the sample. The secondary electrons are collected by the detector and generate an electronic signal which is now amplified and transformed to an image visible on the screen. The ray diagram of *FE-SEM* is shown in Figure 2.6.

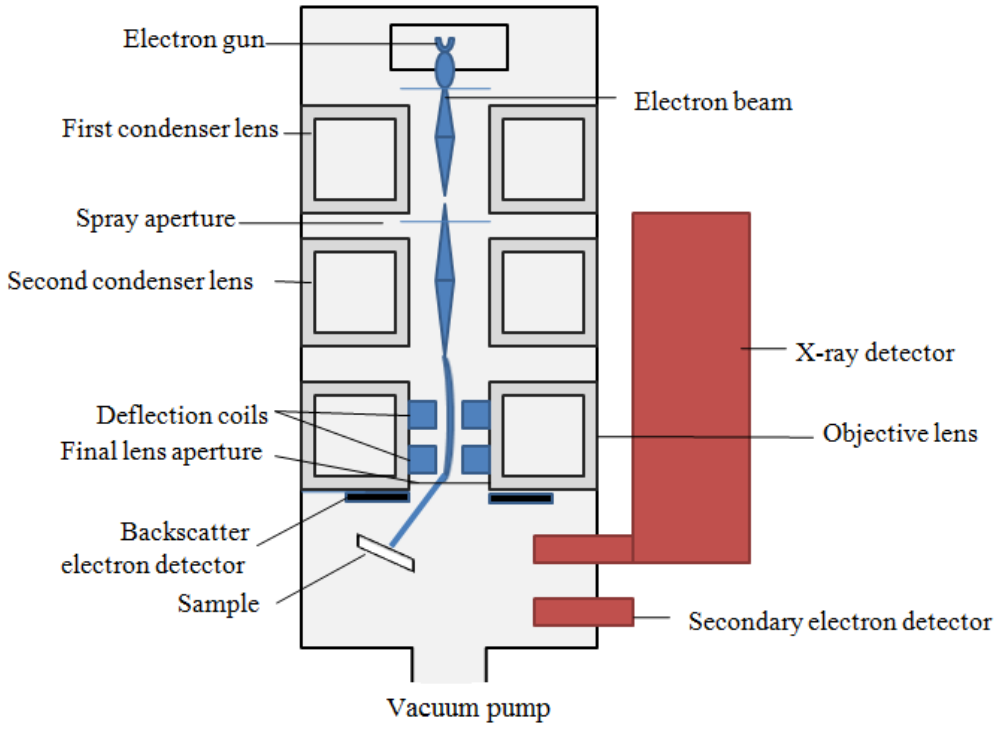

Figure 2.6: Ray diagram of *FE-SEM*

The surface morphology of prepared samples has been investigated using Quanta 200 FEG *FE-SEM*, IIT Roorkee (Figure 2.7), having resolution of less than 2 *nm*. It has magnification of 12X-1000 kX and operated at an accelerating voltage of 200 V -30 kV.

Figure 2.7: Quanta 200 *FEG* Field effect scanning electron microscope

2.4.4 Fourier transform infrared spectroscopy (*FT-IR*)

FT-IR is a sensitive method related with the interaction of infrared radiation with matter. It works on the principle that the molecular bonds vibrate at different frequencies depending on the molecules and bond type. Every single bond vibrates at definite frequency which corresponds to characteristic of molecule and the functional groups present in the molecule. In case of spinel ferrites the *FT-IR* spectroscopy provides an insight regarding the metal ion positions in the lattice sites utilizing the various vibrational bands in the crystal [16]. Spinel ferrites have characteristic infrared spectra. The formation of ferrite spinel structure is indicated from the frequency bands present in the range *400 cm^{-1}-600 cm^{-1}* [16].

Michelson interferometer, radiation source, radiation detector and samples holder are the major parts of a *FT-IR* spectrophotometer. Figure 2.8 shows the graphic of *FT-IR* spectrophotometer.

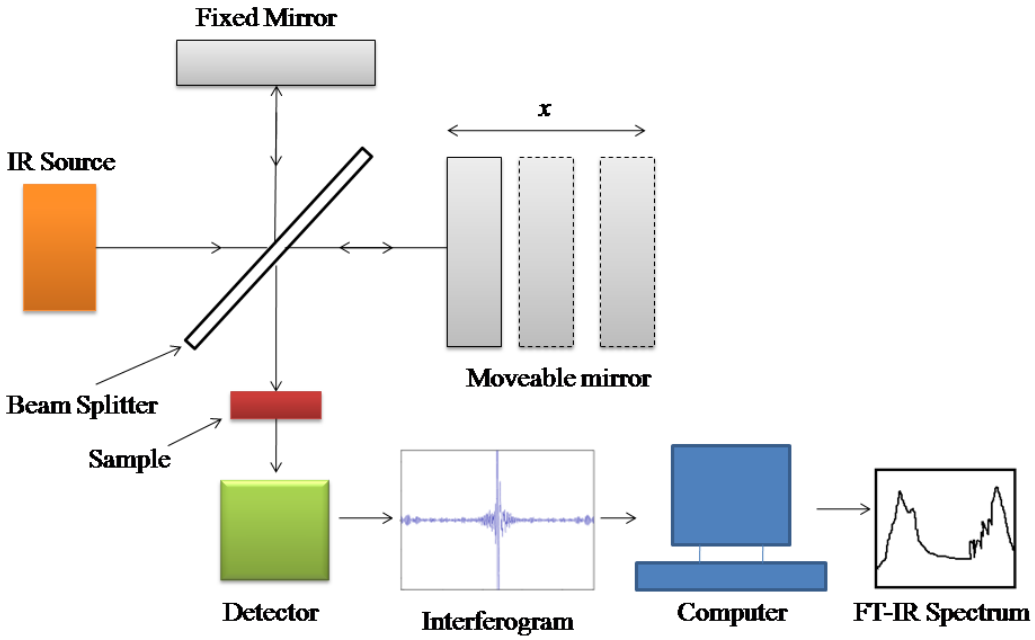

Figure 2.8: Graphic of *FT-IR* spectrophotometer

The *FT-IR* measurements have been carried out from *400 cm^{-1} -1000 cm^{-1}* using Perkin Elmer spectrophotometer model-65 (SAIF Panjab University), by preparing a pellet of powdered sample using solid *KBr*. The spectral resolution was *1 cm^{-1}*. The silicon carbide element and deuterated triglycine sulfate (DTGS) has been used as infrared source and radiation detector

respectively in Perkin Elmer 65 *FT-IR* spectrophotometer. Figure 2.9 displays the *FT-IR* spectrophotometer instrument.

Figure 2.9: *FT-IR* spectrophotometer

2.4.5 Vibrating sample magnetometer (*VSM*)

VSM is the most common experimental tool to investigate the magnetic behavior of a material. This magnetic behavior in case of spinel ferrites can be investigated in terms of different magnetic parameters like coercivity (H_c), saturation magnetization (M_s) and retentivity (M_r) using *M-H* hysteresis loop obtained from *VSM*. It works on Faraday's law of electromagnetic induction. The sample is placed in a stable magnetic field in *VSM*. This magnetic field magnetizes the sample by orientation of its domains along its direction. The stronger the stable magnetic field the more is the magnetization. A magnetic moment is induced in the sample and generates a stray magnetic field around the sample. On vibration of the sample the stray magnetic field shows time dependent alteration which is perceived by pick up coils. This alteration induces an electric field to generate an induced current. The magnitude of induced current is equivalent to the magnetization induced in the sample. This induced current is

amplified by a transimpedance and lock-in amplifier respectively in the *VSM*. Figure 2.10 shows the schematic diagram of *VSM*. The magnetic characteristics of material are estimated by plotting a graph (M-H curve) between magnetization and applied field.

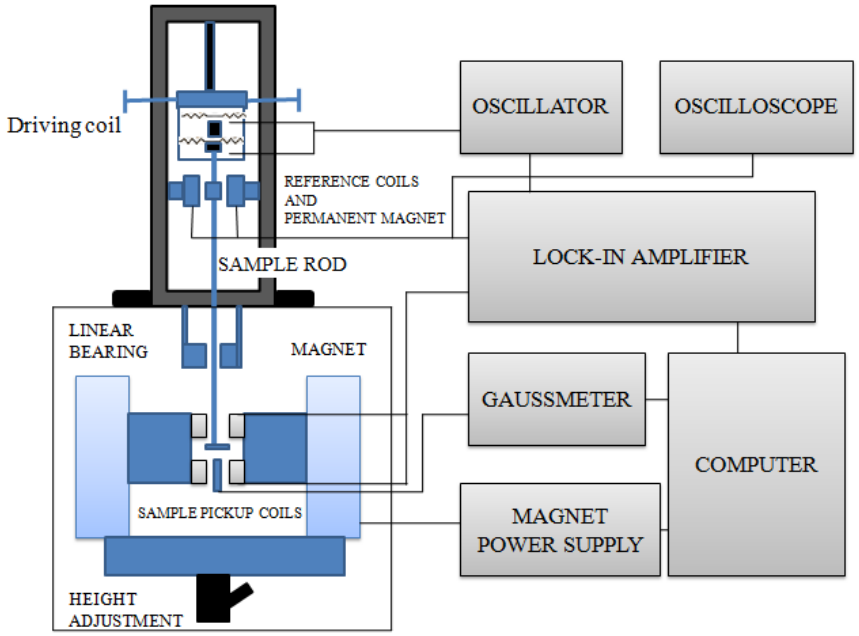

Figure 2.10: Schematic representation of *VSM*

PAR-155 Quantum design *VSM*, (IIT Roorkee) has been utilized for the magnetic characterization. These measurements have been taken from *-10 kOe to +10 kOe* at room temperature.

Figure 2.11: Experimental set up of PAR-155 Vibrating sample magnetometer

The following relations have been utilized for the estimation of various parameters using experimental data obtained with the help of *VSM*.

(i) Magneto-crystalline anisotropy constant (K_a)

K_a is the inherent property of magnetic materials. It decides the coercive nature of magnetic materials. It has been calculated using relation [16]:

$$K_a = (H_c \times M_s)/0.98 \tag{2.7}$$

where K_a is the anisotropy constant and M_s is the saturation magnetization.

(ii) Magnetic moment (η_B)

The value of η_B has been calculated using equation [16]:

$$\eta_B = (M_w \times M_s)/5585 \tag{2.8}$$

here M_s represents the saturation magnetization and M_w represents the molecular weight of the sample.

(iii) Remanence ratio (*R*)

The remanence ratio gives information about the isotropic and anisotropic nature of the samples. The value of *R* has been evaluated using relation [36]:

$$R = M_r / M_s \tag{2.9}$$

where M_r is the retentivity and M_s is the saturation magnetization.

(iv) Yafet-Kittel (*Y-K*) angles

Y-K angles provide insight about the type of magnetic ordering and spin arrangement in ferrites. These angles have been obtained employing the relation [16]:

$$\eta_B = M_B \cos\alpha_{YK} - M_A \tag{2.10}$$

where M_B and M_A are values of magnetic moment at octahedral and tetrahedral sites respectively and $\alpha_{Y\text{-}K}$ is Yafet-Kittel angle.

CHAPTER 3*

STRUCTURAL, MORPHOLOGICAL AND ELEMENTAL STUDIES OF TRANSITION METAL DOPED *Mg-Zn* FERRITES

* **Rohit Sharma,** P. Thakur , M. Kumar , N. Thakur, N. S. Negi, P. Sharma, V. Sharma, Improvement in magnetic behaviour of cobalt doped magnesium-zinc nano-ferrites via co-precipitation route, **Journal of Alloys and Compounds**, 684, 569-581 (2016)

Rohit Sharma, P. Thakur, P. Sharma, V. Sharma, Ferrimagnetic Ni^{2+} doped Mg-Zn spinel ferrite nanoparticles for high density information storage, **Journal of Alloys and Compounds**, 704, 7-17 (2017)

Rohit Sharma, P. Thakur , M. Kumar, P. B. Barman, P. Sharma, V. Sharma , Enhancement in A-B super-exchange interaction with Mn^{2+} substitution in *Mg-Zn* ferrites as a heating source in hyperthermia applications, **Ceramics International**, 43,13661-13669 (2017)

This chapter includes the structural, morphological and elemental studies of transition metal ($M = Co^{2}$, Ni^{2+} and Mn^{2+}) doped *Mg-Zn* ferrites. The effect of transition metal (*M*) doping on these properties of *Mg-Zn* ferrites has been discussed. Several structural parameters calculated using experimental X-ray diffraction data are also described.

3.1 Introduction

Ferrites have excellent magnetic and electrical properties [1] making them appropriate for different functions like as high density storage of information, telecommunication systems, transformer cores, antenna rods, ferro-fluids, ac motors, generators, microwave devices, recording equipments, magnetically guided drug delivery and gas sensors [2-6]. To explore and utilize ferrites for different technological applications, the evaluation of their various physical properties is essential.

The properties of nanomaterials are influenced by their structure and morphology [7]. In the case of ferrite nanoparticles, also the structure and morphology plays an important role in deciding other physical properties [8] which are essential for technological applications of ferrite nanoparticles. The grain size and surface morphology of *Ni-Zn* ferrites are important factors to determine the magnetic and dielectric properties of ferrite nanoparticles [9]. The change in structural parameters of ferrite nanoparticles is responsible for modifying other physical characteristics [10]. The change in morphology leads to change in magnetic characteristics of copper doped *Mg-Zn* ferrites [11]. The impact of structural parameters and morphology of ferrite nanoparticles on other physical properties makes it necessary to investigate their structural and morphological properties.

In the present study the transition metal ($M = Co^{2+}$, Ni^{2+} *and* Mn^{2+}) doped *Mg-Zn* ferrite belongs to spinel ferrite family. *Mg-Zn* ferrite crystallizes into mixed spinel ferrite structure [12]. The crystallization of ferrites into a particular type of structure depends on the distribution of divalent and trivalent metal cations in lattice sites [13]. Co^{2+} and Ni^{2+} metal ions have preference to lodge in B crystallographic sites whereas Mn^{2+} ions prefer to occupy A crystallographic sites [14, 15]. With the substitution of transition metals in Magnesium-Zinc ferrites the metal cation distribution in crystallographic lattice sites gets modified which leads to subsequent changes in various structural parameters and morphology. Several authors have reported that the substitution

of transition metals lead to variation in structural parameters and morphology of spinel ferrites [14-17]. Abraham *et al.* reported that the substitution of Co^{2+} metal ions have significant impact on the structural parameters of magnesium ferrite [18]. Prasad *et al.* have reported that the Ni^{2+} substitution changes structural parameters of *Co-Zn* ferrites and the change in structural parameters also make an impact on various other physical properties [19]. Dolla *et al.* have investigated the Mn^{2+} doped ferrites, the Mn^{2+} substitution changes the shape of nanoparticles from cubical to sphere like structures and also modifies several structural parameters [20]. The X-ray diffraction and *FE-SEM* technique are the useful tools to get information about the structure and morphology of spinel ferrites respectively. Apart from X-ray diffraction, the *FTIR* spectroscopy also provides a suitable mean for structural analysis of spinel ferrites because spinel ferrites have characteristic infrared spectra [10]. Rashmi *et al.* have reported the existence of prominent frequency bands around $400\ cm^{-1}$ and $600\ cm^{-1}$ for samarium doped zinc spinel ferrite [21]. The presence of frequency bands around $400\ cm^{-1}$ and $600\ cm^{-1}$ confirm the formation of spinel structure of ferrites.

There are numerous reports about the structural, morphological and elemental properties of Magnesium-Zinc ferrites [22, 23]. But there are few reports available on structural, morphological and elemental properties of transition metal ($M = Co^{2}$, Ni^{2+} and Mn^{2+}) ions doped *Mg-Zn* ferrites. In the present chapter the calculation of various structural parameters such as crystallite size (D), lattice constant (a), inter-planar spacing (d) and strain (ε_u) *etc.* have also been included.

3.2 Experimental details

The transition metal (M) ions doped *Mg-Zn* ferrites have been prepared employing co-precipitation route. The detailed description of synthesis process has been given in section 2.3 of chapter 2. The structural characterization of prepared powdered samples has been carried out using Shimadzu (*XRD* 6000) diffractometer. The data has been acquired in the angular range of 10°-80° at a scan speed of 2 degree per minute. *FT-IR* measurements in the range $400\ cm^{-1}$ to $1000\ cm^{-1}$ have been performed using Perkin Elmer spectrophotometer model-65. The *KBr* pellet has been utilized for *FT-IR* measurements. The 2 mg powdered sample has been mixed with 200 mg *KBr* to form pellets. The surface morphology of prepared samples has been investigated

using Quanta 200 FEG *FE-SEM*. The elemental characterization of prepared samples has been performed using oxford instruments *EDS.*

3.3 Results and discussion

In this section, the structural, morphological and elemental properties of transition metal (*M*) ions doped *Mg-Zn* ferrites have been described.

3.3.1 Structural, morphological and elemental properties of $Mg_{0.5}Zn_{0.5-x}Co_xFe_2O_4$ ferrites

The structural properties of Co^{2+} doped *Mg-Zn* ferrites have been investigated using *XRD*. Figure 3.1 depicts the *XRD* patterns for Co^{2+} added *Mg-Zn* ferrites.

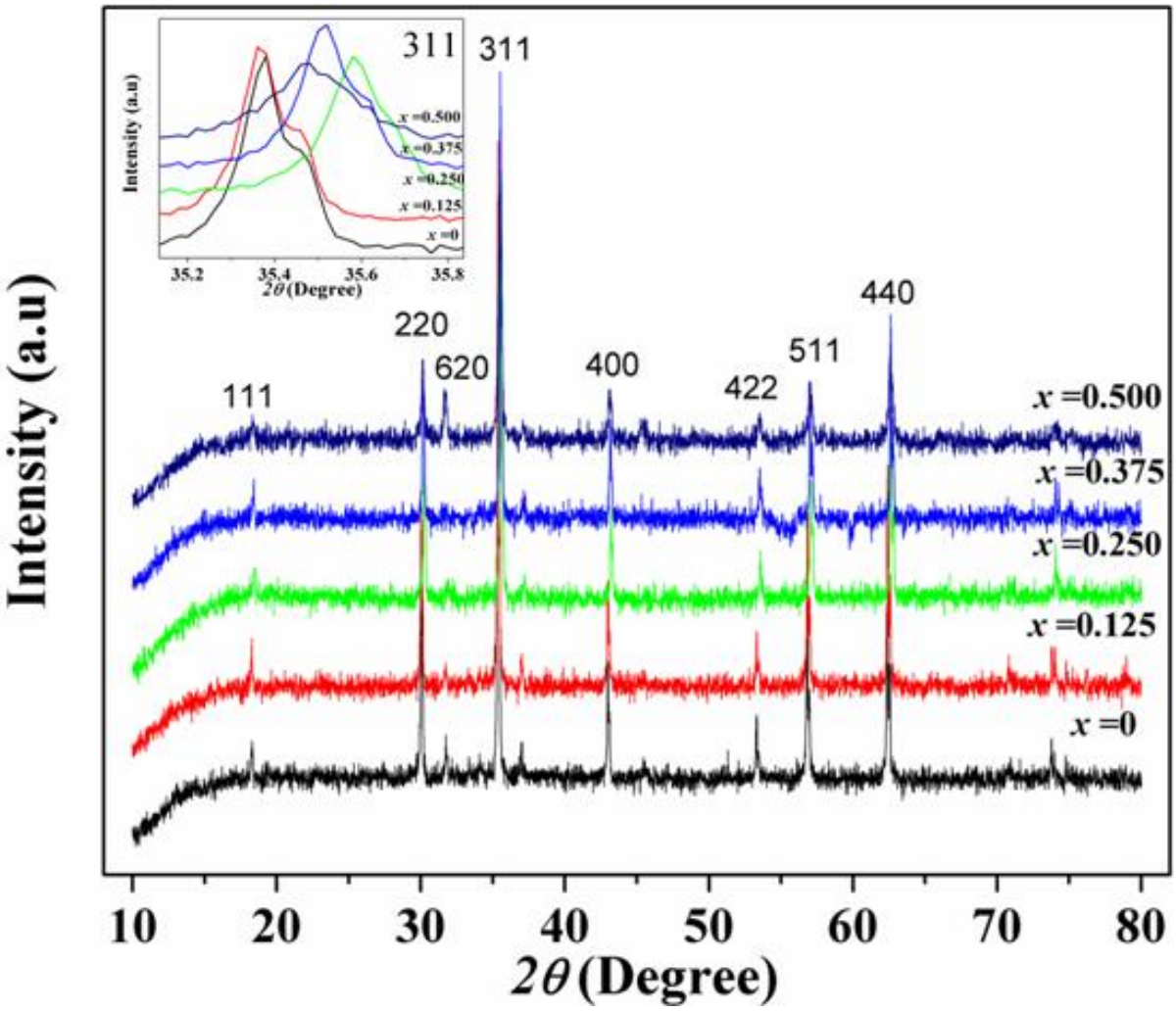

Figure 3.1: *XRD* patterns of Co^{2+} doped *Mg-Zn* ferrites

The peaks indexed as (111), (220), (620), (311), (400), (422), (511) and (440) in Figure 3.1 are the planes characteristic of the face centered cubical (FCC) spinel structure [24]. The presence of these peaks confirm the formation of single phase FCC structure for all prepared samples. The inset in the *XRD* spectra (Figure 3.1) show shift of prominent *XRD* peak (311) with Co^{2+} substitution. The shift of prominent *XRD* peak confirm addition of Co^{2+} ions [25]. To calculate the crystallite size, X-ray diffraction peaks indexed as (111), (220), (311), (422), (511) and (440) have been considered. The average crystallite size has been calculated using equation (2.2). The average crystallite size for $x = 0$, (Table 3.1) is less compared to $x = 0.125$, it is attributed to the migration of Zn^{2+} (0.82 *Å*) metal cations from A lattice sites to B lattice sites and migration of Fe^{3+} (0.67*Å*) metal ions from B lattice sites to A lattice sites. For nano-ferrites, it is possible that some of Zn^{2+} divalent metal ions may shift towards B lattice sites [26]. For $x > 0.125$, the average crystallite size decreases. It is because of the replacement of Zn^{2+} with Co^{2+} because Co^{2+} metal ions has smaller ionic radius (0.74 *Å*) than Zn^{2+} (0.82 *Å*) metal ions [27].

The value of lattice constant for the samples has been computed employing equation (2.4); it shows non-linear behaviour (Table 3.1) with increase in Co^{2+} substitution. The observed non-linear variation in the value of *a* indicates deviation from Vegards's law because of the departure of inverse spinel or normal spinel structure to partially inverted structure [24, 27]. The distribution of divalent metal cations in both tetrahedral and octahedral sites is responsible for partially inverted nature of spinel ferrites. The agglomeration of ferrite nanoparticles at grain boundaries can also be attributed to the nonlinear variation in lattice parameter [28]. The value of d_{hkl} have been computed using equation (2.3) and it ranges between 2.5154 *Å* to 2.5324 *Å*. The non-linear variation with Co^{2+} substitution (Table 3.1) may also attributed to deviation of inverse spinel or normal spinel structure to partially inverted structure.

The packing factor (*p*) for prepared samples has been calculated using equation (2.5). It ranges between 143.36 to 276.97 (Table 3.1). The variation of packing factor is in accordance with crystallite size variation. The sample having least crystallite size has minimum packing factor. The type of strain present in prepared samples has been found using equation (2.6). The value of strain calculated for prepared samples (Table 3.1) indicate that for $x = 0.125$ the tensile strain is present and for all other samples the compressive type of strain has been observed.

Table 3.1: Different structural parameters for Co^{2+} doped *Mg-Zn* ferrites

x	Crystallite size (*D*) nm	Lattice constant (*a*) *Å*	Inter-planar spacing (d_{hkl}) *Å*	Packing factor (*p*)	Strain (ε_u)
0.000	60.97	8.4126	2.5315	240.89	-
0.125	70.13	8.4134	2.5324	276.97	3.95×10^{-4}
0.250	56.49	8.3661	2.5154	224.61	-6.32×10^{-3}
0.375	56.13	8.2588	2.5214	222.64	-3.95×10^{-3}
0.500	36.17	8.3850	2.5230	143.36	-3.16×10^{-3}

To investigate the infrared spectra of prepared samples, the *FT-IR* spectroscopy has been utilized. Figure 3.2 displays *FT-IR* spectra of Co^{2+} added *Mg-Zn* ferrites.

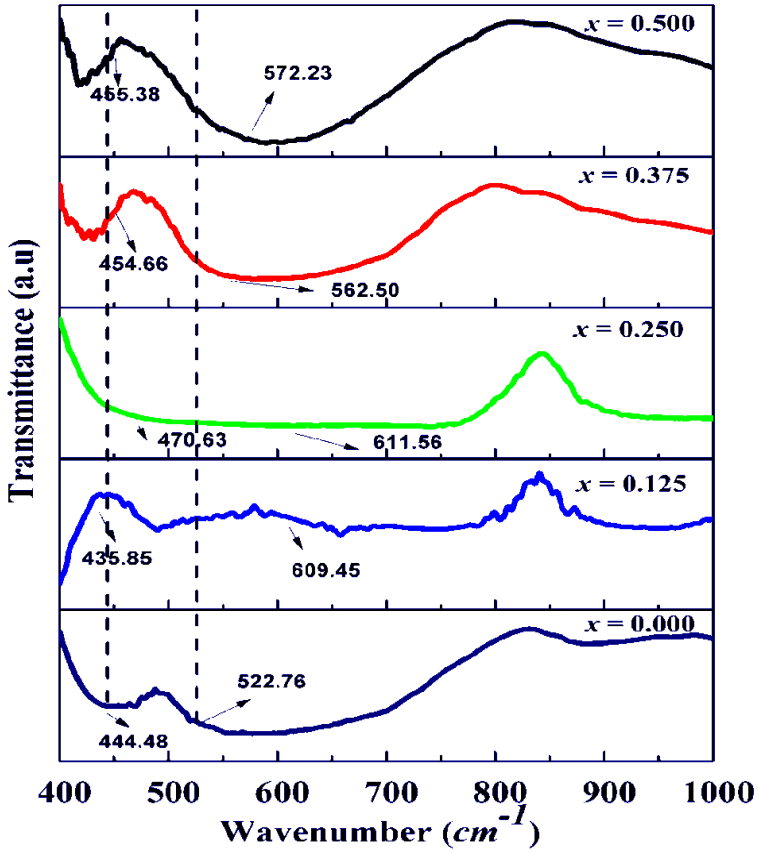

Figure 3.2: *FT-IR* spectra of Co^{2+} doped *Mg-Zn* ferrites

The *FT-IR* spectra shows frequency bands across 400 cm^{-1} and 600 cm^{-1} for all prepared samples. Waldron has been reported that the frequency bands around the wavenumber 400 cm^{-1}

and 600 cm^{-1} represent intrinsic vibration for bond between O^{2-} and the metal cations located at A and B lattice sites [29]. The position of frequency bands is dissimilar due to the difference in Fe^{3+}-O_2^- bond length at A and B sites [24]. The frequency bands observed for samples corroborate the cubical spinel structure. There is change in the location of frequency bands with Co^{2+} substitution which may be due to the alteration in the bond length. The Co^{2+} metal ion substitution migrate Fe^{3+} metal ions from B lattice sites and change bond length. The synthesis method, grain size and ionic radius plays an significant role in deciding the position of vibrational frequency bands [30].

The morphology of samples has been used investigated using *FE-SEM*. Figure 3.3 displays the *FE-SEM* micrographs of Co^{2+} doped *Mg-Zn* ferrites.

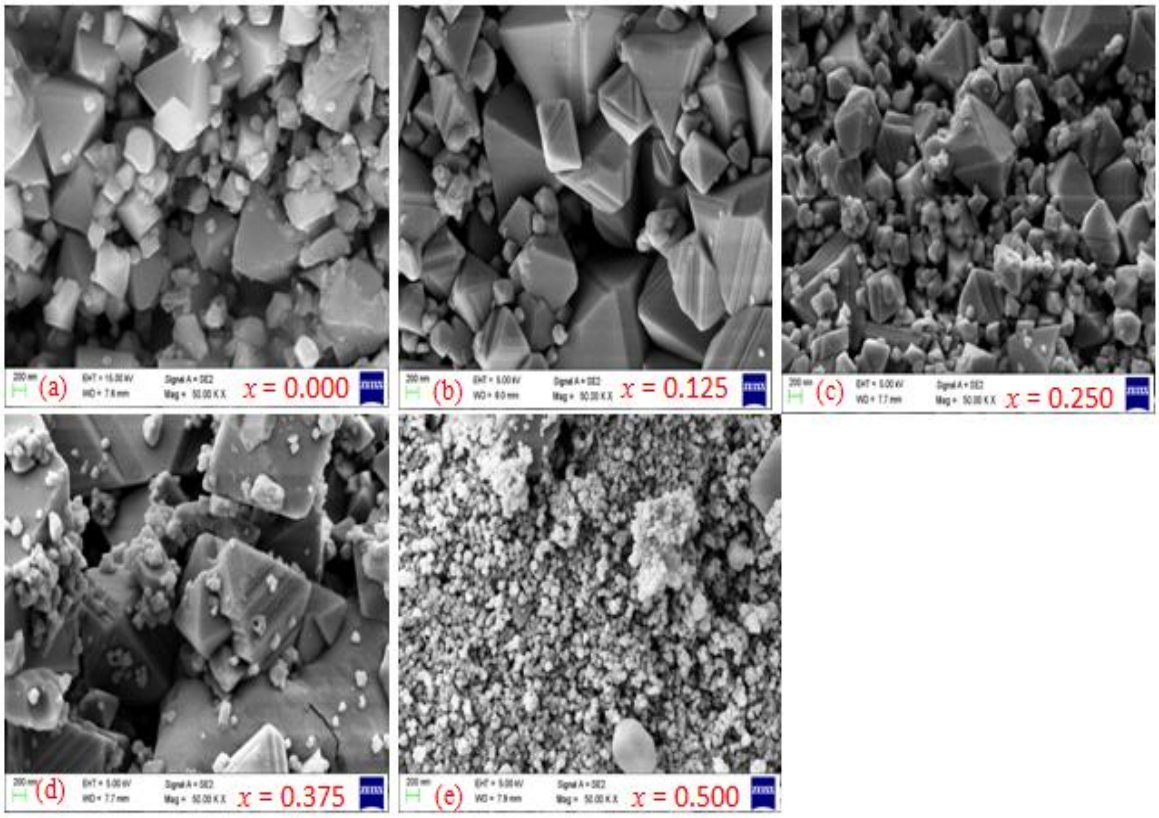

Figure 3.3: *FE-SEM* micrographs for Co^{2+} doped *Mg-Zn* ferrite

FE-SEM micrographs clearly indicate that there is non-uniform distribution of grains for samples. Except for x = 0.500, the sharp edges on the surfaces have been observed for all samples. For x = 0.500, the maximum agglomeration of nanoparticles has been observed. The

agglomeration of nanoparticles increase with Co^{2+} addition. The increase in agglomeration of nanoparticles is due to the substitution of ferromagnetic Co^{2+} by replacing diamagnetic Zn^{2+}. Figure 3.4 shows the *EDS* spectra for the prepared samples. The occurrence of elements *Co*, *Fe*, *Zn*, *Mg* and *O* has been confirmed.

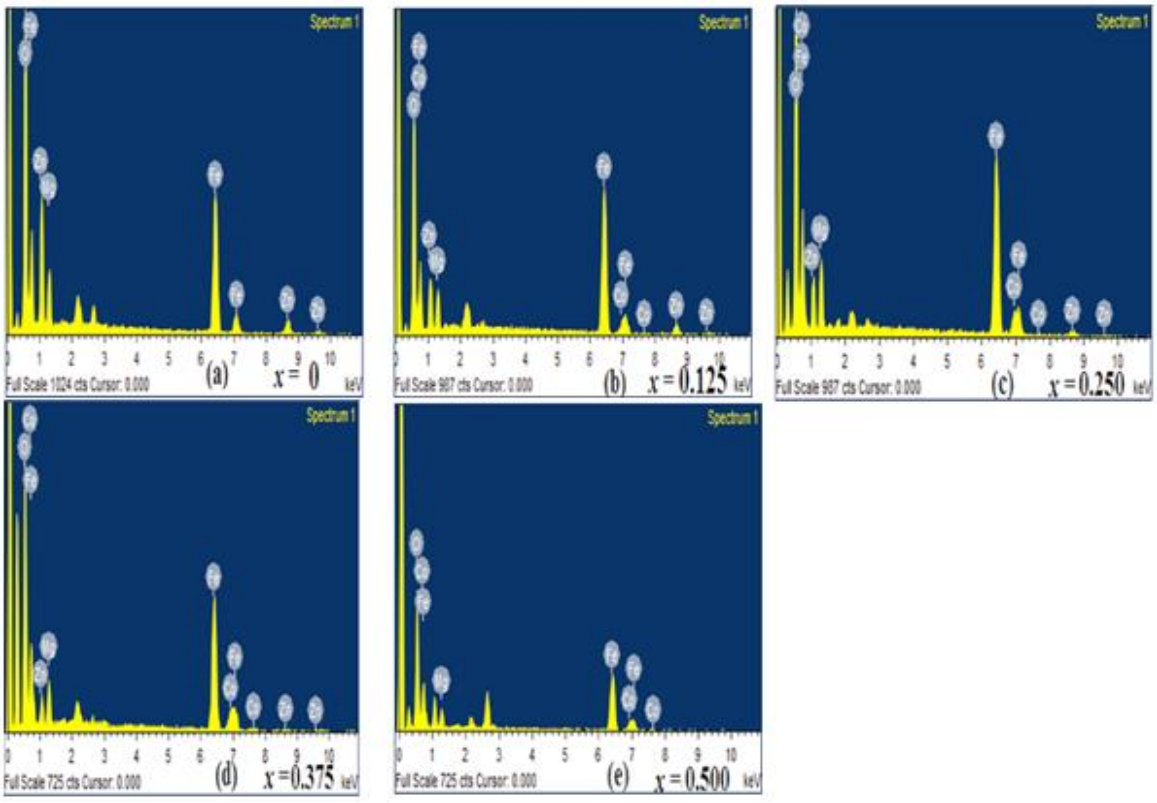

Figure 3.4: *EDS* spectra for Co^{2+} doped *Mg-Zn* ferrites

The values of atomic % (Table 3.2) matches approximately with the estimated values for the samples. The atomic % expected ratio of metal cations w.r.t. anion is 3:4.

Table 3.2: Values of atomic % for Co^{2+} doped *Mg-Zn* ferrites

x	Atomic % Magnesium	Atomic % Zinc	Atomic % Iron	Atomic % Oxygen	Atomic % Cobalt
0.000	5.87	9.56	26.43	58.14	0.00
0.125	5.88	5.87	36.44	49.41	2.39
0.250	6.64	4.16	31.45	53.73	4.02
0.375	5.45	3.09	32.55	53.66	5.26
0.500	5.38	0.00	31.62	56.94	6.06

3.3.2 Structural, morphological and elemental properties of $Mg_{0.5}Zn_{0.5-x}Ni_xFe_2O_4$ ferrites

Figure 3.5 displays the *XRD* patterns of Ni^{2+} added *Mg-Zn* ferrite samples.

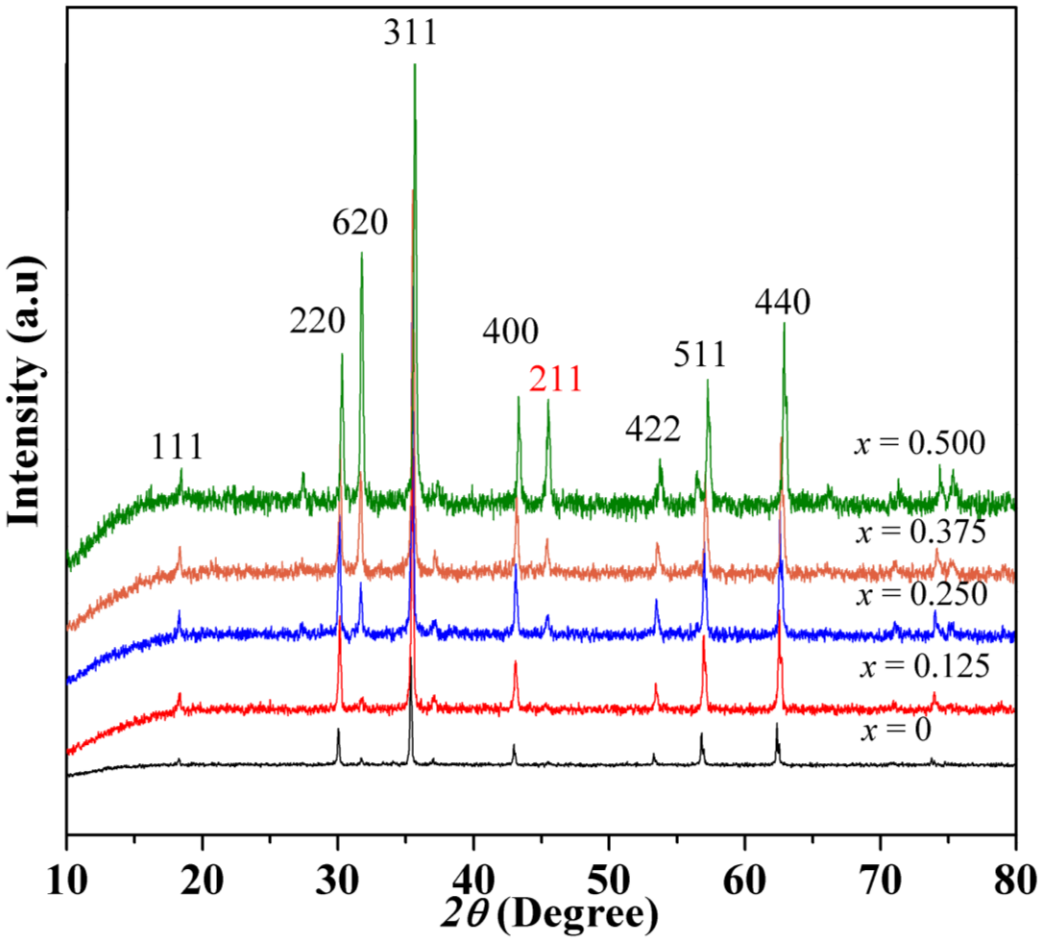

Figure 3.5: *XRD* patterns of Ni^{2+} doped *Mg-Zn* ferrites

The peaks have been indexed as (111), (220), (620), (311), (400), (211), (422), (511) and (440). The peaks (111), (220), (620), (311), (400), (422), (511), (440) are planes specific to single phase (FCC) spinel structure [24]. With increase in Ni^{2+} substitution ($x > 0.125$), the peak marked as (211) appears which indicates the existence of *MgO* phase [32]. The existence of *MgO* phase suggests the transition of $Mg(OH)_2$ into *MgO* [33] and low solubility of Mg^{2+} metal cations with Ni^{2+}cations in the spinel structure. So, only the most prominent peak (311) corresponding to cubical spinel ferrite has been considered for calculation of crystallite size using equation (2.2). It decreases with Ni^{2+} content (Table 3.3). This is because of the replacement of larger Zn^{2+} metal ions with smaller Ni^{2+} metal ions ,as Ni^{2+} has smaller ionic radius (0.69 *Å)* than Zn^{2+} (0.82 *Å*) [14]. Manikandan *et.al* have also reported similar results on the substitution of metal ion

having smaller ionic radii [34]. The *XRD* spectra show shift in most prominent (311) X-ray diffraction peak towards higher diffraction angle with Ni^{2+} substitution. This is because of the replacement of larger Zn^{2+} metal ions by smaller Ni^{2+} ions. The *XRD* peak (311) which is most prominent, shifts from 2θ = 35.37 for x = 0 to 2θ = 35.67 for x = 0.500 (Figure 3.6).

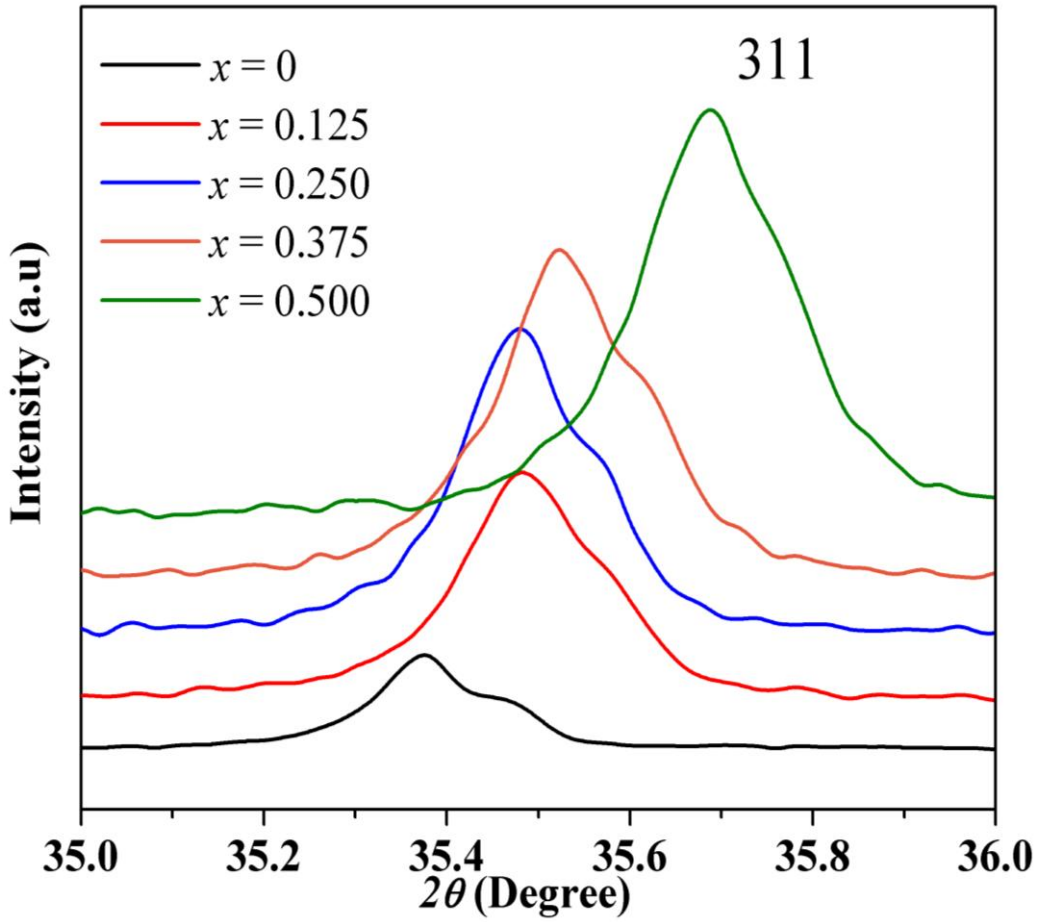

Figure 3.6: Shift in position of most prominent (311) X-ray diffraction peak with Ni^{2+} substitution

The d_{hkl} and a have been calculated using equation (2.3) and (2.4) respectively. The value of a and d_{hkl} (Table 3.3) decreases with Ni^{2+} substitution. It is due to the difference in ionic radii of Ni^{2+} and Zn^{2+} metal ions. For prepared samples the value of p the packing factor has been computed employing equation (2.5). The value of p decreases with Ni^{2+} substitution (Table 3.3). Packing factor depends on crystallite size. For x = 0.500, the smallest crystallite size along with minimum value packing factor has been obtained. The types of strain (ε_u), present in prepared spinel ferrite samples have been calculated using the equation (2.6). The strain increases from -

3.23×10^{-3} for $x = 0.125$ to -8.71×10^{-3} for $x = 0.500$ (Table3.3). The compressive type of strain has been observed for Ni^{2+} substituted samples. The strain varies inversely with crystallite size for prepared samples. The decrease in crystalline nature with reduction in crystallite size is key factor for increase in strain values.

Table 3.3: Different structural parameters for Ni^{2+} doped *Mg-Zn* ferrites

x	Crystallite size (D) nm	Lattice constant (a) Å	Inter-planar spacing (d_{hkl}) Å	Packing factor (p)	Strain (ε_u)
0.125	47.21	8.3847	2.5280	186.74	-3.23×10^{-3}
0.250	46.89	8.3846	2.5280	185.48	-3.23×10^{-3}
0.375	46.04	8.3755	2.5253	182.32	-4.29×10^{-3}
0.500	43.58	8.3392	2.5143	173.33	-8.71×10^{-3}

Figure 3.7 shows the *FT-IR* spectra from *400 cm*$^{-1}$ to *1000 cm* $^{-1}$ for Ni^{2+} added *Mg-Zn* ferrites

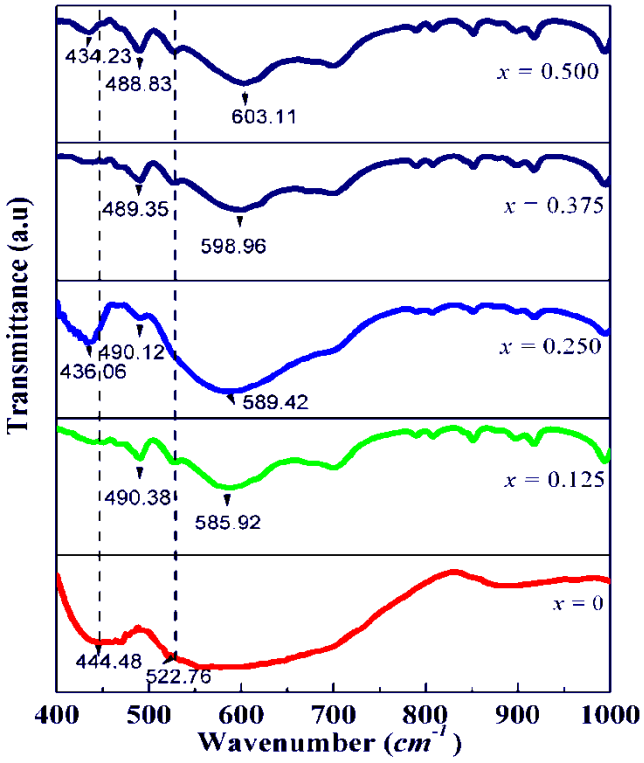

Figure 3.7: *FT-IR* spectra of Ni^{2+} doped *Mg-Zn* ferrites

The occurrence of vibrational frequency bands around *434.23 cm^{-1} to 490.38 cm^{-1}* as well as *522.76 cm^{-1}* to *603.11cm^{-1}* verify the cubical spinel structure for prepared samples. With Ni^{2+} substitution the most prominent frequency bands, related to A lattice sites (Figure 3.6) displace towards the higher wave-number. The decrease of tetrahedral bond length with Ni^{2+} substitution is responsible for the shift of salient frequency bands for higher wave-number because bond length varies inversely with frequency of vibration. The frequency bands corresponding to B site vibration varies non-linearly with Ni^{2+} substitution. Some additional absorption bands at *436.06 cm^{-1}* for $x = 0.250$ and at *434.23 cm^{-1}* for $x = 0.500$ have been observed. They also correspond to B lattice site vibration. The presence of different metal cations having different ionic radius at B lattice sites may be responsible for presence of these additional frequency bands. Some other reasons such as grain size, bond length, synthesis route *etc.* also play significant part in influencing the frequency band positions [30].

There is non-uniform grain growth for all samples (Figure 3.8). The micrographs display particles of unlike shapes and different sizes.

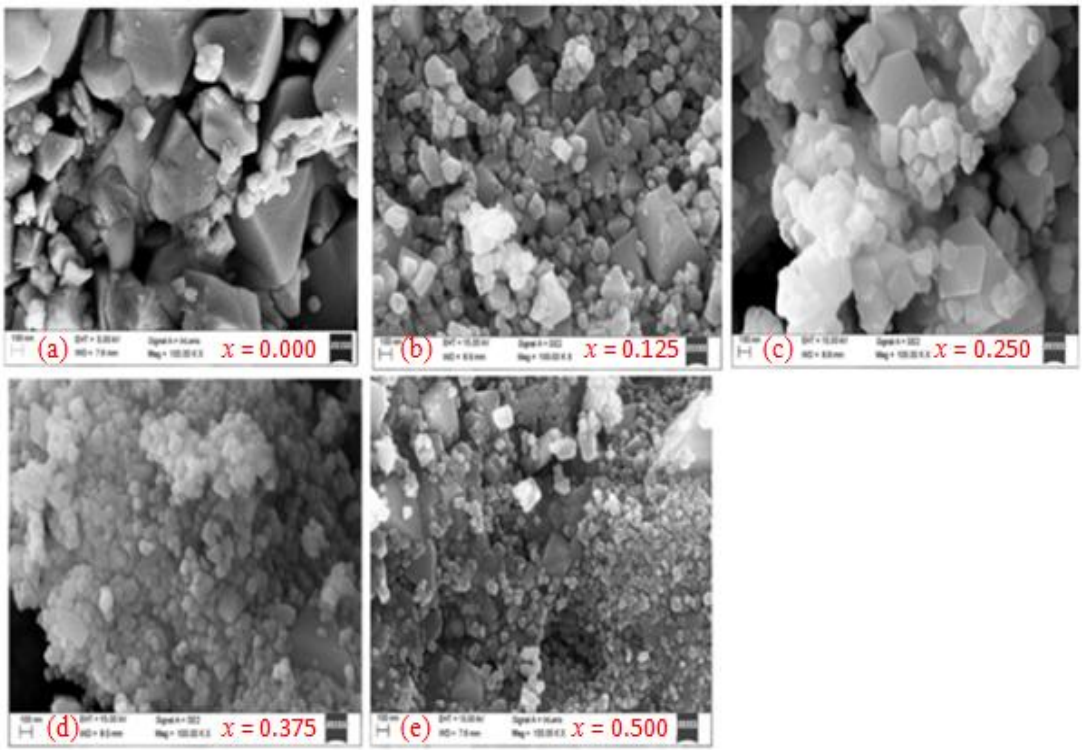

Figure 3.8 : *FE-SEM* micrographs for Ni^{2+} doped *Mg-Zn* ferrites

With increase in Ni^{2+} substitution the agglomeration of nanoparticles become appreciable. The existence of permanent magnetic dipole moment which increases with increase in Ni^{2+} substitution is responsible for agglomeration of nanoparticles [13].

EDS spectra confirm the presence elements such as *Mg, Fe, Zn, Ni* and *O*. Figure 3.9 shows *EDS* spectra for all prepared samples.

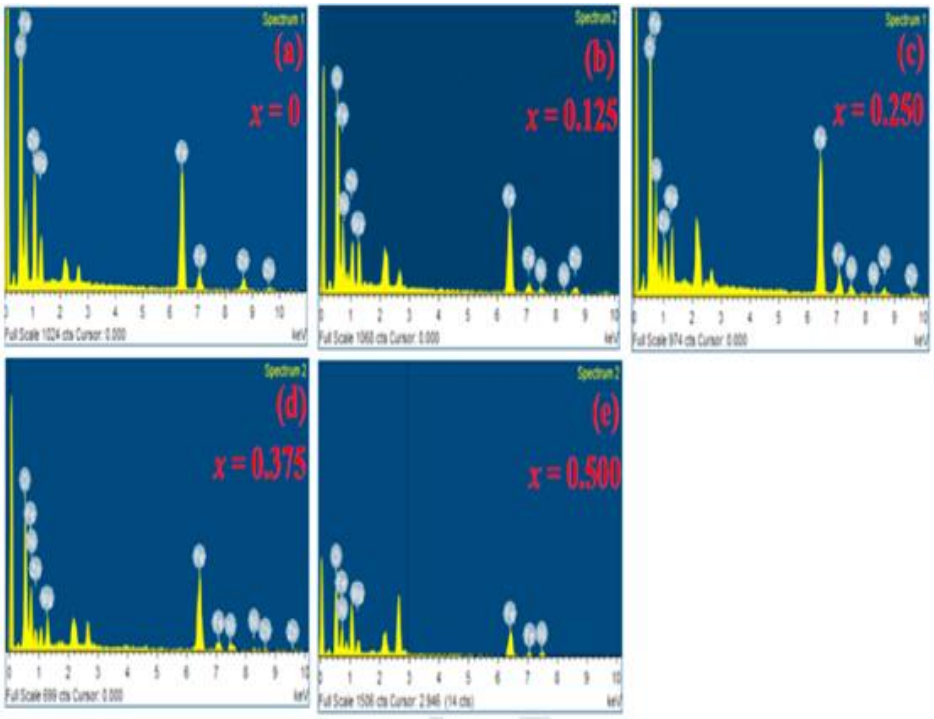

Figure 3.9: *EDS* spectra for Ni^{2+} doped *Mg-Zn* ferrites

The atomic % of metal cations and anions observed in *EDS* spectra have been shown in Table 3.4. The expected ratio of atomic % of cations to anion is 3:4 and observed values (Table 3.4) are also close to the expected values.

Table 3.4: Values of atomic % for Ni^{2+} doped *Mg-Zn* ferrites

x	Atomic % Magnesium	Atomic % Zinc	Atomic % Iron	Atomic% Oxygen	Atomic % Nickel
0.000	5.87	9.56	26.43	58.14	0.00
0.125	8.44	6.71	26.91	55.05	2.89
0.250	6.85	4.99	32.02	52.36	3.78
0.375	6.50	3.49	31.01	53.34	5.66
0.500	8.85	0.00	25.59	57.81	7.75

3.3.3 Structural, morphological and elemental properties of $Mg_{0.5}Zn_{0.5-x}Mn_xFe_2O_4$ ferrites

The *XRD* patterns of Mn^{2+} doped *Mg-Zn* ferrites are shown in Figure 3.10.

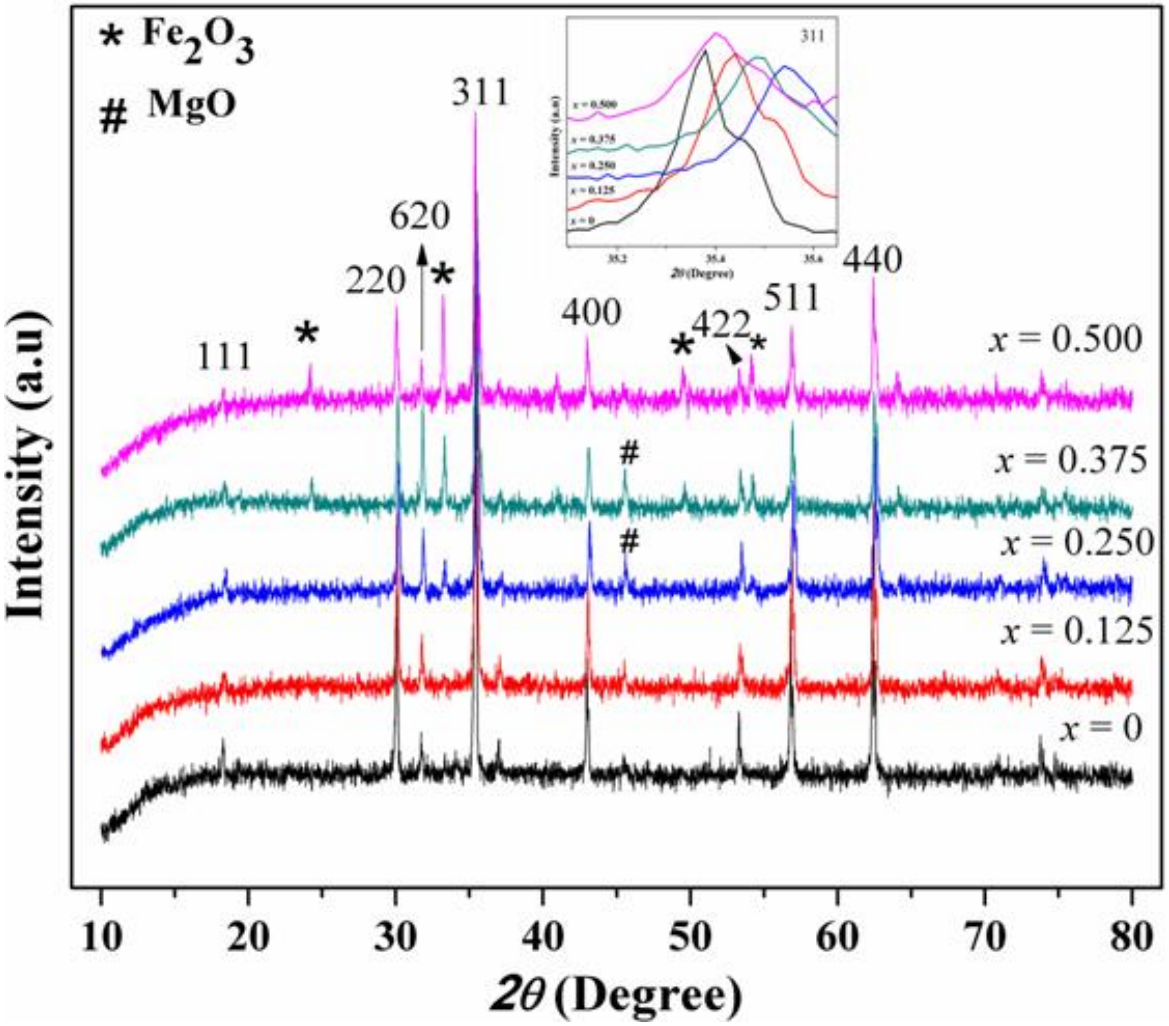

Figure 3.10: *XRD* patterns of Mn^{2+} doped *Mg-Zn* ferrites

The *XRD* peaks marked as (220), (620), (311), (400), (422), (511), (440) represent characteristic planes of FCC spinel structure [24]. The inset in the *XRD* spectra (Figure 3.10) show shift of prominent *XRD* peak (311) with Mn^{2+} substitution. The shift of prominent *XRD* peak confirm addition of Mn^{2+} ions. For $x \geq 0.250$, the hematite phase has been observed. On heating iron hydroxides, it may get converted to hematite. The *Mn* doped ferrites annealed up to a temperature of 1173 *K* have also shown the existence of hematite phase [35]. For $x = 0.250$ and $x = 0.375$ samples the magnesium oxide formation has been observed. During sintering, the heat

treatment of magnesium hydroxide transforms it into magnesium oxide [33]. The presence of this phase of magnesium oxide for magnesium ferrite has been observed by other researchers also [36]. Due to the presence of X-ray diffraction peaks corresponding to magnesium oxide and hematite phase for Mn^{2+} doped samples, the crystallite size has been calculated by considering only the most prominent X-ray diffraction peak (311) using equation (2.2). The value of *D* the crystallite size shows variation from 57.05 *nm* to 48.68 *nm* (Table 3.5). It decreases with Mn^{2+} substitution, except for x = 0.375. The existence of hematite phase and magnesium oxide may reduce the growth of spinel ferrite phase which results in the reduction of crystallite size. The presence of hematite phase for *Mn-Zn* ferrites has also been observed [37]. The value of d_{hkl} the inter-planar spacing and *a* the lattice constant have been calculated from equation (2.3) and (2.4) respectively. The value of *a* as well as d_{hkl} decrease (Table 3.5) up to x = 0.250 sample and then increases (Table 3.5). This decrease in the value of *a* and d_{hkl} is on account of the replacement of Zn^{2+} ions (0.82 *Å*) of larger ionic radius with Mn^{2+} (0.66 *Å*) ions of smaller ionic radius [38]. The hematite phase may develop along the interstitial sites or lattice increasing the value of *a* and d_{hkl} of x = 0.375, 0.500 samples. The equation (2.5) has been used for the estimation of *p* the packing factor. It varies (Table 3.5) similar to the crystallite size. For prepared samples the strain has been calculated using equation (2.6). The prepared samples show compressive strain (Table 3.5).

Table 3.5: Different structural parameters for Mn^{2+} doped *Mg-Zn* ferrites

x	Crystallite size (D) nm	Lattice constant (a) *Å*	Inter-planar spacing (d_{hkl}) *Å*	Packing factor (p)	Strain (ε_u)
0.125	57.05	8.3979	2.5320	225.34	-1.63×10^{-3}
0.250	53.31	8.3730	2.5245	211.19	-4.59×10^{-3}
0.375	55.50	8.3875	2.5289	219.48	-2.86×10^{-3}
0.500	48.68	8.4059	2.5344	192.09	-6.80×10^{-4}

The frequency bands corresponding to vibrational modes of metal cations present on A and B lattice sites have been confirmed with the help of *FT-IR* spectroscopy (Figure 3.11)

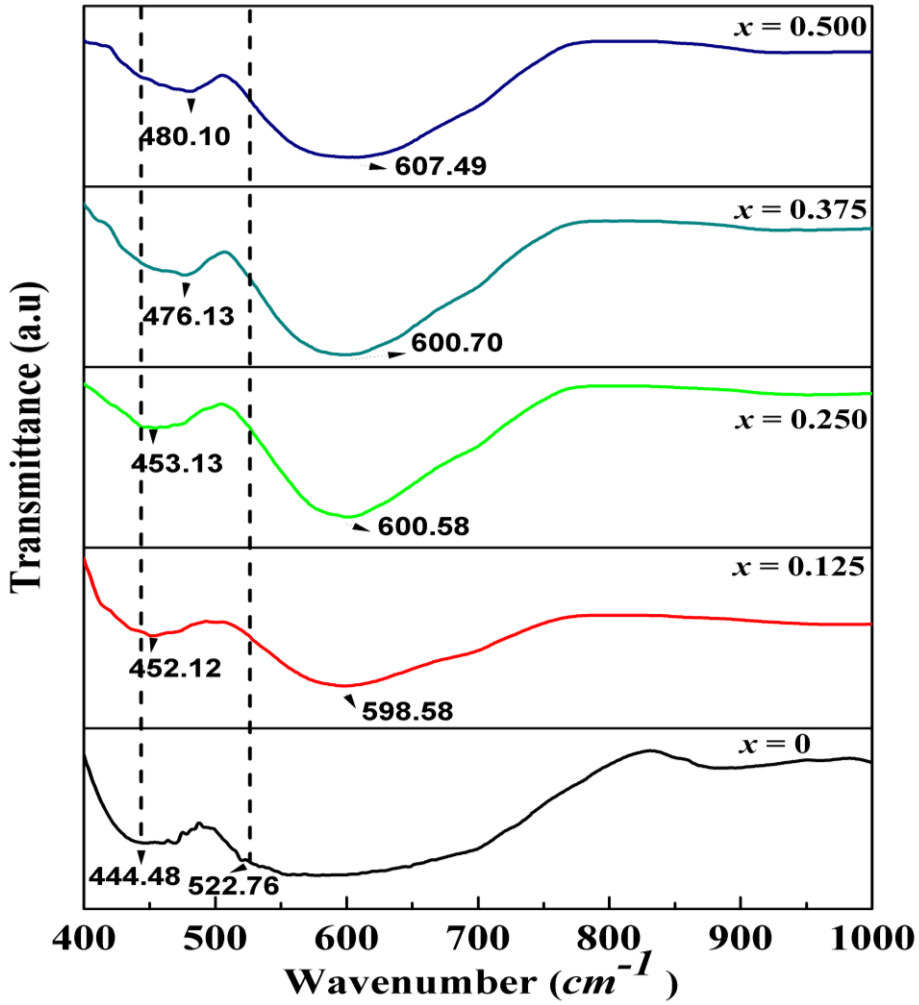

Figure 3.11: *FT-IR* spectra of Mn^{2+} doped *Mg-Zn* ferrites

The frequency band υ_1 from 444.48 cm^{-1} to 480.10 cm^{-1} and v_2 from 522.76 cm^{-1} to 607.49 cm^{-1} have been observed for Mn^{2+} added samples. The lower frequency band (v_1) and higher frequency band (v_2) are the fundamental vibration of metal cations situated at B and A lattice sites respectively [38]. The presence of these frequency bands confirms the formation of spinel structure. With Mn^{2+} substitution, the bands v_1 and v_2 move towards higher value of wave-number. The dissimilarity in Fe^{3+}-O^{2-} distances for A and B lattice sites may be the key factor liable for the difference in position and shift of frequency bands [39].

It has been clearly shown in *FE-SEM* micrographs (Figure 3.12) that the nano-particles of different sizes are present for all prepared samples. For $x \geq 0.250$, the agglomeration of nanoparticles becomes appreciable. The magnetic nature of Mn^{2+} metal ions may lead to the aggregation of nanoparticles.

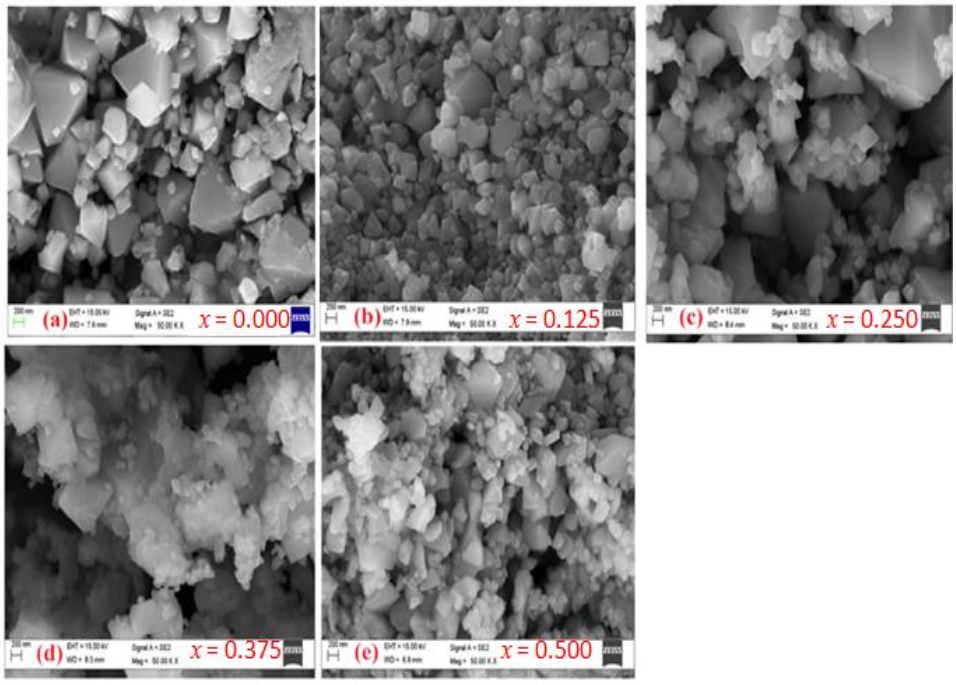

Figure 3.12: *FE-SEM* micrographs for Mn^{2+} doped *Mg-Zn* ferrites

EDS spectra (Figure 3.13) affirm the presence of constituent elements for Mn^{2+} doped *Mg-Zn* ferrite samples

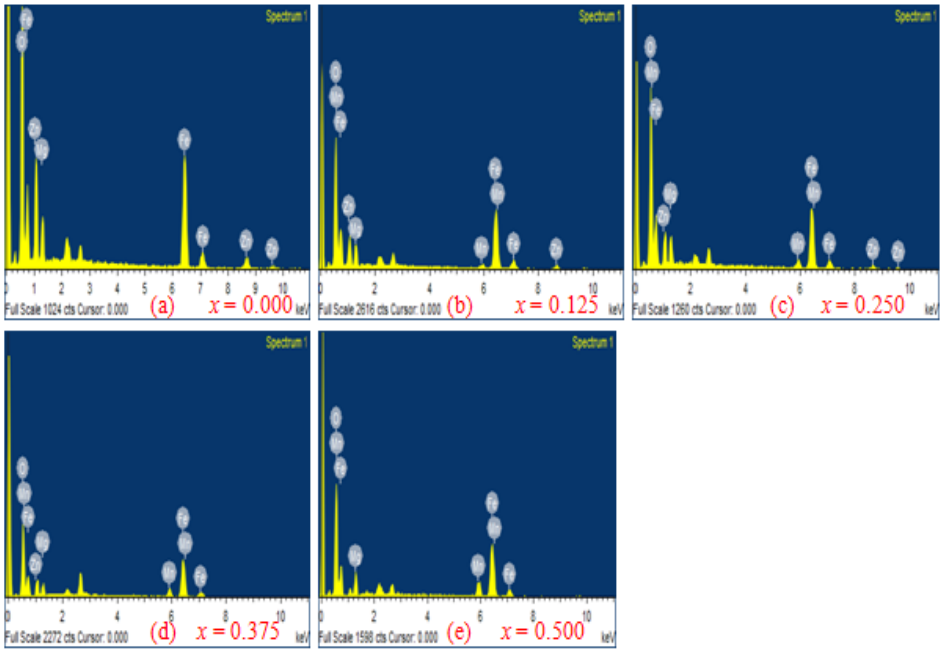

Figure 3.13 : *EDS* spectra for Mn^{2+} doped *Mg-Zn* ferrites

The values of atomic % for oxygen anion and metal cations have been shown in Table 3.6, the observed values of atomic % and ratio of atomic % of cations to anions are close to expected values for all prepared samples.

Table 3.6 Values of atomic % for Mn^{2+} doped *Mg-Zn* ferrites

x	Atomic % Magnesium	Atomic % Zinc	Atomic % Iron	Atomic % Oxygen	Atomic % Manganese
0.000	5.87	9.56	26.43	58.14	0.00
0.125	6.60	6.69	30.01	55.23	1.47
0.250	6.81	5.76	25.63	58.65	3.14
0.375	6.43	5.49	30.58	52.09	5.41
0.500	7.21	0.00	33.65	51.22	7.92

3.4 Conclusion

XRD patterns confirm the formation of FCC spinel structure for transition metal ($M = Co^{2+}$, Ni^{2+} and Mn^{2+}) doped *Mg-Zn* ferrites. For Co^{2+} doped samples, pure spinel structure without any single impurity has been observed. The formation of pure spinel structure indicates the complete incorporation of Co^{2+} metal ions into their respective crystallographic lattice sites. There is formation of magnesium oxide for Ni^{2+} doped samples. For Mn^{2+} doped samples the hematite phase has been present. The change in structural parameters of prepared samples has shown dependence on ionic radius of transition metal ions and their preference for crystallographic lattice sites. For Co^{2+} doped samples, the non linear variation in the value of *a* and d_{hkl} is due to metal cation allocation at lattice sites. The replacement of larger Zn^{2+} ions by smaller Ni^{2+} metal ions is responsible for the variation in structural parameters of Ni^{2+} doped samples. For Mn^{2+} doped samples, presence of hematite phase influences various structural parameters. It indicates that the hematite phase may grow along lattice or interstitial sites of spinel structure which leads to subsequent variation in structural properties. The investigation of *FT-IR* spectra for prepared samples confirm the presence of frequency bands corresponding to A and B site vibration. The change in the prominent frequency band positions on the addition of transition metal ions is due to the change in bond lengths. The surface morphology of prepared samples has been investigated using *FE-SEM*. There is non-uniform grain growth and increase in aggregation of

nanoparticles with substitution of transition metal ions. It signifies that the presence of permanent magnetic moment is responsible for the agglomeration of spinel ferrite nanoparticles. *EDS* spectra for prepared samples confirm the presence of elements corresponding to their chemical compositions. The observed ratios of atomic % of cations to anion are close to the expected values. It confirms that the stoichiometry is maintained for all prepared samples.

CHAPTER 4*

CATION DISTRIBUTION FOR TRANSITION METAL DOPED *Mg-Zn* FERRITES

* **Rohit Sharma,** P. Thakur , M. Kumar , N. Thakur, N. S. Negi, P. Sharma, V. Sharma, Improvement in magnetic behaviour of cobalt doped magnesium-zinc nano-ferrites via co-precipitation route, **Journal of Alloys and Compounds**, 684,569-581 (2016)

Rohit Sharma, P. Thakur, P. Sharma, V. Sharma, Ferrimagnetic Ni^{2+} doped Mg-Zn spinel ferrite nanoparticles for high density information storage, **Journal of Alloys and Compounds**, 704, 7-17 (2017)

Rohit Sharma, P. Thakur, M. Kumar, P. B. Barman, P. Sharma, V. Sharma , Enhancement in A-B super-exchange interaction with Mn^{2+} substitution in *Mg-Zn* ferrites as a heating source in hyperthermia applications, **Ceramics International**, 43,13661-13669 (2017)

This chapter describes the theoretical cation distribution in crystallographic lattice sites with respect to the choice of metal ions for A or B sites and *XRD* results for transition ($M = Co^{2+}$, Ni^{2+} and Mn^{2+}) metal doped *Mg-Zn* ferrites. Several theoretical parameters calculated using the cation distribution have been discussed.

4.1 Introduction

Ferrite nano-particles crystallize into face centered cubical spinel structure. They belong to *Fd3m* space group having closed pack arrangement of 24 metal cations and 32 oxygen anions [1]. There are two different types of crystallographic lattice sites, *i.e.* A and B sites in spinel structure. The 8 cations are distributed in A lattice sites and remaining ones occupy 16 B lattice sites which makes spinel structure electrically neutral [2].

Normal, inverse and mixed spinel are the three types of spinel structures. The crystallization of spinel ferrites in these structures depend upon the metal cation distribution in crystallographic lattice sites [3]. The octahedral lattice sites are large as compared to tetrahedral sites. So the divalent metal ions which are larger in comparison to trivalent metal ions prefer to occupy octahedral sites and smaller trivalent ions can occupy tetrahedral as well as octahedral sites. Zn^{2+} and Cd^{2+} metal ions because of their electronic configuration prefer tetrahedral bonding with oxygen anions, therefore they occupy the tetrahedral sites [2]. In few cases of nano-ferrites, the Zn^{2+} ions have also been reported to occupy the octahedral (B) sites [4].

On the account of preference of metal cations to occupy lattice sites the cation distribution for spinel ferrites can be proposed. Several theoretical parameters can be calculated using proposed cation distribution which may be useful in the analysis of different physical properties of spinel ferrites. Various research groups have reported about the cation distribution and have calculated different theoretical parameters for spinel ferrites [5, 6]. The cation distribution also helps in understanding the magnetic properties of spinel ferrites by investigating cation-anion distances and bond angles. Patange *et al.* have reported cation distribution for chromium substituted nickel ferrites and explained magnetic behavior with the help of proposed cation distribution [7]. The X-ray diffraction results can also be used to propose cation distribution if R (agreement factor) has the least value. The value of R corresponds to the difference of the ratios for X-ray diffraction intensity of the calculated and experimentally observed peaks for a particular set of

diffraction pairs. Reflections at (220), (440) and (400) are considered sensitive for estimation of agreement factor because these peaks are not sensitive to temperature and absorption factors [6]. Considering preference of metal cations for crystallographic lattice sites and X-ray diffraction (*XRD*) results, the cation distribution have been studied for transition metal ($M = Co^{2+}$, Ni^{2+} and Mn^{2+}) added *Mg-Zn* ferrites. The parameters such as mean ionic radii, theoretical lattice parameter, tetrahedral edge length, *etc*. have been calculated theoretically.

4.2 Cation distribution for $Mg_{0.5}Zn_{0.5-x}Co_xFe_2O_4$ ferrites

In $Mg_{0.5}Zn_{0.5-x}Co_xFe_2O_4$ ferrites, Zn^{2+} metal ions prefer to occupy A sites while Mg^{2+} and Co^{2+} metal ions have choice to occupy B sites [2]. The trivalent Fe^{3+} metal ions can occupy any of the A or B lattice sites. The ionic radius of metal ions *i.e.* Mg^{2+} (0.72 *Å*), Fe^{3+} (0.67 *Å*), Zn^{2+} (0.82 *Å*) and Co^{2+} (0.74 *Å*) plays an essential part in cation distribution [8, 9]. After taking *XRD* results and preference of metal cations into account, the most appropriate cation distribution for $Mg_{0.5}Zn_{0.5-x}Co_xFe_2O_4$ ferrites has been proposed (Table 4.1).

Table 4.1: Proposed cation distribution for $Mg_{0.5}Zn_{0.5-x}Co_xFe_2O_4$ ferrites

x	A- site	B- site
0	$Fe_{0.5}\,Zn_{0.5}$	$Fe_{1.5}Mg_{0.5}$
0.125	$Fe_{0.625}\,Zn_{0.375}$	$Fe_{1.375}Mg_{0.5}\,Co_{0.125}$
0.250	$Fe_{0.625}\,Zn_{0.250}\,Mg_{0.125}$	$Fe_{1.375}Mg_{0.375}Co_{0.250}$
0.375	$Fe_{0.750}\,Zn_{0.125}\,Mg_{0.125}$	$Fe_{1.250}Mg_{0.375}\,Co_{0.375}$
0.500	$Fe_{1.0}$	$Fe_{1.0}\,Mg_{0.5}Co_{0.5}$

The r_A mean ionic radii corresponding to A and r_B mean ionic radii corresponding to B lattice sites have been calculated according to cation distribution using following equations [10];

$$r_A = [C_{Mg^{2+}} . r_{Mg^{2+}} + C_{Zn^{2+}} . r_{Zn^{2+}} + C_{Co^{2+}} . r_{Co^{2+}} + C_{Fe^{3+}} . r_{Fe^{3+}}] \quad (4.1)$$

$$r_B = 0.5 \times [C_{Mg^{2+}} . r_{Mg^{2+}} + C_{Zn^{2+}} . r_{Zn^{2+}} + C_{Co^{2+}} . r_{Co^{2+}} + C_{Fe^{3+}} . r_{Fe^{3+}}] \quad (4.2)$$

where *C* is the ionic concentration and *r* is the ionic radii of metal cations. Figure 4.1 shows the change in mean value of r_A and r_B with cobalt substitution.

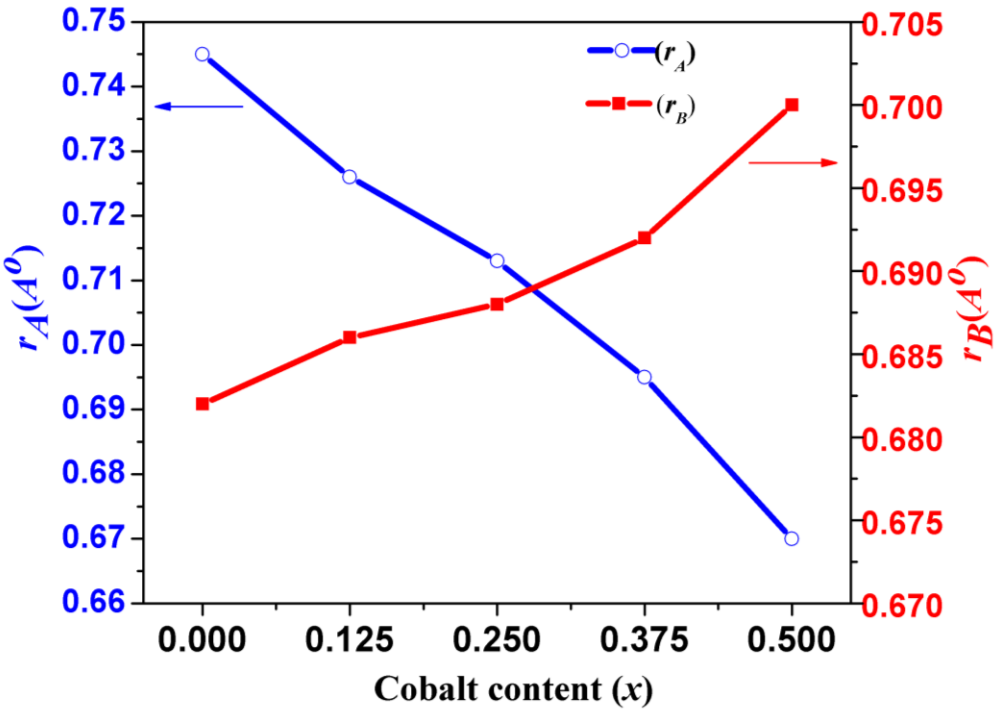

Figure 4.1: Variation of mean ionic radii of A and B lattice sites with Co^{2+} substitution

The mean value of r_A decrease with Co^{2+} substitution (Table 4.2). It is due to the replacement of Zn^{2+} metal ions of larger ionic radius from A lattice sites with smaller trivalent Fe^{3+} metal ions. The mean value of r_B increase with Co^{2+}substitution. The incorporation of larger Co^{2+} metal ions in B lattice sites and migration of smaller trivalent Fe^{3+} metal ions to A lattice sites increases the mean ionic radii of B lattice sites. The cobalt metal ions prefer to reside in B lattice sites which results in the migration of Fe^{3+} metal ions from B lattice sites to A lattice sites [9]. The a_{th} the theoretical lattice parameter has been calculated using the equation [10];

$$a_{th} = (8/3\sqrt{3})[(r_A + R_o) + \sqrt{3}(r_B + R_o)] \quad (4.3)$$

where R_o represents the oxygen anion radius which is 1.32 *Å*. The a_{th} decreases with Co^{2+} substitution (Table 4.2). It is due to the replacement of Zn^{2+} (0.82 *Å*) metal ions with Co^{2+} (0.74 *Å*) metal ions [8]. The difference in experimental (Table 3.1) and theoretical lattice parameter is because of the approximation considered for the calculation of theoretical lattice parameter. The approximation considered the unit cell as an ideal one having anions and cations as rigid spheres arranged in a regular array [11]. Figure 4.2 shows the change in a_{th} and a with Co^{2+} substitution.

Table 4.2: Several structural parameters calculated theoretically using proposed cation distribution

x	r_A (Å)	r_B (Å)	a_{th} (Å)	u (Å)	δ (Å)	R_A (Å)	R_B (Å)	R (Å)	R' (Å)	R'' (Å)
0	0.745	0.682	8.517	0.3899	0.0143	2.030	1.989	3.328	2.619	2.984
0.125	0.726	0.686	8.499	0.3889	0.0139	2.023	1.993	3.304	2.643	2.983
0.250	0.713	0.688	8.484	0.3883	0.0133	2.003	1.986	3.272	2.642	2.966
0.375	0.695	0.692	8.467	0.3873	0.0123	1.963	1.968	3.206	2.631	2.926
0.500	0.670	0.700	8.450	0.3859	0.0109	1.973	2.009	3.222	2.705	2.970

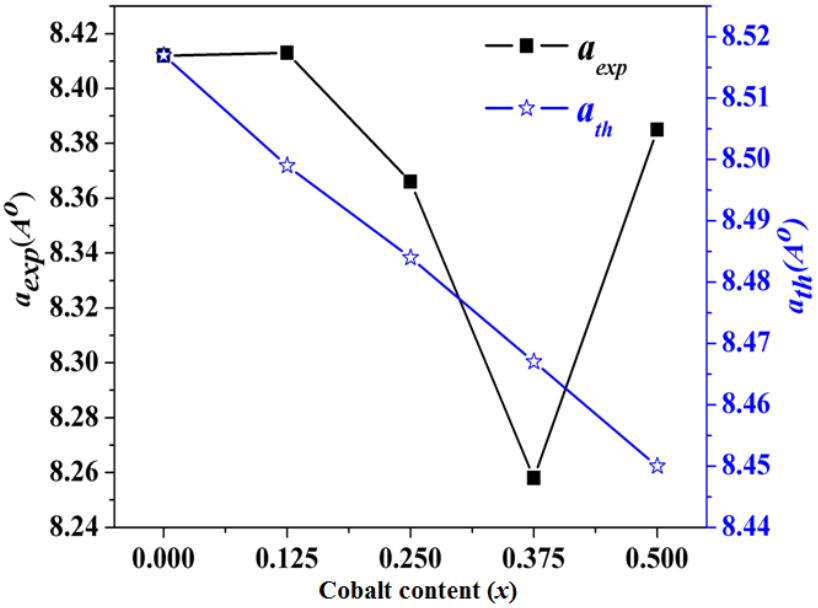

Figure 4.2: Variation of a_{exp} and a_{th} with Co^{2+} substitution

The value of u the oxygen positional parameter has been computed using equation [10];

$$u=(1/a_{th}\sqrt{3})(r_A+R_o)+1/4 \qquad (4.4)$$

It decreases (Table 4.2) with Co^{2+} substitution. The A lattice sites are small enough to adjust metal cations, so oxygen anions connected with octahedral sites slightly move to incorporate them. This results in the contraction of the B sites by the amount equivalent to A sites expansion. This type of drift of O^{2-} ions represent the oxygen positional parameter [10]. Figure 4.3 shows the change in u with Co^{2+} substitution.

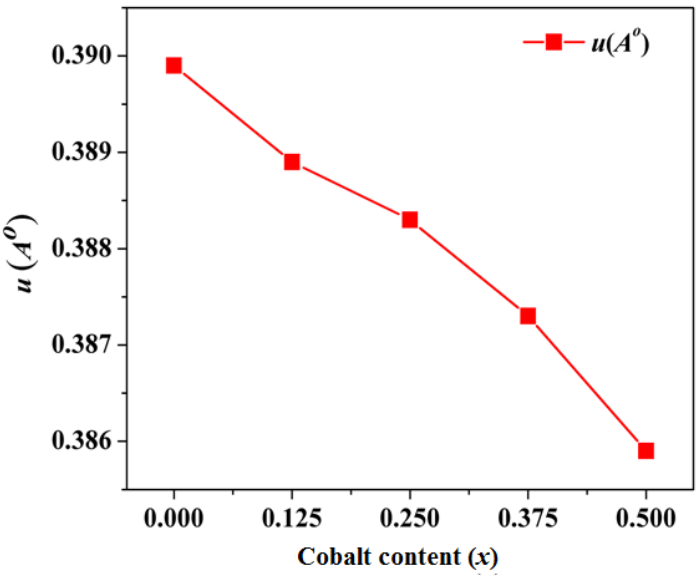

Figure 4.3: Variation of oxygen positional parameter *(u)* with Co^{2+} substitution

In ideal spinel ferrite structure [9] all O^{2-} anions behave identically which result in the perfect closed cubical packing having the ideal value of u_{ideal} equal to 0.375 *Å*. But, actually the real spinel lattice is marginally distorted. The computed values of *u* for these samples (Table 4.2) are larger than 0.375 *Å*. This is due to the movement of oxygen anions towards A lattice sites. The value of *u* shows a decrease on Co^{2+} substitution (Table 4.2). The enlargement of A lattice sites decreases on Co^{2+}substitution, since the smaller Fe^{3+} metal ions migrated from B lattice sites have to be accommodated in A lattice sites [9, 11]. R_A and R_B the cation-anion lengths for A and at B lattice sites respectively have been computed from the following relations [11];

$$R_A = a\sqrt{3}(\delta + 1/8) \tag{4.5}$$

$$R_B = a\left(\frac{1}{16} - \frac{\delta}{2} + 3\delta^2\right)^{1/2} \tag{4.6}$$

where, $\delta = u - u_{ideal}$ is inversion parameter and *a* is the experimental lattice parameter. The δ value decreases (Table 4.2) on Co^{2+} substitution. The variation in inversion parameter is in accordance with oxygen positional parameter. R_A represents the minimum distance for the A site metal cation and O^{2-} anion and R_B the minimum distance for the B site metal cation and O^{2-} anion. The calculated R_A and R_B values (Table 4.2) depend on the values of *u* and *a*. The change in R_A and R_B is due to the replacement of larger Zn^{2+} metal cations from A lattice sites by Co^{2+} ions causing the transfer of smaller Fe^{3+} cations from B to A lattice sites. *R* the tetrahedral edge

length, $R^{'}$ the shared octahedral length and $R^{''}$ the unshared octahedral edge length have been computed from the equations [12];

$$R = a(\sqrt{2})(2u - 0.5) \tag{4.7}$$

$$R' = a(\sqrt{2})(1 - 2u) \tag{4.8}$$

$$R'' = a\sqrt{(4u^2 - 3u + (11/16))} \tag{4.9}$$

The calculated values of R, $R^{'}$ and $R^{''}$ have been shown in Table 4.2. The values of R and $R^{''}$ decrease with Co^{2+} substitution up to x = 0.375. Their variation with Co^{2+} shows dependence on the value of a.

4.3 Cation distribution for $Mg_{0.5}Zn_{0.5-x}Ni_xFe_2O_4$ ferrites

For $Mg_{0.5}Zn_{0.5-x}Ni_xFe_2O_4$ ferrites, Mg^{2+} and Ni^{2+} ions show preference to occupy the B lattice sites where as Zn^{2+} ions prefer to reside at the A lattice sites [2]. The trivalent Fe^{3+} metal ions can occupy any of these lattice sites [2]. Table 4.3 gives the most suited cation distribution using the experimental *XRD* data and taking the choice of metal cations for their respective crystallographic sites in consideration.

Table 4.3: Proposed cation distribution for $Mg_{0.5}Zn_{0.5-x}Ni_xFe_2O_4$ ferrites

x	A- site	B - site
0	$Fe_{0.5}\,Zn_{0.5}$	$Fe_{1.5}Mg_{0.5}$
0.125	$Fe_{0.625}\,Zn_{0.375}$	$Fe_{1.375}\,Mg_{0.5}\,Ni_{0.125}$
0.250	$Fe_{0.750}\,Zn_{0.250}$	$Fe_{1.250}\,Mg_{0.5}Ni_{0.250}$
0.375	$Fe_{0.875}\,Zn_{0.125}$	$Fe_{1.125}\,Mg_{0.5}\,Ni_{0.375}$
0.500	$Fe_{1.0}$	$Fe_{1.0}\,Mg_{0.5}Ni_{0.5}$

.

The r_A mean ionic radii corresponding to A and r_B mean ionic radii corresponding to B lattice sites have been calculated using equations [10];

$$r_A = [C_{Mg^{2+}}.r_{Mg^{2+}} + C_{Zn^{2+}}.r_{Zn^{2+}} + C_{Ni^{2+}}.r_{Ni^{2+}} + C_{Fe^{3+}}.r_{Fe^{3+}}] \tag{4.10}$$

$$r_B = 0.5 \times [C_{Mg^{2+}}.r_{Mg^{2+}} + C_{Zn^{2+}}.r_{Zn^{2+}} + C_{Ni^{2+}}.r_{Ni^{2+}} + C_{Fe^{3+}}.r_{Fe^{3+}}] \tag{4.11}$$

The value of r_A decreases (Table 4.4) with Ni^{2+} substitution. This is because of the substitution of Ni^{2+} (0.69 *Å*) [13] metal ions, which replaces larger Zn^{2+} (0.82 *Å*) metal ions from A lattice sites

with smaller Fe^{3+} (0.67 Å) metal ions. The value of r_B lattice increases (Table 4.4) with Ni^{2+} substitution. This is due to the incorporation of larger Ni^{2+} metal ions and transfer of smaller Fe^{3+} metal ions towards A lattice sites. Figure 4.4 shows the change in r_A and r_B with Ni^{2+} substitution.

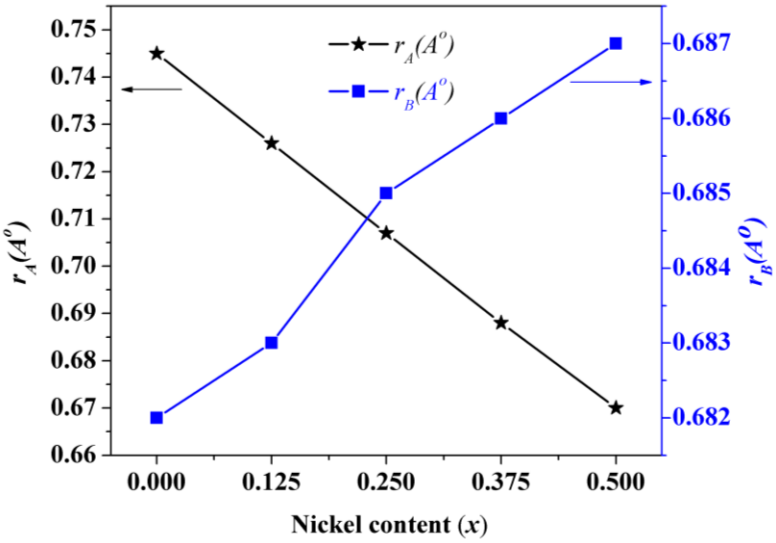

Figure 4.4: Variation of r_A and r_B with Ni^{2+} substitution

For Ni^{2+} doped samples, a_{th} has also been calculated using equation (4.3). The theoretical lattice parameter decreases with Ni^{2+} substitution (Table 4.4) as the smaller Ni^{2+} metal ions replace the larger Zn^{2+} metal ions . The observed values of theoretical lattice parameter (Table 4.4) and experimental lattice parameter (Table 3.3) indicate that they are in good agreement. There is a small difference between experimental and theoretical lattice parameter because for the calculation of theoretical lattice parameter the unit cell considered is ideal one having regularly arranged anions and cations [14].

Table 4.4: Several structural parameters calculated theoretically using proposed cation distribution

x	r_A (Å)	r_B (Å)	a_{th} (Å)	u (Å)	δ (Å)	R_A (Å)	R_B (Å)	R (Å)	R' (Å)	R'' (Å)
0.125	0.726	0.683	8.491	0.3891	0.0141	2.020	1.985	3.298	2.630	2.973
0.250	0.707	0.685	8.467	0.3882	0.0132	2.007	1.991	3.277	2.651	2.972
0.375	0.688	0.686	8.440	0.3873	0.0123	1.991	1.996	3.252	2.669	2.968
0.500	0.670	0.687	8.415	0.3865	0.0115	1.971	1.993	3.219	2.677	2.954

Equation (4.4) has been employed to calculate the value of *u*. It decreases with Ni^{2+} substitution (Table 4.4). The migration of smaller Fe^{3+} metal ions from B lattice sites to A lattice sites on Ni^{2+} substitution decreases A lattice site expansion resulting in the decrease of parameter *u*. Figure 4.5 shows the variation of oxygen positional parameter with Ni^{2+} substitution.

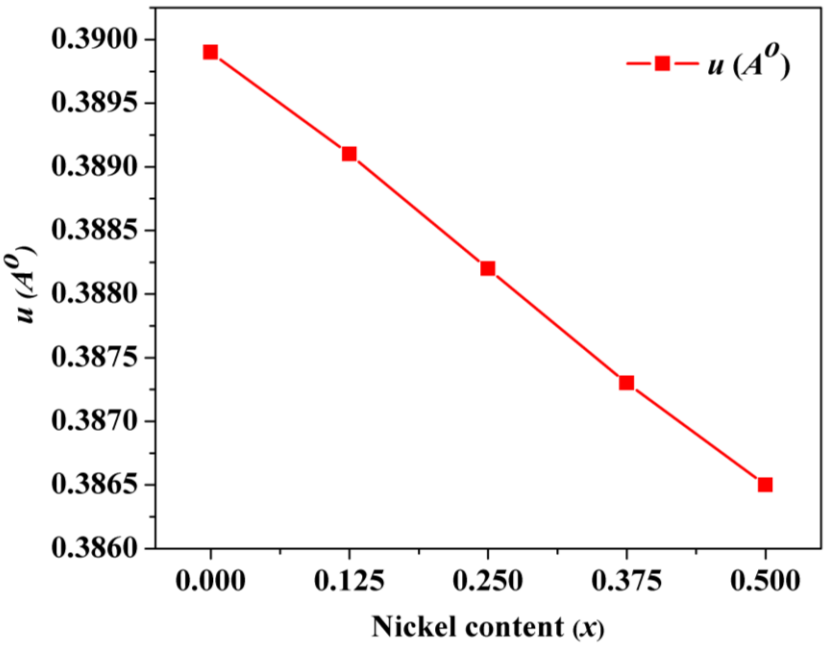

Figure 4.5: Variation of oxygen positional parameter *(u)* with Ni^{2+} substitution

The inversion parameter decreases with Ni^{2+} substitution (Table 4.4). The variation in the value of δ is in accordance with that of oxygen positional parameter. R_A the tetrahedral bond length and R_B the octahedral bond length have been calculated using equation (4.5) and (4.6) respectively. The tetrahedral bond length decreases with Ni^{2+} substitution (Table 4.4). The Ni^{2+} substitution transfers smaller Fe^{3+} metal ions from B lattice sites to A lattice sites which decrease the mean value of r_A with subsequent decrease of R_A. The variation in R_B is non-linear with Ni^{2+} substitution, which may be due to the occurrence of different unequal ionic radius metal ions (Fe^{3+}, Mg^{2+} and Ni^{2+}) at B lattice sites.

The values for *R*, *R′* and *R″* have been computed from equation (4.7), (4.8) and (4.9) respectively. The metal ions distribution at A and B lattice sites causes the change in the *R*, *R′* and *R″* values (Table 4.4) [5]. The decrease in the value of *R* (Table 4.4) with Ni^{2+} addition is

due to the reduction in r_A. On the other hand the increase in r_B with Ni^{2+} addition leads to increase of R' and R'' (Table 4.4).

4.4 Cation distribution $Mg_{0.5}Zn_{0.5-x}Mn_xFe_2O_4$ ferrites

In $Mg_{0.5}Zn_{0.5-x}Mn_xFe_2O_4$ ferrites, Mg^{2+} and Mn^{2+} ions have choice to reside at the B and A lattice sites respectively [15]. Ionic radius of metal cations play important role in deciding their preference for lattice sites. Mn^{2+} is a divalent metal cation, but due to its smaller size than Fe^{3+} metal ion, the Mn^{2+} metal ions selects to reside at A sites [2]. Zn^{2+} ions choice for A lattice sites, while Fe^{3+} ions can occupy any of the A or B lattice sites. Table 4.5 presents the most appropriate cation distribution for $Mg_{0.5}Zn_{0.5-x}Mn_xFe_2O_4$ ferrites, based on the choice of metal ions for crystallographic sites and experimental XRD results.

Table 4.5: Proposed cation distribution for $Mg_{0.5}Zn_{0.5-x}Mn_xFe_2O_4$ ferrites

x	A- site	B- site
0	$Fe_{0.5}\ Zn_{0.5}$	$Fe_{1.5}Mg_{0.5}$
0.125	$Fe_{0.525}\ Zn_{0.375}\ Mn_{0.1}$	$Fe_{1.475}Mg_{0.5}\ Mn_{0.025}$
0.250	$Fe_{0.550}\ Zn_{0.250}\ Mn_{0.2}$	$Fe_{1.450}Mg_{0.5}Mn_{0.050}$
0.375	$Fe_{0.575}\ Zn_{0.125}\ Mn_{0.3}$	$Fe_{1.425}Mg_{0.5}\ Mn_{0.075}$
0.500	$Fe_{0.6}\ Mn_{0.4}$	$Fe_{1.4}Mg_{0.5}Mn_{0.1}$

The r_A mean ionic radii corresponding to A and r_B mean ionic radii corresponding to B lattice sites have been calculated by using equations [10];

$$r_A = [C_{Mg^{2+}}.r_{Mg^{2+}} + C_{Zn^{2+}}.r_{Zn^{2+}} + C_{Mn^{2+}}.r_{Mn^{2+}} + C_{Fe^{3+}}.r_{Fe^{3+}}] \quad (4.12)$$

$$r_B = 0.5\times[C_{Mg^{2+}}.r_{Mg^{2+}} + C_{Zn^{2+}}.r_{Zn^{2+}} + C_{Mn^{2+}}.r_{Mn^{2+}} + C_{Fe^{3+}}.r_{Fe^{3+}}] \quad (4.13)$$

The mean ionic radii r_A and r_B decrease with the addition of Mn^{2+} (Table 4.6). The smaller Mn^{2+} (0.66 Å) metal ions replace the larger Zn^{2+} (0.82 Å) metal ions, thus migrating the Fe^{3+} (0.67 Å) towards A lattice sites and decreases the r_A. Some Mn^{2+} ions present at B lattice sites causes the observed variation in mean ionic radii of r_B.

The a_{th} relies on the ionic radii of the metal cations. Equation (4.3) has been used to compute a_{th}. It decreases with Mn^{2+} substitution (Table 4.6). It is due to the substitution of Mn^{2+} (0.66 Å) metal ions by replacing Zn^{2+} (0.82 Å) metal ions.

Equation (4.4) has been used to compute the *u* value, which reduces with Mn^{2+} addition as shown in Table 4.6. The smaller Fe^{3+} migrate from B- to A-sites on Mn^{2+} substitution. This results in restricted enlargement of A-sites causing reduction in the *u* value. The R_A and R_B bond lengths have been calculated using equation (4.5) and (4.6) respectively. The inversion parameter decreases with Mn^{2+}substitution (Table 4.6). The tetrahedral bond length decreases (Table 4.6) with increasing Mn^{2+} content. The decrease in r_A with Mn^{2+} substitution is responsible for decrease in R_A. While the R_B enhances (Table 4.6) with Mn^{2+} substitution. The equations (4.7), (4.8) and (4.9) respectively have been used to compute of edge lengths *R*, *R′*and *R″* values.

R the tetrahedral edge length reduces on adding Mn^{2+} metal cations (Table 4.6) on account of the decrease in r_A. The variation of *R′*,*R″* is credited to the distribution of metal cations in A and B lattice sites. The *R′* enhances (Table 4.6) on Mn^{2+} addition and the *R″* (Table 4.6) shows variation in accordance with *a*.

Table 4.6: Several structural parameters calculated theoretically using proposed cation distribution

x	r_A (Å)	r_B (Å)	a_{th} (Å)	*u* (Å)	δ (Å)	R_A (Å)	R_B (Å)	*R* (Å)	R' (Å)	R'' (Å)
0.125	0.7252	0.6823	8.488	0.3891	0.0141	2.023	1.9881	3.304	2.634	2.978
0.250	0.7055	0.6822	8.457	0.3882	0.0132	2.004	1.9888	3.272	2.647	2.968
0.375	0.6857	0.6821	8.426	0.3874	0.0124	1.996	1.9982	3.259	2.671	2.972
0.500	0.6660	0.6820	8.396	0.3865	0.0115	1.987	2.0094	3.245	2.698	2.978

4.5 Conclusion

Taking choice of metal cations for crystallographic sites and experimental results of *XRD* results into consideration the chapter suggests the suitable distribution of cations for transition metal (*M*) doped *Mg-Zn* ferrites. The cation distribution provides a useful mean to investigate the various structural parameters of spinel ferrites. The observed variation in theoretically calculated structural parameters is mainly due to the dissimilarity in ionic radius of metal cations. The tetrahedral and octahedral mean ionic radii have been calculated for all prepared samples. The alteration in r_A and r_B depends on the ionic radius as well as on the preference of metal cations

for their respective crystallographic lattice sites. The investigation of theoretical lattice parameter for all prepared samples is in close agreement with experimental lattice parameter which also validates the proposed cation distribution. But, the variation in theoretically and experimentally calculated lattice parameter matches best with each other for Ni^{2+} doped samples as compared to Co^{2+} and Mn^{2+} doped samples. The oxygen positional parameter decreases for all prepared samples with increase in substitution of transition metal ions. The replacement of larger Zn^{2+} metal ions with smaller transition metal ions reduces tetrahedral sites expansion which is responsible for the decrease in oxygen positional parameter. The minimum value of inversion parameter has been observed for ferrite sample having maximum content of Co^{2+}. The tetrahedral and octahedral bonds lengths have been calculated for all prepared samples using proposed cation distribution. The distribution of metal cations in their corresponding crystallographic lattice sites plays dominant role in deciding the variation of tetrahedral and octahedral bonds lengths. The distribution of cations indicate that the preference of metal cations for crystallographic lattice sites and their ionic radii plays important role in varying the various structural parameters of spinel ferrites.

CHAPTER 5*

MAGNETIC STUDIES OF TRANSITION METAL DOPED *Mg-Zn* FERRITES

* **Rohit Sharma,** P. Thakur , M. Kumar , N. Thakur, N. S. Negi, P. Sharma, V. Sharma, Improvement in magnetic behaviour of cobalt doped magnesium-zinc nano-ferrites via co-precipitation route, **Journal of Alloys and Compounds**, 684,569-581 (2016)

Rohit Sharma, P. Thakur, P. Sharma, V. Sharma, Ferrimagnetic Ni^{2+} doped Mg-Zn spinel ferrite nanoparticles for high density information storage, **Journal of Alloys and Compounds**, 704, 7-17 (2017)

Rohit Sharma, P. Thakur , M. Kumar, P.B. Barman, P. Sharma, V. Sharma , Enhancement in A-B super-exchange interaction with Mn^{2+} substitution in *Mg-Zn* ferrites as a heating source in hyperthermia applications, **Ceramics International**, 43,13661-13669 (2017)

This chapter describes the magnetic studies of transition metal ($M = Co^{2}$, Ni^{2+} and Mn^{2+}) doped *Mg-Zn* ferrites. Several parameters such as coercivity, retentivity, saturation magnetization *etc.* which are important to explain the magnetic nature of prepared samples have been calculated.

5.1 Introduction

Nanoparticles of spinel ferrites have fascinated the scientific community for their distinctive and interesting magnetic properties. These magnetic nanoparticles show importance in various applications like information storage, magnetic recording, power transformers, magnetic resonance imaging, magnetically targeted delivery of drugs, magnetic hyperthermia and magnetic contrast agents *etc.* [1-5]. Bhongale *et al.* have reported that the higher saturation magnetization in Nd^{3+} substituted *Mg-Cd* spinel nano ferrites make them useful in high density recording applications [6]. Mansour *et al.* have investigated the Cr^{3+} doped manganese-zinc nano ferrites and reported that they are valuable in computer memories and magnetic recording applications [7].

Mg-Zn ferrite is one of the vital metal oxide system among spinel ferrites due to its soft magnetic nature, high resistivity, low dielectric losses, high Curie temperature, cost effectiveness and superior environmental persistence [8]. There are numerous reports in the literature on magnetic properties of *Mg-Zn* ferrites [8, 9]. *Mg-Zn* spinel ferrites are useful in several technologically important applications such as memory recording devices, loading coils, recording heads, transformer cores and microwave devices [9]. These also show potential applications in biomedical and sensing applications. The *Mg-Zn* spinel ferrites can be explored for magnetic hyperthermia applications [10]. These materials are also suitable for sensor based applications [11].

The magnetic behavior of spinel ferrites is decided by the magnitude of A-B super-exchange interaction between metal cations. But, in *Mg-Zn* ferrite system, the Mg^{2+} and Zn^{2+} metal ions are diamagnetic in nature and hence decrease the magnitude of super-exchange interaction [12, 13]. The placement of metal cations in crystallographic lattice sites play key role in deciding the magnitude of A-B super-exchange interaction. In order to enhance the magnitude of A-B super-exchange interaction the replacement of Zn^{2+} metal ions with magnetic metal ions may be useful. The divalent Zn^{2+} ions have strong preference for tetrahedral sites (A) and their replacement with

magnetic metal ions will align magnetic metal ions in antiparallel arrangement which may result in enhancement of A-B super-exchange interaction [14]. Among various metal ions the substitution of transition metal ions is known for modifying the magnetic properties of spinel ferrites [15]. Co^{2+} metal ions are considered as useful dopant because of large coercivity, chemical stability, moderate saturation magnetization and good mechanical strength [16]. The large magneto-crystalline anisotropy of Co^{2+} metal ions enhances the A-B super-exchange interaction as well as their magnetic behaviour. The substitution of Ni^{2+} metal ions also leads to modification in the magnetic behaviour of spinel ferrites [17, 18]. Ni^{2+} metal ions have magnetic moment of 2 μB and are of soft magnetic nature [19]. Several authors have reported for the Ni^{2+} substituted ferrites. Padmapriya *et al.* have reported that the substitution of ferromagnetic Ni^{2+} doping on replacing Zn^{2+} metal ions enhances the coercivity of zinc ferrite [20]. Jalaiah *et al.* and Topkaya *et al.* and have explained that the substitution of Ni^{2+} metal ions increase the coercivity of *Mn –Zn* and *Mn* spinel ferrites respectively [21, 22]. Numerous reports show the substitution of Mn^{2+} metal ions to alter the magnetic characteristics of spinel ferrites. Mn^{2+} doped Zn ferrites show high permeability with low magnetic losses [23]. The Mn^{2+} added *Mg-Zn* spinel ferrites may also be explored for high frequency device applications [24]. The possible bio-compatibility and desired thermal properties also make Mn^{2+} doped spinel ferrites useful for hyperthermia applications [25].In the present work the divalent Zn^{2+} metal ions have been replaced by transition metal ($M = Co^{2+}$, Ni^{2+} and Mn^{2+}) metal ions to modify the magnetic properties of *Mg-Zn* ferrites.

5.2 Experimental details

The transition metal (*M*) doped *Mg-Zn* ferrites have been synthesized using co-precipitation route described with detail in section 2.3. The magnetic properties for prepared powdered samples have been investigated using Vibrating sample magnetometer (PAR-155). The magnetic field in the range *-10 kOe* to *+10 kOe* has been applied for magnetic measurements.

5.3 Results and discussion

In this section, the magnetic properties of transition metal (*M*) doped *Mg-Zn* ferrites have been described.

5.3.1 Magnetic properties of $Mg_{0.5}Zn_{0.5-x}Co_xFe_2O_4$ ferrites

The M-H curves for $Mg_{0.5}Zn_{0.5-x}Co_xFe_2O_4$ ferrite samples have been shown in figure 5.1.

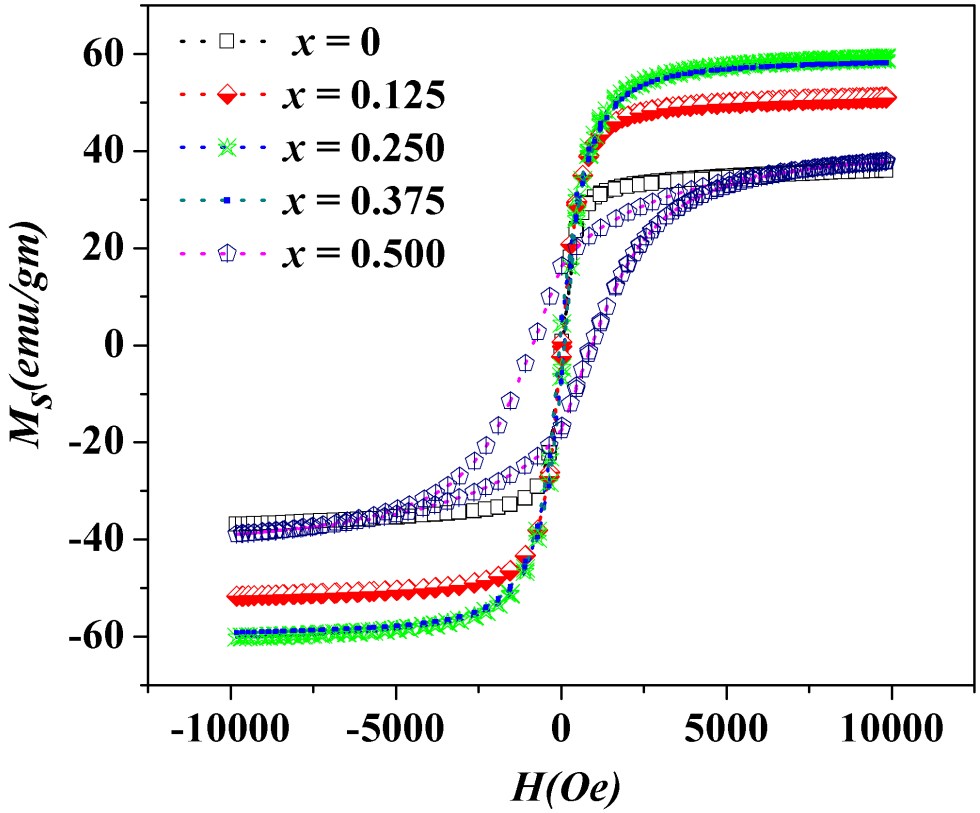

Figure 5.1: M-H curves for $Mg_{0.5}Zn_{0.5-x}Co_xFe_2O_4$ ferrites

For x = 0 and 0.125 samples, typical S shaped curves have been observed. The presence of S shaped curves for these samples signify their superparamagnetic character. Figures 5.2 show zoomed M-H curves for x = 0 and x = 0.125 samples which confirm the superparamagnetic nature. The presence of superparamagnetic character indicate that the thermal energy have been sufficient to overcome the magneto-crystalline anisotropy which holds the magnetic ordering in certain directions [26]. The Mg^{2+} and Zn^{2+} metal ions are diamagnetic in nature and do not contribute to magneto-crystalline anisotropy. The magneto-crystalline anisotropy is contributed only by trivalent Fe^{3+} metal ions which may not be enough to keep the magnetic ions in particular direction. The presence of superparamagnetism indicates that the blocking temperature have been overcome by thermal energy [27]. The less disorder in spin leads to decrease in magneto-crystalline anisotropy which may also be responsible for superparamagnetic behaviour [28].

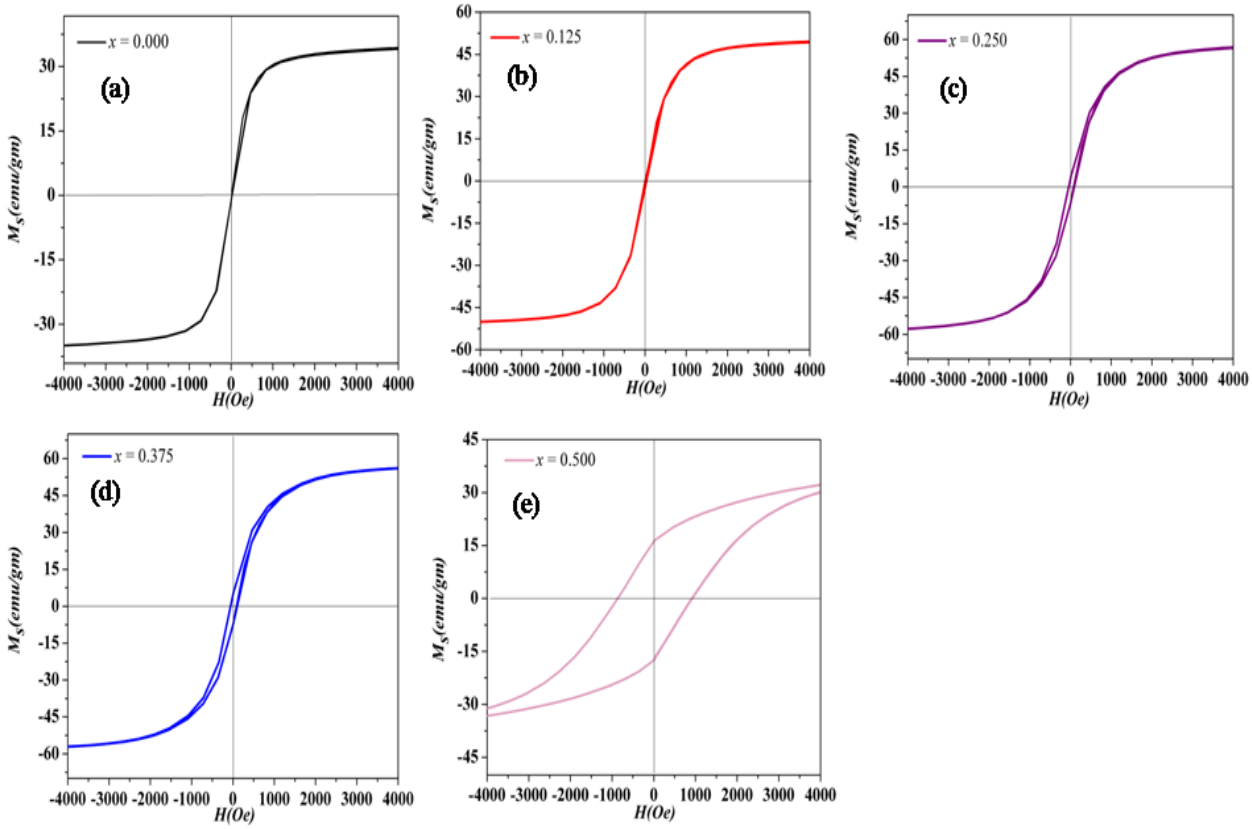

Figure 5.2 : Zoomed image of M-H curves for $Mg_{0.5}Zn_{0.5-x}Co_xFe_2O_4$ ferrite samples

The magnetic nature of prepared samples transform from superparamagnetic to ferrimagnetic for $x > 0.125$. The substitution of Co^{2+} metal ions create anti-parallel alignment between trivalent Fe^{3+} and divalent Co^{2+} ions at A and B sites respectively. The anti-parallel alignment between Co^{2+} and Fe^{3+} ions enhances the A-B super-exchange interaction which may be responsible for transition of magnetic character of prepared samples from super-paramagnetic to ferrimagnetic [29]. The zoomed M-H curves for prepared samples (Figure 5.2 (c-e)) which clearly indicate that $x = 0.250$, $x = 0.375$ and $x = 0.500$ sample are ferrimagnetic in nature. The coercivity (H_c) and retentivity (M_r) values increase (Table 5.1) with increase in Co^{2+} substitution. It is due to the large magneto-crystalline anisotropy of Co^{2+} metal ions because of strong L-S coupling and three unpaired electrons [30]. The magneto-crystalline anisotropy, shape anisotropy, size anisotropy and surface anisotropy are the major factors influencing the value of coercivity [31]. The magneto-crystalline anisotropy is mainly responsible for the variation in coercivity. The value of K_a for Co^{2+} is +ve as it has single easy magnetization axis [31].

Table 5.1: Magnetic parameters calculated for $Mg_{0.5}Zn_{0.5-x}Co_xFe_2O_4$

x	M_r (emu/gm)	H_c (Oe)	M_s (emu/gm)	η_B (μ_B)	K_a (erg/cm^3)	R
0	-	-	36.18	1.42	-	-
0.125	-	-	50.92	2.00	-	-
0.250	4.95	66.40	59.41	2.32	4025.33	0.083
0.375	6.11	73.72	58.52	2.28	4402.13	0.104
0.500	16.60	883.40	37.30	1.48	34524.71	0.433

For $x > 0.125$, the value of K_a has been calculated according to Stoner- Wohlfarth theory using equation (2.7).The anisotropy constant increases with Co^{2+} substitution (Table 5.1). The values of anisotropy constant indicate that the free and easy movement of domain walls get inhibited. Stoner–Wohlfarth theory states that the saturation magnetization and coercivity are related inversely with each other [32] and the same has been observed for $x > 0.125$. Figure 5.3 shows the change in values of H_c *and* M_s with cobalt content.

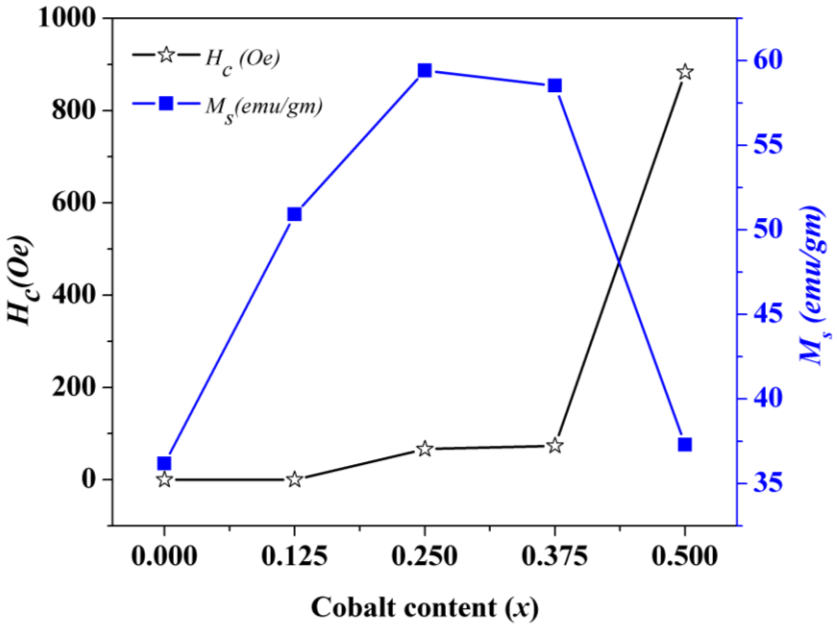

Figure 5.3: Variation of H_c and M_s with cobalt substitution

The equation (2.8) has been used to calculate the observed magnetic moment (η_B) for prepared samples. The value of magnetic moment varies between 1.42 μB to 2.32μB. This change in magnetic moment (Table 5.1) is in accordance with variation in the value of M_s. The value of the remanence ratio (R) has been calculated using equation (2.9). The value of R has shown variation

from 0.083 to 0.433. Remanence ratio signifies that how easily the magnetization gets aligned along the direction of easy axis on removing the applied magnetic field [33]. The increase in remanence ratio (Table 5.1) confirms the emergence of anisotropic behaviour for prepared samples.

The super-exchange interaction among metal ions at A and B crystallographic sites is responsible for magnetic properties in spinel ferrites. The magnetic moment for the non-collinear alignment of cations at A and B crystallographic sites have collinear spin arrangement, known as Neel's collinear arrangement.

Figure 5.4 shows the collinear arrangement of spins suggested by Neel.

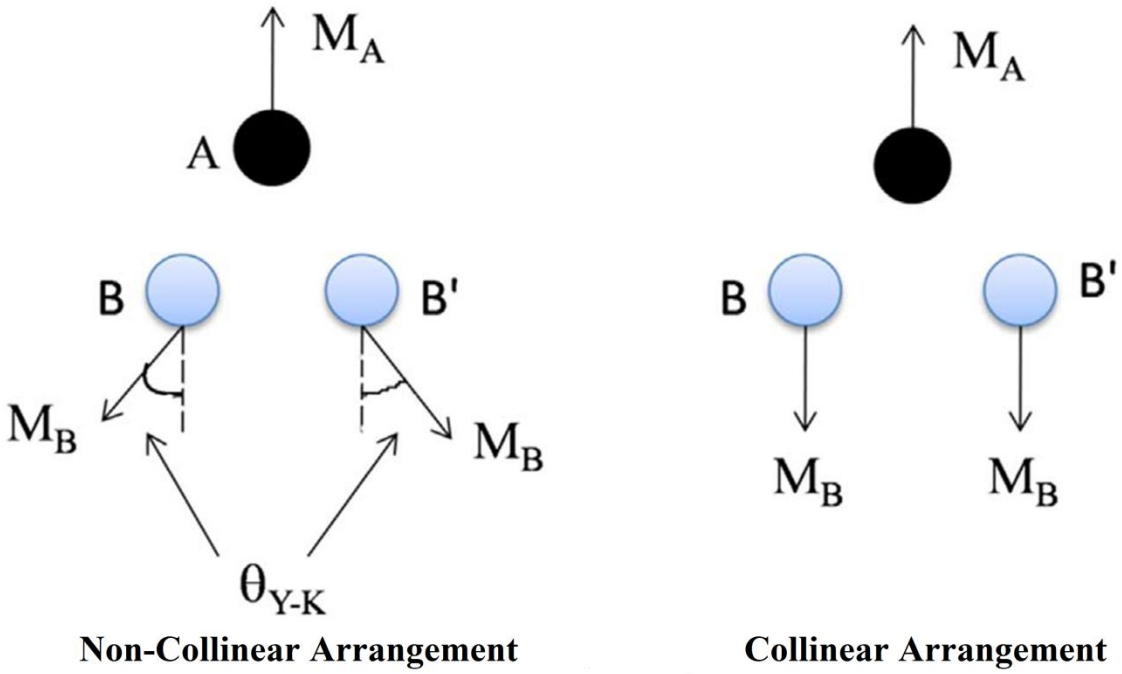

Figure 5.4: Neel's collinear and Yafet-Kittel's non-collinear arrangement of spins

According to proposed cation distribution (Table 4.1) and utilizing the magnetic moment values of Mg^{2+} (0 μB), Zn^{2+} (0 μB), Fe^{3+} (5 μB) and Co^{2+} (3 μB) metal ions, the net magnetic moment ($M_{cal.}$) has been calculated using equation [34];

$$M_{cal.} = M_B - M_A \tag{5.1}$$

where M_A and M_B represent net magnetic moment of respective lattice sites at A and B. The value of $M_{cal.}$ changes from 5 μB to 1.5 μB (Table 5.2) with increase in Co^{2+} substitution. Using

proposed cation distribution (Table 4.1) the cation-anion distances, cation- cation distances and bond angles between different ion pairs have been calculated. This helps to further analyze the effect of Co^{2+} substitution on magnetic exchange interactions.

Figure 5.5 shows cation- anion and cation-cation pairs with their distances and angles between them.

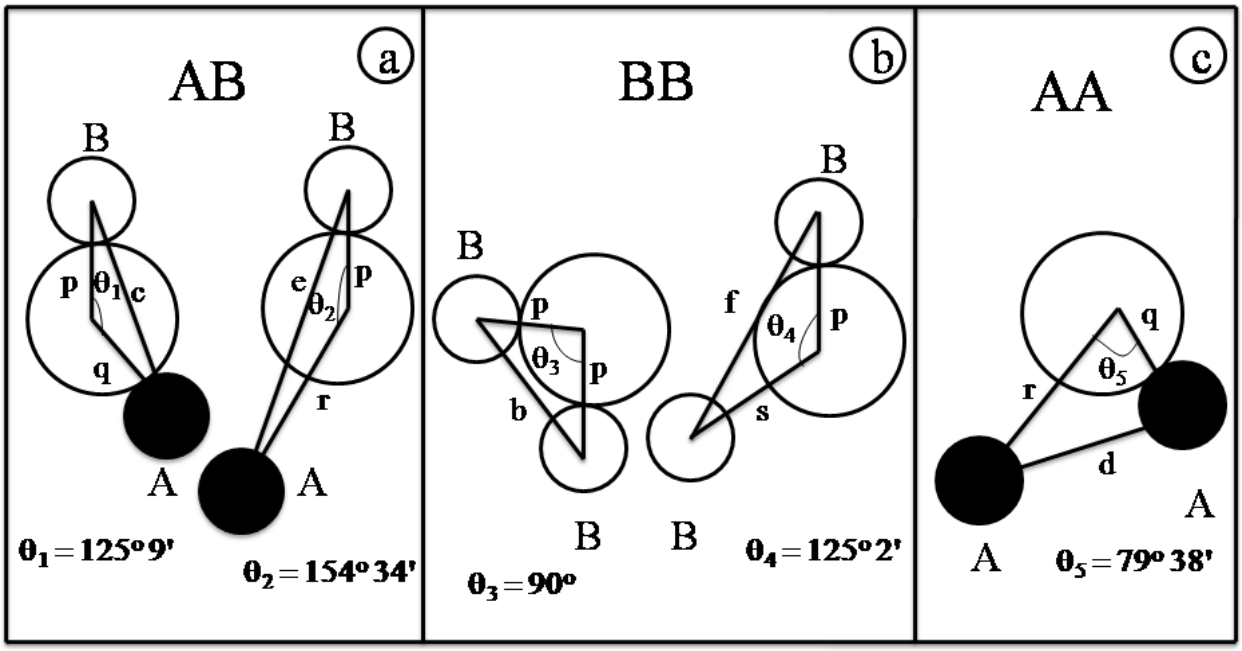

Figure 5.5: The interionic distances and bond angles

The interionic distances have been computed employing following equations [35];

For cation–anion inter distances

$$p = a((5/8) - u) \tag{5.2}$$

$$s = a((1/3u) + (1/8))\sqrt{3} \tag{5.3}$$

where p and s are the interionic distance separating cation at B site and O^{2-} anion.

$$r = a(u - 1/4)\sqrt{11} \tag{5.4}$$

$$q = a(u - 1/4)\sqrt{3} \tag{5.5}$$

where r and q are the interionic distance separating cation at A site and O^{2-} anion.

For cation-cation inter distances

$$b = (a/4)\sqrt{2} \tag{5.6}$$

$$f = (a/4)\sqrt{6} \tag{5.7}$$

where b and f are the interionic distance between cations situated at two different B sites.

$$c = (a/8)\sqrt{11} \tag{5.8}$$

$$e = (3a/8)\sqrt{3} \tag{5.9}$$

where c and e are the interionic distance between A site cation and B site cation.

$$d = (a/4)\sqrt{3} \tag{5.10}$$

where d is the distance between cations situated at two different A sites.

The calculated values of interionic distances are shown in Table 5.2.

Table 5.2: Net calculated magnetic moment and interionic distances for $Mg_{0.5}Zn_{0.5-x}Co_xFe_2O_4$ ferrites

x	$M_{cal.}$ (μ_B)	p (Å)	q (Å)	r (Å)	s (Å)	b (Å)	c (Å)	d (Å)	e (Å)	f (Å)
0	5.00	1.977	2.038	3.902	3.714	2.973	3.486	3.642	5.463	5.131
0.125	4.125	1.986	2.023	3.874	3.710	2.973	3.487	3.642	5.464	5.131
0.250	4.500	1.980	2.000	3.836	3.686	2.957	3.467	3.622	5.433	5.103
0.375	3.625	1.962	1.966	3.759	3.634	2.919	3.422	3.575	5.363	5.037
0.500	1.500	2.00	1.973	3.778	3.683	2.964	3.475	3.630	5.446	5.114

The bond angles have been computed employing interionic distances (Table 5.2) using the following equations [36].

$$\theta_1 = \cos^{-1}[(p^2 + q^2 - c^2)/2pq] \tag{5.11}$$

where θ_1 is the angle between inter-ionic distance p and inter-ionic distance q.

$$\theta_2 = \cos^{-1}[(p^2 + r^2 - e^2)/2pr] \tag{5.12}$$

where θ_2 is the angle between inter-ionic distance p and inter-ionic distance r.

$$\theta_3 = \cos^{-1}[(2p^2 - b^2)/2p^2] \quad (5.13)$$

where θ_3 is the angle between two different p inter-ionic distances.

$$\theta_4 = \cos^{-1}[(p^2 + s^2 - f^2)/2ps] \quad (5.14)$$

where θ_4 is the angle between inter-ionic distance p and inter-ionic distance s.

$$\theta_5 = \cos^{-1}[(r^2 + q^2 - d^2)/2rq] \quad (5.15)$$

where θ_5 is the angle between inter-ionic distance q and inter-ionic distance r.

The values obtained for interionic bond angles have been shown in Table 5.3. The bond angle θ_1, θ_2 and θ_5 increase while θ_3 and θ_4 decrease with Co^{2+} substitution. The increase in value of θ_1, θ_2 and θ_5 signify the enhancement of A-B and A-A exchange interaction while the decrease of θ_3 and θ_4 indicate decrease in the strength of B-B exchange interactions. [37]. The Co^{2+} ions at B sites and Fe^{3+} ions at A sites enhances the A-B super-exchange interaction. Alike variation in magnetic exchange interactions has been described for various other spinel ferrites [37].

Yafet–Kittel (*Y-K*) model has also been used to get insight about the magnetic exchange interactions and spin arrangement. *Y-K* model states that the B sub-lattice can be alienated into B_1 and B_2 sublattice. The B_1 and B_2 sub-lattices have non-collinear arrangement of spin which is also known as triangular spin arrangement [38]. Figure 5.4 shows the Yafet-Kittel non collinear arrangement of spin. The calculation of *Y-K* angles ($\alpha_{Y\text{-}K}$) has been done using equation (2.10). The *Y-K* angles decreases (Table 5.3) from $\alpha_{Y\text{-}K}$ = 58.48 for x = 0 to $\alpha_{Y\text{-}K}$ = 22.61 for x = 0.500. This indicates the enhancement of the A-B super-exchange interaction and the transition of non-collinear arrangement of spin to collinear arrangement.

Table 5.3: Bond angles and Y-K angles for $Mg_{0.5}Zn_{0.5-x}Co_xFe_2O_4$ ferrites

x	θ_1	θ_2	θ_3	θ_4	θ_5	$\alpha_{Y\text{-}K}$
0	120.53	133.91	97.51	126.91	67.37	58.48
0.125	120.78	134.80	97.07	126.82	67.96	45.24
0.250	121.06	135.83	96.58	126.71	68.64	50.15
0.375	121.35	136.88	96.09	126.62	69.33	46.67
0.500	121.60	137.82	95.67	126.52	69.95	22.61

5.3.2 Magnetic properties of $Mg_{0.5}Zn_{0.5-x}Ni_xFe_2O_4$ ferrites

Figure 5.6 shows the room temperature M-H curves for $Mg_{0.5}Zn_{0.5-x}Ni_xFe_2O_4$ ferrites.

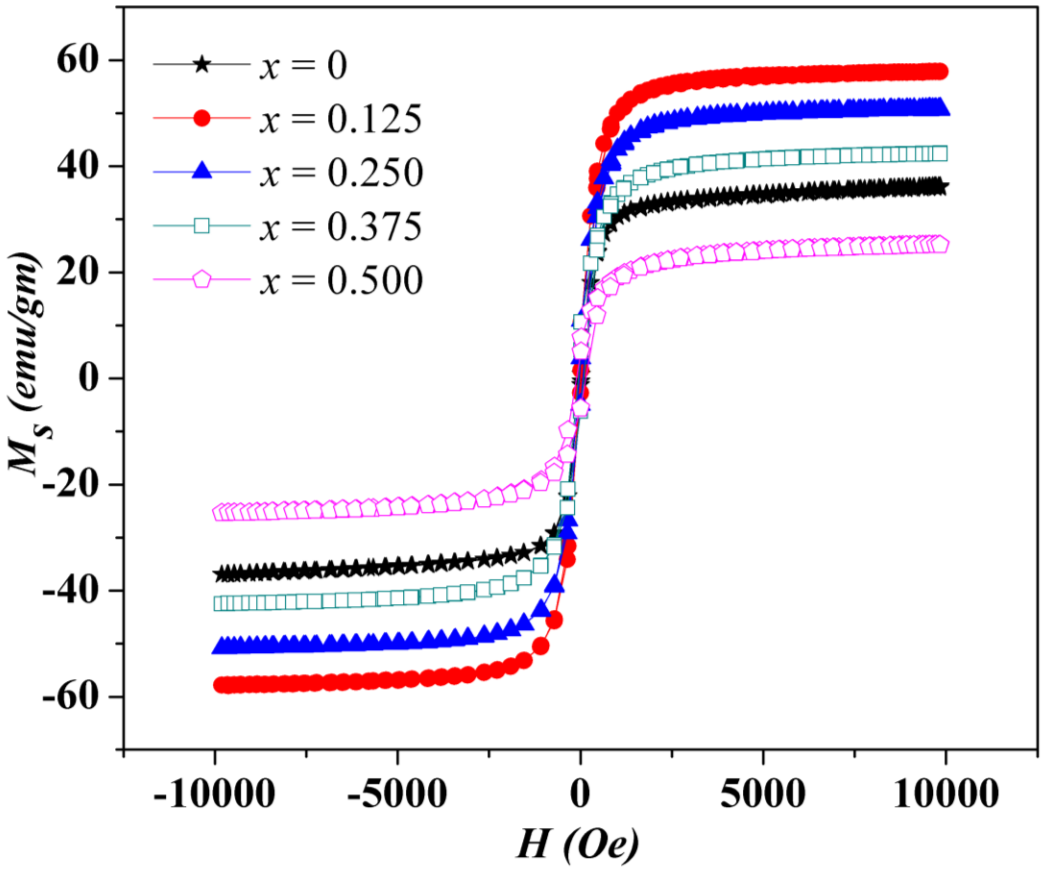

Figure 5.6: M-H curves for $Mg_{0.5}Zn_{0.5-x}Ni_xFe_2O_4$ ferrites

The magnetic behaviour changes from superparamagnetic to soft ferrimagnetic behaviour with Ni^{2+} substitution. The magnetic Ni^{2+} metal ions having magnetic moment of $2\mu B$ are responsible for transition from superparamagnetic to ferrimagnetic nature. Figure 5.7 shows the zoomed image of M-H curves for $Mg_{0.5}Zn_{0.5-x}Ni_xFe_2O_4$ ferrite samples which clearly indicate the presence of ferrimagnetic nature for prepared samples ($x \geq 0.125$).

The substitution of Ni^{2+} metal ions enhances the magneto-crystalline anisotropy. This enables the samples to be capable of sustaining magnetic order in certain direction and show soft ferrimagnetic nature. Several authors have reported presence of soft magnetic nature for Ni^{2+} doped spinel ferrites [20-22].

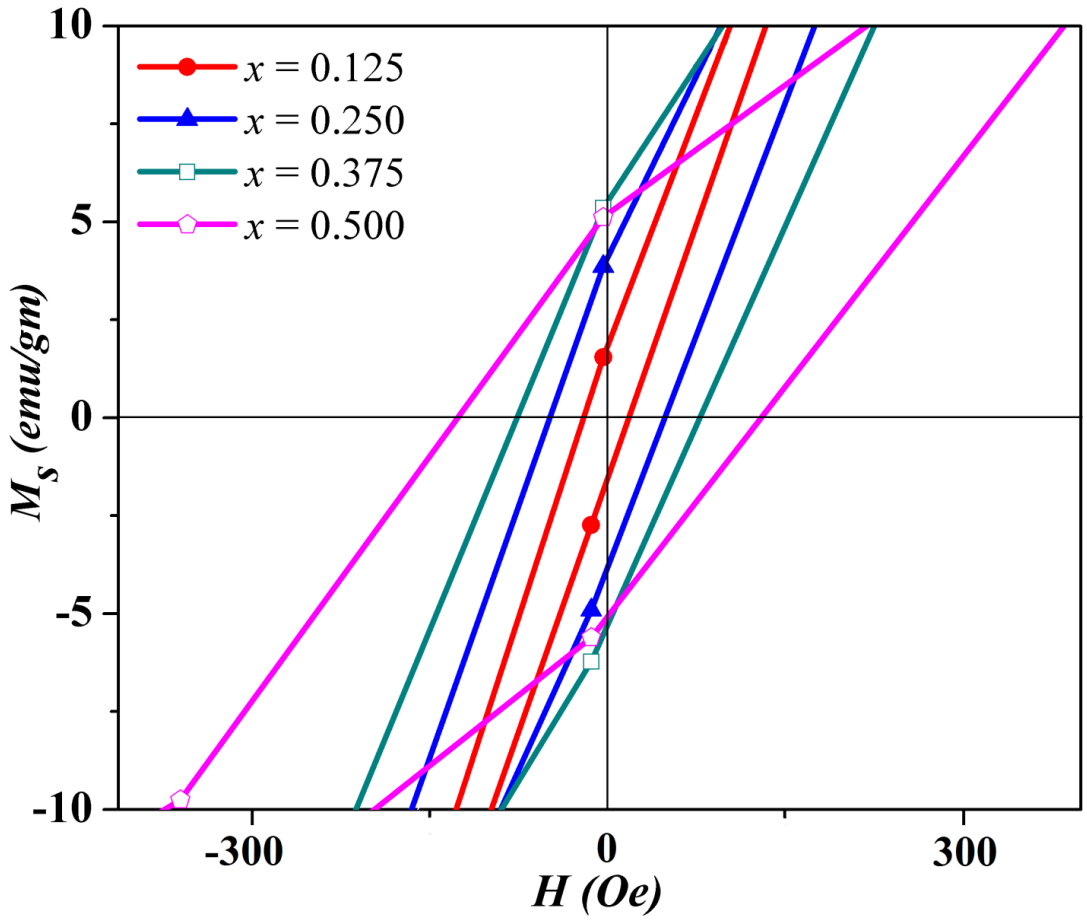

Figure 5.7: Zoomed image of M-H curves for $Mg_{0.5}Zn_{0.5-x}Ni_xFe_2O_4$ ferrites

The values of H_c, M_r and M_s determined using curves for M versus H (Table 5.4). The saturation magnetization decreases (Table 5.4) with Ni^{2+} substitution. The interaction of transition metal cations with O^{2-} anions gives rise to surface distortions which decrease the saturation magnetization. The disorder and frustration of the spins at the surface of the nanoparticles increase with decrease in size due to large ratio of surface/volume [39]. The value of H_c and M_r increases with Ni^{2+} substitution (Table 5.4). The values of coercivity obtained in present work are large in comparison to the values reported by Padmapriya *et al.* [20] on replacing Zn^{2+} metal ions with Ni^{2+} metal ions. This is because of the large K_a value of Ni^{2+} metal ions [40]. Magneto-crystalline anisotropy is inherent property of magnetic materials which decides their coercive nature [31]. The K_a has been calculated using equation (2.7) and it increases (Table 5.4) from 1.103×10^3 erg/cm^3 to 3.242×10^3 erg/cm^3 with Ni^{2+} content. The observed value of η_B for has been computed from equation (2.8), it decreases (Table 5.4) with increase in Ni^{2+} substitution.

The increase in interaction between the oxygen anions and transition metal ion decreases the magnetic moment with Ni^{2+}addition. The remanence ratio has been calculated using equation (2.9) and it increases (Table 5.4) from 0.028 for x = 0.125 to 0.203 for x = 0.500. The smaller value of remanence ratio suggests that the prepared samples are isotropic in nature [33].

Table 5.4: Magnetic parameters calculated for $Mg_{0.5}Zn_{0.5-x}Ni_xFe_2O_4$ ferrites

x	M_r (emu/gm)	H_c (Oe)	M_s (emu/gm)	η_B (μ_B)	K_a (erg/cm^3)	R
0.125	1.64	18.69	57.84	2.26	1103.00	0.028
0.250	3.78	48.05	50.75	1.98	2488.00	0.074
0.375	5.11	75.13	42.18	1.64	3233.00	0.121
0.500	5.15	125.58	25.30	0.99	3242.00	0.203

Using the proposed cation distribution for $Mg_{0.5}Zn_{0.5-x}Ni_xFe_2O_4$ ferrites (Table 4.4) and the magnetic moment values of Mg^{2+} (0 μB), Fe^{3+} (5 μB), Zn^{2+}(0 μB) and Ni^{2+} (2 μB) metal ions the $M_{cal.}$ has been calculated employing equation (5.1). The value of $M_{cal.}$ decreases (Table 5.5) with Ni^{2+} substitution on account of choice of occupation of divalent Ni^{2+} ions for B lattice sites. Ni^{2+} substitution migrates Fe^{3+} metal ions from B to A lattice sites which raises the value of magnetic moment at A lattice sites and therefore, decrease the value of net calculated magnetic moment. The cation-cation distances, cation-anion distances and interionic bond angles have been computed from relations (5.2) to (5.11) and listed in Table 5.5.

Table 5.5: Net calculated magnetic moment and interionic distances *for* $Mg_{0.5}Zn_{0.5-x}Ni_xFe_2O_4$ ferrites

x	$M_{cal.}$ (μB)	p (Å)	q (Å)	r (Å)	s (Å)	b (Å)	c (Å)	d (Å)	e (Å)	f (Å)
0.125	4	1.977	2.020	3.868	3.698	2.964	3.476	3.630	5.446	5.134
0.250	3	1.985	2.007	3.843	3.694	2.964	3.476	3.630	5.445	5.134
0.375	2	1.990	1.991	3.813	3.686	2.961	3.472	3.626	5.440	5.128
0.500	1	1.988	1.971	3.775	3.666	2.948	3.457	3.610	5.416	5.106

The increase in bond angle θ_1, θ_2 and θ_5 has been observed while θ_3 and θ_4 decrease with Ni^{2+} substitution (Table 5.6). The increase in θ_1, θ_2 and θ_5 signify enhancement of A-B and A-A

exchange interactions respectively. Ni^{2+} metal ions on replacing the diamagnetic Zn^{2+} metal ions create an antiparallel arrangement of magnetic metal ions which strengthens the magnitude of A-B super-exchange interaction. The Ni^{2+} ion addition migrates Fe^{3+} ions from lattice sites B to A enhancing the A-A exchange interaction.

The angle θ_3 and θ_4 decreases on Ni^{2+} substitution signifying the weakening of the magnetic exchange interaction between B lattice site metal ions *i.e.* B-B exchange interaction. The Fe^{3+} ($5\mu B$) migration from B to A lattice sites on substituting Ni^{2+} ($2\mu B$) which reduces the value of net magnetic moment of B lattice site metal ions. This depreciates the B-B exchange interaction. The Yafet-Kittel angles $\alpha_{Y\text{-}K}$ have been calculated to get an insight about magnetic exchange interaction using equation (2.10). The values of *Y-K* angle decrease (Table 5.6) with Ni^{2+} substitution which suggests the strengthening of A-B super-exchange interaction [38]

The variation in *Y-K* angles with Ni^{2+} substitution also indicate that the wave functions corresponding to nearby magnetic metal ions get overlapped which raises the magnitude of A-B super-exchange interaction [41].

Table 5.6: Bond angles and Y-K angles for $Mg_{0.5}Zn_{0.5-x}Ni_xFe_2O_4$ ferrites

x	θ_1	θ_2	θ_3	θ_4	θ_5	$\alpha_{Y\text{-}K}$
0.125	120.78	134.80	97.07	126.82	67.96	40.90
0.250	121.06	135.83	96.58	126.71	68.64	31.90
0.375	121.35	136.88	96.09	126.62	69.33	19.34
0.500	121.60	137.82	95.67	126.52	69.95	3.30

5.3.3 Magnetic properties of $Mg_{0.5}Zn_{0.5-x}Mn_xFe_2O_4$ ferrites

The M-H curves for $Mg_{0.5}Zn_{0.5-x}Mn_xFe_2O_4$ ferrites obtained at room temperature have been shown in figure 5.8. The magnetic nature of prepared samples shows transition from superparamagnetic (for $x = 0$) to ferrimagnetic behaviour (for $x \geq 0.125$) with Mn^{2+} substitution.

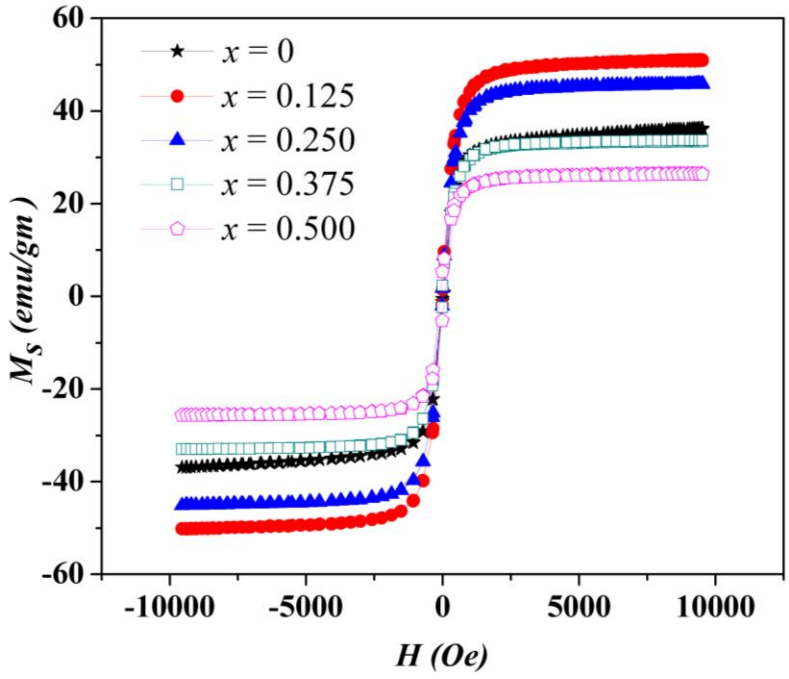

Figure 5.8: M-H curves for $Mg_{0.5}Zn_{0.5-x}Mn_xFe_2O_4$ ferrites

Figure 5.9 shows the zoomed image of M-H curves for prepared samples indicating the ferrimagnetic nature.

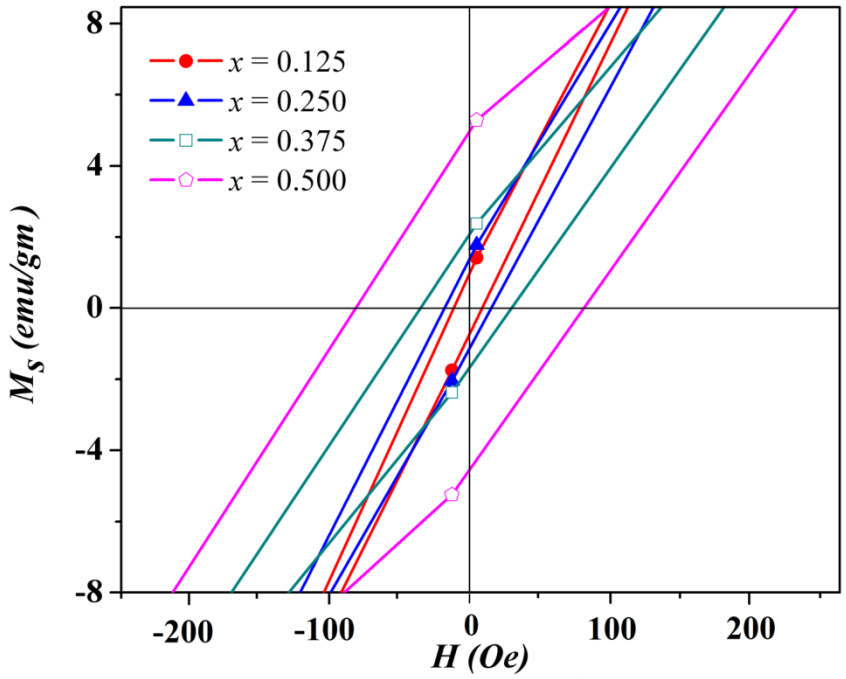

Figure 5.9: Zoomed image of M-H curves for $Mg_{0.5}Zn_{0.5-x}Mn_xFe_2O_4$ ferrite samples

The replacement of diamagnetic Zn^{2+} metal ions by magnetic Mn^{2+} (5 μB) metal ions lead to the appearance of soft ferrimagnetic behaviour. The M versus H curves in Figure 5.6 has been used to calculate M_r and H_c values (Table 5.7). There is an increase in value of retentivity and coercivity (Table 5.7) with Mn^{2+} substitution. The Mn^{2+} metal ions have zero angular momentum. Hence the contribution of lattice coupling and magneto crystalline anisotropy are not present. Therefore, the magnetic moment (5 μB) corresponding to spin motion of Mn^{2+} ions increases the value of H_c [9]. The increase in coercivity with Mn^{2+} substitution signifies A-B super-exchange interaction enhancement. The increase of Mn^{2+} causes the existence of magnetic ions on A and B sites intensifying the A-B super-exchange interaction. The value of M_s varies contrary to the coercivity. The equation (2.7) has been used to calculate the anisotropy constant. It increases (Table 5.7) with Mn^{2+} substitution. The observed value of η_B has been computed using equation (2.8). It decreases (Table 5.7) with Mn^{2+} substitution. This is due to the increase in net value of magnetic moment at A lattice sites. The R has been computed using equation (2.9). The values of R for all prepared samples (Table 5.7) are less than 0.5 which indicates multi-magnetic domain presence in prepared samples.

Table 5.7: Magnetic parameters calculated for $Mg_{0.5}Zn_{0.5-x}Mn_xFe_2O_4$ ferrites

x	M_r (emu/gm)	H_c (Oe)	M_s (emu/gm)	η_B (μ_B)	K_a (erg/cm^3)	R
0.125	0.851	10.22	50.58	1.98	527.00	0.016
0.250	1.267	17.10	45.34	1.76	791.00	0.027
0.375	1.863	32.76	33.85	1.31	1130.00	0.055
0.500	4.712	81.63	26.05	1.00	2160.00	0.180

The value of $M_{cal.}$ for Mn^{2+} substituted samples has been calculated using equation (5.1) The values of magnetic moment for Mg^{2+} (0μB), Mn^{2+} (5μB), Zn^{2+} (0μB) and Fe^{3+} (5μB) have been used in accordance with the suggested distribution of cations for $Mg_{0.5}Zn_{0.5-x}Mn_xFe_2O_4$ ferrites (Table 4.5) in equation (5.1) to calculate the net magnetic moment. The value of $M_{cal.}$ decreases (Table 5.8) with Mn^{2+} substitution. The substitution of Mn^{2+} migrate Fe^{3+} metal ions from B-lattice sites to A-lattice sites as the value of magnetic moment at A sites increase which decreases the $M_{cal.}$ value. The magnetic exchange interactions have been investigated using Table 4.5.

Table 5.8: Net calculated magnetic moment and interionic distances for $Mg_{0.5}Zn_{0.5-x}Mn_xFe_2O_4$ ferrites

x	$M_{cal.}$ μB	p (Å)	q (Å)	r (Å)	s (Å)	b (Å)	c (Å)	d (Å)	e (Å)	f (Å)
0.125	4.375	1.981	2.023	3.874	3.704	2.969	3.481	3.636	5.454	5.142
0.250	3.750	1.982	2.004	3.837	3.689	2.960	3.471	3.625	5.438	5.127
0.375	3.125	1.992	1.996	3.822	3.691	2.965	3.477	3.631	5.447	5.136
0.500	2.500	2.004	1.987	3.805	3.695	2.971	3.484	3.639	5.459	5.147

The interionic bond angles (Table 5.9) have been computed using cation-cation distances and cation anion lengths (Table 5.8).The increase in calculated value of angles θ_1, θ_2 and θ_5 suggest strengthening of A-B super-exchange and A-A exchange interactions respectively [36]. The bond angles θ_3 and θ_4 decrease (Table 5.9) with Mn^{2+} substitution which suggests the decrease in magnitude of B-B exchange interactions [36].

The Yafet-Kittel (*Y-K*) model has been used to investigate the nature of magnetic exchange interactions. The equation (2.10) has been used to calculate the *Y-K* angles ($\alpha_{Y\text{-}K}$). The *Y-K* angles decrease (Table 5.9) with Mn^{2+} substitution suggesting the transition of arrangement of spins from non-collinear to collinear type of magnetic ordering [42].

Table 5.9: Bond angles and *Y-K* angles for $Mg_{0.5}Zn_{0.5-x}Mn_xFe_2O_4$ ferrites

x	θ_1	θ_2	θ_3	θ_4	θ_5	$\alpha_{Y\text{-}K}$
0.125	120.78	134.80	97.07	126.82	67.96	47.10
0.250	121.06	135.83	96.58	126.71	68.64	42.72
0.375	121.32	136.76	96.15	126.62	69.26	40.71
0.500	121.60	137.82	95.70	126.52	69.96	36.86

5.4 Analysis of retentivity and coercivity for transition metal doped *Mg-Zn* ferrites.

The value of retentivity, coercivity, anisotropy constant and remanence ratio increases with increase in transition metal content. The value of retentivity and coercivity has been observed to be larger in case of Co^{2+} doped samples in comparison to Ni^{2+} and Mn^{2+} doped samples (Figure 5.10). The value of coercivity has been observed to be maximum for Co^{2+} content *i.e.* $x = 0.500$.

The larger value of retentivity and coercivity for transition metal doped samples make them suitable for memory storage applications.

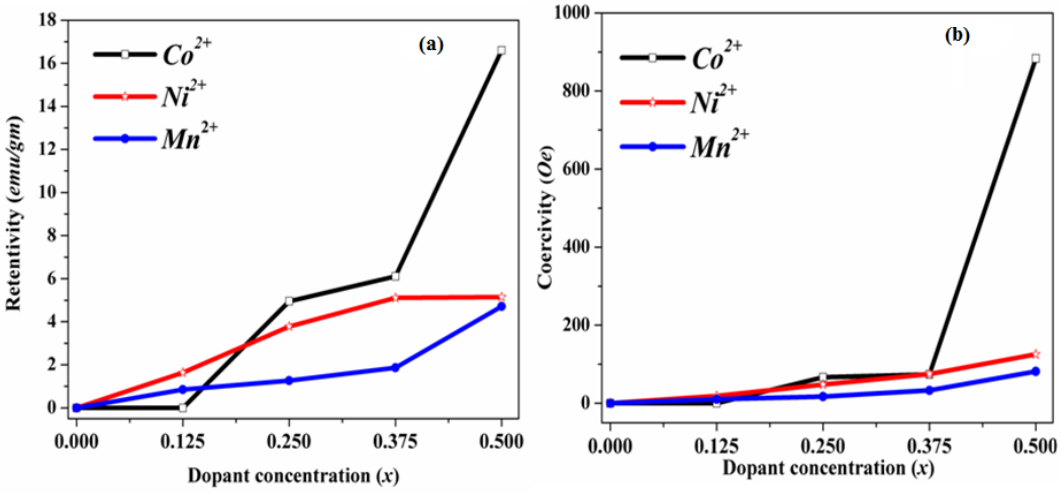

Figure 5.10: (a) Variation of retentivity& (b) Variation of coercivity with Co^{2+}, Ni^{2+} and Mn^{2+} doping

5.5 Conclusion

The magnetic properties of transition metal (*M*) doped $Mg_{0.5}Zn_{0.5-x}M_xFe_2O_4$ ferrites have been determined by analyzing their respective *M-H* curves. The super-paramagnetic character has been observed for $x = 0$ i.e. undoped sample. The super-paramagnetic character has also been observed for Co^{2+} doped *i.e.* $x = 0.125$ sample. With further increase in Co^{2+} substitution ($x > 0.125$) the magnetic behaviour has shown change from superparamagnetic to ferrimagnetic. It may be ascribed to the magnetic behaviour and high magneto-crystalline anisotropy of Co^{2+} ions. For Ni^{2+} and Mn^{2+} doped samples, the magnetic nature transforms from superparamagnetic to ferrimagnetic. The magnetic nature of Ni^{2+} and Mn^{2+} metal ions is responsible for appearance of ferrimagnetic behaviour. The Co^{2+} doped samples are more coercive in comparison to Ni^{2+} and Mn^{2+} doped samples. The higher magneto crystalline anisotropy of Co^{2+} metal ions in comparison to Ni^{2+} and Mn^{2+} metal ions make Co^{2+} doped samples more coercive. The remanence ratio has been calculated for all prepared samples. The smaller value of remanence ratio for prepared samples indicates the formation of multi-magnetic domain type of structure.

The magnetic parameters such as retentivity, saturation magnetization, calculated magnetic moment and *Y-K* angles have been calculated for all prepared samples. The observed values of magnetic parameters for Co^{2+}, Ni^{2+} and Mn^{2+} doped samples suggest their suitability for magnetic memory recording. The magnitude of exchange interactions present between magnetic

metal ions have been investigated theoretically using proposed cation distribution and Yafet-Kittel model. The theoretical calculation show an enhancement of A-B super-exchange interaction and indicate flipping of spin alignment from non-collinear to collinear on addition of transition metal element. The increase in the value of coercivity and retentivity with transition metal content supports the theoretical analysis of magnetic exchange interactions.

CHAPTER 6

SUMMARY AND FUTURE SCOPE

In present time, the spinel ferrite nanoparticles are of significant interest because of their remarkable magnetic and electrical properties. These remarkable properties make them industrially and technologically an important magnetic material. Spinel ferrites are utilized in several essential applications like memory storage, sensing, microwave instruments, photo-catalytic degeneration of toxic substances and for several biomedical applications such as magnetically targeted drug delivery, magnetic resonance imaging, magnetic hyperthermia, *etc.* There are various spinel ferrite systems such as magnesium, zinc, nickel, lithium, cobalt, manganese, nickel-zinc, manganese-zinc *etc.* The magnesium-zinc (*Mg-Zn*) ferrite system is one of the most important and promising ferrite system on account to its interesting behaviour showing soft magnetic nature, high magnetic permeability, low magnetic losses, high electrical resistivity, high thermal and chemical stability, better environmental stability *etc.* A large number of applications of *Mg-Zn* ferrite rely on its magnetic properties which depend on the super-exchange interaction between metal cations positioned on two different crystallographic lattice sites.

The existence of diamagnetic Zn^{2+} and Mg^{2+} metal ions at tetrahedral and octahedral lattice sites respectively in ferrite system of *Mg-Zn* reduce the magnitude of super-exchange interaction and diminishes magnetic character. It stressed upon the requirement for the addition of some metal ions which may strengthen the super-exchange interaction and enhance magnetic character. The replacement of diamagnetic Zn^{2+} metal ions having strong preference for A sites with transition metal ions enhances the magnetic behaviour. In present work the transition metal ($M = Co^{2+}$, Ni^{2+} and Mn^{2+}) replaces the diamagnetic Zn^{2+} metal ions and modifies the magnetic behaviour of *Mg-Zn* ferrite system. The synthesis technique plays an important part in governing the various physical attributes of spinel ferrites. There are several physical and chemical methods such as ball milling, sputtering, sol-gel, micro-emulsion, hydrothermal, co-precipitation *etc.* available for the synthesis of spinel ferrite nanoparticles. The availability of several parameters like pH, stirring time, stirring rate, synthesis temperature and requirement of a simple experimental setup make co-precipitation route an effective method for the synthesis of spinel ferrite nanoparticles. The current work has been performed using chemical route of co-precipitation. The prepared ferrite samples have been characterized for different properties like structural, morphological, elemental and magnetic using various sophisticated experimental techniques.

The co-precipitation method utilized in the present work proves to be an effective route for the preparation of spinel nanoferrites with good crystallinity. The evaluation of crystalline spinel structure for all prepared samples has been confirmed using *XRD* results. It also confirms the incorporation of transition metal ions into the lattice of *Mg-Zn* spinel ferrite. There is the presence of magnesium oxide and hematite phases for Mn^{2+} doped samples confirmed using *XRD* results. The heating of iron-hydroxide in the presence of air is the major factor responsible for the emergence of hematite phase. The existence of magnesium oxide phase has also been confirmed for Ni^{2+} doped samples. The *XRD* results provides an effective mean to estimate the various of structural parameters like crystallite size, inter-planar spacing, lattice constant, packing factor *etc.* for all prepared samples. The ionic radius of transition metal cations and their preference for their respective crystallographic lattice sites play major role in influencing the structural parameters. The calculation of crystallite size confirmed that all of the prepared samples are in nano-regime. The spinel structure for all prepared samples has also been confirmed using *FT-IR* spectroscopy. The presence of frequency bands for the tetrahedral and octahedral lattice site vibration confirm formation of spinel structure. The frequency band corresponding to tetrahedral lattice site is due the vibration of bond between metal cations situated at tetrahedral lattice site and oxygen anions. On the other hand the frequency band corresponding to octahedral lattice site is due the vibration of bond between metal cations situated at octahedral lattice site and oxygen anions. The cation distribution has been proposed for all prepared samples by taking the preference of metal cations for their respective crystallographic lattice sites and experimental *XRD* results into account. Cation distribution helps in the calculation of several parameters related to structure like mean ionic radii, inversion parameter, oxygen positional parameter, cation-cation and cation-anions distances, inter-ionic bond angles *etc.* which helps in understanding the different physical properties of prepared spinel ferrite samples.

The effect of transition metal substitution on morphology of prepared samples has been investigated from Field effect scanning electron microscope. The micrographs show that the transition metal substitution leads to the agglomeration of nanoparticles. The magnetic nature of transition metal ions is attributed to the agglomeration of nanoparticles. The *EDS* spectroscopy has been utilized to confirm the stoichiometry for all prepared samples. The obtained values of atomic % of cations and anion are approximately same to the expected values. The obtained

values of atomic % of cations and anions indicate that the co-precipitation route is efficient in keeping the prepared samples in stoichiometry.

The magnetic properties of prepared samples have been investigated using Vibrating sample magnetometer. The super-paramagnetic character has been observed for undoped sample. The super-paramagnetic character has also been observed for cobalt doped sample *i.e.* $x = 0.125$. The magneto-crystalline anisotropy which holds the spin orientation in definite direction is overcome by thermal energy. On increase in Co^{2+} ($x > 0.125$) substitution the superparamagnetic behaviour changes to ferrimagnetic. For Ni^{2+} and Mn^{2+} doped samples, transition from superparamagnetic to ferrimagnetic nature has been observed. The magnetic nature of Co^{2+}, Ni^{2+} and Mn^{2+} metal ions is responsible for the appearance of ferrimagnetic behaviour. The maximum enhancement in magnetic character has been observed for Co^{2+} doped samples in comparison to Ni^{2+} and Mn^{2+} doped samples. The high magneto-crystalline anisotropy of cobalt is attributed to the observed behaviour. Several magnetic parameters such as retentivity, saturation magnetization, calculated magnetic moment and *Y-K* angles have also been calculated for all prepared samples. The nature of magnetic interactions has also been investigated with the help of proposed cation distribution using Neel's model and *Y-K* model. The *Y-K* model proposes the increase in strength of A-B super-exchange interaction on substituting the transition metal ions. The variation in magnetic interactions computed using suggested distribution of cations has been supported by experimentally obtained data.

The moderate saturation magnetization and soft ferrimagnetic nature has been obtained for transition metal doped *Mg-Zn* ferrites. These samples are useful in memory storage application. The soft magnetic nature of prepared samples also makes them useful for biomedical applications. In future the prepared samples can be explored for magnetic hyperthermia and antimicrobial studies.

BIBLIOGRAPHY

BIBLIOGRAPHY

CHAPTER 1

[1] Jaswal L., Singh B., "Ferrite materials: A chronological review", *Journal of Integrated Science and Technology*, vol. 2, pp. 69-71, 2014.

[2] Hilpert S., Verf V., "*Genetische und constitutive Zussammenhange in den magnetischen Eigenschaften bei Ferriten and Eisenoxyden*", Chemische Berichte, vol. 42, pp. 2248-2261, 1909.

[3] Forestier H., "*Transformations magnetiques du sesquioxide de fer, de ses solutions solides, et des ses combinations ferromagnetiques*", Annali di chimica, vol. 9, pp. 316-401, 1928.

[4] Kato Y. and Takei T., ''*Manufacturing Method of Ferrite Coves*'', Japan Patent No. 98844, 1932.

[5] Kato Y., Takei T., " *Permanent oxide magnet and its characteristics*", The journal of the institute of Electrical Engineers of Japan, vol.53, pp. 408, 1933.

[6] Snoek J. "*Magnetic and electrical properties of ferrites*," Physica, vol.3, pp.463-43, 1936.

[7] Verwey J., Heilman E., "*Cation arrangements in spinels*", Journal of Chemical Physics, vol.15, pp. 174-180, 1947.

[8] Bozorth R., "*Basic research and applications in Magnetism*", IEEE TRANSACTIONS ON MAGNETICS, vol.5, pp. 692-700, 1969.

[9] Anderson P., "*Anti-ferromagnetism: Theory of super-exchange interaction*", Physical Review, vol. 79, pp. 350-356, 1950.

[10] Sugimoto M., "*The Past, Present, and Future of Ferrites",* Journal of the American Ceramic Society, vol. 82, pp. 269-280, Feb. 1999.

[11] Coey J. M. D., *"History of magnetism",* 24th Riso International Symposium on Materials Science , Denmark, pp. 10-13, 2003.

[12] Groenou AB. van, Bongers P. F., Stuyts A. L., "*Magnetism, microstructure and crystal chemistry of spinel ferrites",* Materials Science and Engineering, vol. 3, pp. 317-392, Feb. 1969.

[13] Goldman A., "*Modern Ferrite Technology*", Springer, 2006.

[14] Jadhav P., Patankar K. , Mathe V., Tarwal N. L., Jang J-H. , Puri V., "*Structural and magnetic properties of* $Ni_{0.8}Co_{0.2-2x}Cu_xMn_xFe_2O_4$ *spinel ferrites prepared via solution combustion route*", Journal of Magnetism and Magnetic Materials, vol. 385, pp. 160-165, Jul. 2015.

[15] Goswami P.P., Choudhury H. A., Chakma S., Moholkar V. S., "*Sonochemical Synthesis and Characterization of Manganese Ferrite Nanoparticles*", Industrial and Engineering Chemistry Research, vol. 52, pp. 17848-17855, Oct. 2013.

[16] Shaikh P. A., Kambale R. C., Rao A. V., Kolekar Y. D., "*Structural, magnetic and electrical properties of Co–Ni–Mn ferrites synthesized by co-precipitation method*", Journal of Alloys and Compounds, vol. 492, pp. 590-596, Mar. 2010.

[17] Rehman M., Malik M. A., Akram M., Khan K., Maqsood A., "*Proficient magnesium nanoferrites: synthesis and characterization*", Physica Scripta, vol. 83, pp.015602, Jan. 2011.

[18] Joshi S., Kumar M., Chhoker S., Srivastava G., Jewariya M., Singh V. N., "*Structural, magnetic, dielectric and optical properties of nickel ferrite nanoparticles synthesized by co-precipitation method*", Journal of Molecular Structure, vol. 1076, pp. 55-62, Nov. 2014.

[19] Sanpo, Noppakun, "*Literature review. In: Solution Precursor Plasma Spray System*", Springer Briefs in Materials, pp 5-51, Jun. 2014.

[20] Mathew D. S., Juang R-S, "*An overview of the structure and magnetism of spinel ferrite nanoparticles and their synthesis in microemulsions*", Chemical Engineering Journal, vol. 129, pp.51–65, May 2007.

[21] Pandey B., Litterst F. J., Baggio-Saitovitch E. M., "*Preferential spin canting in nanosize zinc ferrite", Journal of Magnetism and Magnetic Materials*, vol. 385 pp. 412–417, Jul. 2015.

[22] Sickafus K. E., Wills J. M., Grimes N. W., "*Spinel Coumpounds: Structure and Property Relations*", Journal of the American Ceramic Society, vol. 82, pp. 3279-3292, Dec. 1999.

[23] Pullar R. C., "*Hexagonal ferrites: A review of the synthesis, properties and applications of hexaferrite ceramics*", Progress in Materials Science, vol. 57, pp. 1191-1334, Sept. 2012.

[24] Akhtar M. N., Yousaf M., Khan S. N., Nazir M. S., Ahmad M., Khan M. A., "*Structural and Electromagnetic Evaluations of YIG Rare Earth Doped (Gd, Pr, Ho,Yb) Nanoferrites For High Frequency Applications*", Ceramics International, vol. 43, pp. 17032-17040. Dec. 2017.

[25] Akhtar M. N., Sulong A. B., Ahmad M., Khan M. A., Ali A., Islam M. U., "*Impacts of Gd–Ce on the structural, morphological and magnetic properties of garnet nanocrystalline ferrites synthesized via sol–gel route*", Journal of Alloys and Compounds, vol. 660, pp. 486-495, Mar. 2016.

[26] Akhtar M. N., Ali K., Umer A., Ahmad T., Khan M. A., "*Structural Elucidation, and Morphological and Magnetic Behavior Evaluations, of Low-Temperature Sintered, Ce-doped, Nanostructured Garnet Ferrites*", Materials Research Bulletin, vol. 101, pp. 48-55, May 2018.

[27] Opuchovic O., Kareivaa A., Mazeika K. , Baltrunas D., "*Magnetic nanosized rare earth iron garnets $R_3Fe_5O_{12}$: Sol–gel fabrication, characterization and reinspection*", Journal of Magnetism and Magnetic Materials, vol. 422, pp. 425–433, Jan. 2017.

[28] Tianshu Z., Hing P. , Jiancheng Z. , Lingbing K., "*Ethanol-sensing characteristics of cadmium ferrite prepared by chemical coprecipitation*", Materials Chemistry and Physics, vol.61, pp.192-198, Nov. 1999.

[29] Reddy C.V.G, Manorama S. V., Rao V. J., "*Semiconducting gas sensor for chlorine based on inverse spinel nickel ferrite*", Sensors and Actuators B: Chemical, vol. 55, pp. 90-95, Apr. 1999.

[30] Zeng X., Zhang J., Zhu S., Deng X., Ma H., Zhang J., Zhang Q., Li P., Xue D., Mellors N.J., Zhang X., Peng Y., "*Direct observation of cation distributions of ideal inverse spinel $CoFe_2O_4$ nano fibres and correlated magnetic properties*" Nanoscale, vol. .9, pp. 7493-7500, Apr. 2017.

[31] S. Hajarpour S., Raouf A. H., Gheisari Kh., "*Structural evolution and magnetic properties of nanocrystalline magnesium–zinc soft ferrites synthesized by glycine–nitrate combustion process*", Journal of Magnetism and Magnetic Materials, vol. 363, pp.21-25, Aug. 2014.

[32] Ammar S., Jouini N., Fi´evet F., Beji Z., Smiri L., Molin´e P., Danot M., Gren`eche J-M., "*Magnetic properties of zinc ferrite nano particles synthesized by hydrolysis in a polyol medium*", Journal of Physics : Condensed Matter, vol.18, pp. 9055-9069, Sept. 2006

[33] Carta D., Marras C., Loche D., Mountjoy G., Ahmed S. I., Corrias A., **"***An X-ray absorption spectroscopy study of the inversion degree in zinc ferrite nanocrystals dispersed on a highly porous silica aerogel matrix*", Journal of Applied Physics, vol. 138, pp. 054702, Feb. 2013.

[34] Tanaka K., Nakashima S., Fujita K., Hirao K, "*High magnetization and the Faraday effect for ferrimagnetic zinc ferrite thin film*", Journal of Physics: Condensed Matter, vol. 30, pp. L469-L482, Jul. 2003.

[35] Zhang D., Li W., Ye R., Guo X., Wang S., Wang X., Xiang Q., "*A facile strategy for $ZnFe_2O_4$ coating preparing by electrophoretic deposition and its supercapacitor*

performances", Journal of Materials Science: Materials in Electronics, vol.29, pp. 5454-5458, Apr. 2018.

[36] Bini M., Tondo C., Capsoni D., Mozzati M.C., Albini B., Galinetto P., "*Superparamagnetic $ZnFe_2O_4$ nanoparticles: the effect of Ca and Gd doping*" , Materials Chemistry And Physics, vol. 204, pp.72-82, Jan.2018.

[37] Gharagozlou M., Bayati R., "*Low temperature processing and magnetic properties of zinc ferrite nanoparticles*", Superlattices and Microstructures, vol. 78, pp. 190–200, Feb. 2015.

[38] Thomas N., Shimna T., Jithin P. V., Sudheesh V. D., Choudhary H. K., Sahoo B., Nair S. S., Lakshmi N., Sebastian V., *"Comparative study of the structural and magnetic properties of alpha and beta phases of lithium ferrite nanoparticles synthesized by solution combustion method",* Journal of Magnetism and Magnetic Materials, vol. 462, pp. 136-143, Sept. 2018.

[39] Mazen S. A., Abu-Elsaad N. I., "*Structural, magnetic and electrical properties of the lithium ferrite obtained by ball milling and heat treatment*", Applied Nanoscience, vol. 5, pp.105-114, Jan. 2015.

[40] Hessien M. M., *"Synthesis and characterization of lithium ferrite by oxalate precursor route",* Journal of Magnetism and Magnetic Materials, vol. 320, pp. 2800-2807, Nov. 2018.

[41] Chinnasamy C. N., Narayanasamy A., Ponpandian N., "*Mixed spinel structure in nanocrystalline $NiFe_2O_4$*", Physical Review B, vol. 63, pp.184108, Apr. 2001.

[42] Naik S., Parveez A., Chaudhuri A., Khadera S. A, "*Structural, dielectric and electrical properties of Ni (Cd, Zn) Fe_2O_4 by Auto Combustion method*", Materials Today: Proceedings, vol. 4, pp. 12103–12108, Nov. 2017

[43] Lv L., Zhou J-P, Liu Q., Zhu G., Chen X-Z, Bian X-B, Liu P., "*Grain size effect on the dielectric and magnetic properties of $NiFe_2O_4$ ceramics*", Physica E, vol. 43, pp. 1798-1803, June 2011.

[44] Alarifi A., Deraz N. M., Shaban S., "*Structural, morphological and magnetic properties of $NiFe_2O_4$ nano-particles*", Journal of Alloys and Compounds, vol. 486, pp. 501–506, July 2009.

[45] Bae S., Lee S. W.,Takemura Y., "*Applications of $NiFe_2O_4$ nanoparticles for a hyperthermia agent in biomedicine*", Applied Physics Letters, vol. 89, pp. 252503, Dec. 2006.

[46] Golkhatmi F. M., Bahramian B., Mamarabadi M., "*Application of surface modified nano ferrite nickel in catalytic reaction (epoxidation of alkenes) and investigation on its antibacterial and antifungal activities*", Materials Science and Engineering : C, vol. 78, pp. 1-11, Sept . 2017.

[47] Thant A. A., Srimala S., Kaung P., Itoh M., Radzali O., Fauzi M. N., " *Low Temperature Synthesis of $MgFe_2O_4$ Soft Ferrite Nanocrystallites*", Journal of the Australian Ceramic Society, vol. 46, pp. 11-14, 2014.

[48] Jung K. W., Lee S., Lee Y. J., "*Synthesis of novel magnesium ferrite ($MgFe_2O4$)/biochar magnetic composites and its adsorption behavior for phosphate in aqueous solutions*", Bioresource Technology, vol. 245, pp. 751-759, Dec. 2017.

[49] Kurian J. , Mathew M., "*Structural, optical and magnetic studies of $CuFe_2O_4$, $MgFe_2O_4$ and $ZnFe_2O_4$ nanoparticles prepared by hydrothermal/ solvothermal method*", Journal of Magnetism and Magnetic Materials, vol. 451, pp. 121-130, Oct. 2017.

[50] Maensiri S., Sangmanee M.,Wiengmoon A., "*Magnesium Ferrite ($MgFe_2O_4$) Nanostructures Fabricated by Electrospinning*", Nanoscale Research Letters, vol. 4, pp. 221-228, Dec. 2008.

[51] Maehara T., Konishi K., Kamimori T., Aono H., Naohara T., Kikkawa H., Watanabe Y., Kawachi K., "*Heating of Ferrite Powder by an AC Magnetic Field for Local Hyperthermia*", Japanese Journal of Applied Physics, vol. 41, pp. 1620-1621, Dec. 2001.

[52] Tang W., Su Y. , Li Q., Gao S., Shang J. K., "*Superparamagnetic magnesium ferrite nanoadsorbent for effective arsenic (III, V) removal and easy magnetic separation*", Water Research, vol. 47, pp. 3624-3634, Apr. 2013.

[53] Thang P. D., Rijnders G., Blank D. H. A., "*Spinel cobalt ferrite by complexometric synthesis*", Journal of Magnetism and Magnetic Materials, vol. 295, pp. 251–256, Sept. 2005.

[54] Amirthavalli C., Thomas J. M., Nagaraj K., Prince A. A. M., "*Facile room temperature CTAB-assisted synthesis of mesoporous nano-cobalt ferrites for enhanced magnetic behaviour*", Materials Research Bulletin, vol. 100, pp. 289-294, Apr. 2008.

[55] Zolio R. F., US Patent, Patent Number 4744866, 1984.

[56] Prabhakaran T., Mangalaraja R.V., Denardin J. C., "*The structural, magnetic and magnetic entropy changes on $CoFe_2O_4/CoFe_2$ composites for magnetic refrigeration application*", Journal of Magnetism and Magnetic Materials, vol. 444, pp. 297-306, Dec. 2017.

[57] Jung J., Kim S., Kim H., Park J., Oh J. H., "*High-Performance Flexible Organic Nano-Floating Gate Memory Devices Functionalized with Cobalt Ferrite Nanoparticles*", Small, vol. 11, pp.4976-4984, Oct. 2015.

[58] Dey C., Baishya K., Ghosh A., Goswami M.M., Ghosh A., Mandal K., "*Improvement of drug delivery by hyperthermia treatment using magnetic cubic cobalt ferrite nanoparticles*", Journal of Magnetism and Magnetic Materials, vol. 427, pp. 168-174, Apr. 2017.

[59] Oh Y., Moorthy M. S., Manivasagan P., Bharathiraja S., Oh J., "*Magnetic hyperthermia and pH-responsive effective drug delivery to the sub-cellular level of human breast cancer cells by modified $CoFe_2O_4$ nanoparticles*", Biochimie, vol. 133, pp. 7-19, Feb. 2017.

[60] Gopalan E. V., Malini K. A., Saravanan S., Kumar D. S., Yoshida Y., Anantharaman M. R., "*Evidence for polaron conduction in nanostructured manganese ferrite*", Journal of Physics D : Applied Physics, vol. 41, pp. 185005, Aug. 2008.

[61] Vijaya J. J., Sekaran G., Bououdina M, "*Effect of Cu^{2+} doping on structural, morphological, optical and magnetic properties of $MnFe_2O_4$particles/sheets/flakes-like nanostructures*", Ceramics International, vol.41, pp.15-26, Jan. 2015.

[62] Vignesh V., Subramani K., Sathish M., Navamathavan R., "*Electrochemical investigation of manganese ferrites prepared via a facile synthesis route for supercapacitor applications*", Colloids and Surfaces A, vol. 538, pp. 668–677, Feb. 2018.

[63] Pradhan P., Giri J., Banerjee R., Bellare J., Bahadur D., "*Preparation and characterization of manganese ferrite-based magnetic liposomes for hyperthermia treatment of cancer*", Journal of Magnetism and Magnetic Materials, vol. 311, pp. 208–215, Apr. 2007.

[64] Jacintha A. M., Umapathy V., Neeraja P., Rajkumar S. R., *"Synthesis and comparative studies of MnFe2O4nanoparticles with different natural polymers by sol–gel method: structural, morphological, optical, magnetic, catalytic and biological activities",* Journal of nanostructure in Chemistry, vol. 7, pp. 375-387, Nov. 2017.

[65] Singh N. H., Bera A., Debnath A., Saha B., *"Mixed Phase Crystalline Hausmannite and Manganese Ferrite Nanoparticles with Magnetic Properties for Environmental Application",* Materials Today: Proceedings, vol. 5, pp. 2300–2305, 2018.

[66] Doaga A., Cojocariu A. M., Amin W., Heib F., Bender P., Hempelmann R., Caltun O.F., "*Synthesis and characterizations of manganese ferrites for hyperthermia applications*", Materials Chemistry and Physics, vol. 143, pp. 305-310, Dec. 2013.

[67] Sutka A., Gross K., Mezinskis G., Bebris G., Knite M., "*The effect of heating conditions on the properties of nano- and microstructured Ni–Zn ferrite*", Physica Scripta, vol. 83, pp. 025601, Jan. 2011.

[68] Ponpandian N., Narayanasamy A., Chinnasamy C. N., Sivakumar N., Greneche J. M., Chattopadhyay K., Shinoda K., Jeyadevan B., Tohji K., "*Néel temperature enhancement in nanostructured nickel zinc ferrite*", Applied Physics Letters, vol. 86, pp. 192510, Apr. 2005.

[69] Sun K., Liu H., Yang Y., Yu Z., Chen C., Wu G. , Jiang X., Lan Z., Li L., "*Contribution of magnetization mechanisms in nickel zinc ferrites with different grain sizes and its temperature relationship*", Materials Chemistry and Physics, vol. 175, pp. 131-137, June 2016.

[70] Mondal R., Deya S., Majumder S., Poddar A., Dasgupta P., Kumar S., "*Study on magnetic and hyperfine properties of mechanically milled $Ni_{0.4}Zn_{0.6}Fe_2O_4$ nanoparticles*", Journal of Magnetism and Magnetic Materials, vol. 448, pp.135-145, Feb. 2018.

[71] Oliveira E. E.C., Araujo W. C., Assis P. C., Vieira M. S., Dassuncao A. G. "*Small-Size Compact Nickel-Zinc Ferrite Dieletric Resonator Antenna With High Dielectric Constant*", International Microwave and Optoelectronics Conference (IMOC), pp. 1-4, 2015.

[72] Huang X., Zhang J., Lai M., Sang T., "*Preparation and microwave absorption mechanisms of the NiZn ferrite nanofibers*", Journal of Alloys and Compounds, vol. 627, pp. 367-373, Apr. 2015.

[73] Afkhami A., Sayari S., Moosavi R., Madrakian T. , "*Magnetic nickel zinc ferrite nanocomposite as an efficient adsorbent for the removal of organic dyes from aqueous solutions*", Journal of Industrial and Engineering Chemistry, vol. 21, pp. 920-924, Jan. 2015.

[74] Pawar C. S., Gujar M. P., Mathe V. L., "*Synthesis and characterization of nano crystalline nickel zinc ferrite for chlorine gas sensor at room temperature*", AIP Conference Proceedings, vol. 1665, pp. 050060, June 2015.

[75] Gopalan E.V., Malini K. A., Sagar S., Sakthi D. K., Yoshida Y., Al-Omari I. A., Anantharaman M. R., "*Mechanism of ac conduction in nanostructured manganese zinc mixed ferrites*", Journal of Physics D: Applied Physics, vol. 42, pp. 165005, Jul. 2009.

[76] Syue M. R., Wei F., Chou C., Fu C., "*Magnetic and electrical properties of Mn–Zn ferrites synthesized by combustion method without subsequent heat treatments*", Journal of Applied Physics, vol. 109, pp. 07A324, Mar. 2011.

[77] Praveena, K., Chena H.W., Liu H. L., Sadhana K., Murthy S. R., "*Enhanced magnetic domain relaxation frequency and low power losses in Zn^{2+} substituted manganese ferrites potential for high frequency applications*", Journal of Magnetism and Magnetic Materials, vol. 420, pp. 129-142, Dec. 2016.

[78] Ahmed M.A., Rady K. E., Shams M. S., "*Enhancement of electric and magnetic properties of Mn–Zn ferrite by Ni–Ti ions substitution*", Journal of Alloys and Compounds, vol. 622, pp. 269–275, Feb. 2015.

[79] Ismail F. M. , Ramadan M., Abdellah A. M., Ismail I., Allam N. K., *"Mesoporous spinel manganese zinc ferrite for high performance supercapacitors"*, Journal of Electroanalytical Chemistry, vol. 817, pp.111-117, May 2018.

[80] Phong P. T., Nam P. H., Manh D. H., Lee I. J., "*$Mn_{0.5}Zn_{0.5}Fe_2O_4$ nanoparticles with high intrinsic loss power for hyperthermia therapy*", Journal of Magnetism and Magnetic Materials, vol. 433, pp. 76-83, July 2017.

[81] Silva S. W., Nakagomi F., Silva M. S., Franco A., Garg V. K., Oliveira A. C., Morais P. C., "*Effect of the Zn content in the structural and magnetic properties of $Zn_xMg_{1-x}Fe_2O_4$ mixed ferrites monitored by Raman and Mössbauer spectroscopies*", Journal of Applied Physics, vol. 107, pp. 09B503, Apr. 2010.

[82] Rafiq M. A., Khan M. A., Asghar M., Ilyas S. Z., Shakir I., "Shahid M., Warsi M. F., *"Influence of Co^{2+} on structural and electromagnetic properties of Mg-Zn nanocrystals synthesized via co-precipitation route"*, Ceramics *International*, vol. 41, pp. 10501-10505, Nov. 2015.

[83] Mansour S. F.,*"Frequency and Composition Dependence on the Dielectric Properties for Mg-Zn Ferrite",* Egyptian Journal of Solids, vol. 28, pp. 263-273, 2005.

[84] SamoÏlenko Z. A., Ivakhnenko N. N., Pashchenko V. P., Kopaev O. V., OstafiÏchuk B. K., Gasyuk I. M., *"Evolution of Short-Range, Mesoscopic, and Long-Range Orders in Magnesium–Zinc Ferrites"*, Technical Physics, vol. 47, pp. 364-367, 2002.

[85] Skołyszewska B., Tokarz W., Przybylski K., Kakol Z., *"Preparation and magnetic properties of MgZn and MnZn ferrites",* Physica C, vol. 387, pp. 290-294, May 2003.

[86] Hajarpour S., Gheisari Kh., Raouf A.H., "*Characterization of nanocrystalline $Mg_{0.6}Zn_{0.4}Fe_2O_4$ soft ferrites synthesized by glycine-nitrate combustion process"*, Journal of Magnetism and Magnetic Materials, vol. 329, pp.165-169, Mar. 2013.

[87] Cao C , Xia A., Liu S., Tong L., *"Synthesis and magnetic properties of hydrothermal magnesium–zinc spinel ferrite powders",* Journal of Materials Science : Materials in Electronics, vol. 24, pp. 4901-4905, Dec. 2013.

[88] Barbosa G. F., Machado F. L.A., Rodrigues A. R., Silva M. S., Franco A., *"Enhanced Magnetic Properties of Zn Substituted Mg Ferrite"*, IEEE TRANSACTIONS ON MAGNETICS, vol. 49, pp. 4562-4564, Aug. 2013.

[89] Choodamani C., Nagabhushana G. P., Rudraswamy B., Chandrappa G. T., *"Thermal effect on magnetic properties of Mg-Zn ferrite nanoparticles"*, Materials Letters, vol. 116, pp. 227-230, Feb. 2014.

[90] Singh S. B., Srinivas Ch., Tirupanyam B. V., Prajapat C. L., Singh M. R., Meena S. S., Bhatt P., Yusuf S. M., Sastrye D. L., "*Structural, Thermal and Magnetic studies of $Mg_xZn_{1-x}Fe_2O_4$ nanoferrites: Study of exchange interactions on magnetic anisotropy",* Ceramics International, vol. 42, pp. 19179-19186, Dec. 2016.

[91] Rahman S., Nadeem K., Rehman M., Mumtaz M., Naeem S., Papst I., *"Structural and magnetic properties of ZnMg-ferrite nanoparticles prepared using the co-precipitation method"*, Ceramics International, vol. 39, pp. 5235-5239, July 2013.

[92] Gore S. K., Tumberphale U. B., Jadhav S. S., Kawale R. S., Naushad M., Mane R . S., *"Microwave-assisted synthesis and magneto-electrical properties of Mg-Zn ferrimagnetic oxide nanostructures",* Physica B: Physics of Condensed Matter, vol. 530, pp.177–182, Feb. 2018.

[93] Choodamani C., Rudraswamy B., Chandrappa G. T., *"Structural, electrical, and magnetic properties of Zn substituted magnesium ferrite",* Ceramics International, vol. 42, pp. 10565-10571, July 2016.

[94] Bharti D. C., Mukherjee K., Majumder S. B., "*Wet chemical synthesis and gas sensing properties of magnesium zinc ferrite nano-particles",* Materials Chemistry and Physics, vol. 120, pp.509-517, Apr. 2010.

[95] Kassabova-Zhetcheva V. D., Pavlova L. P., Samuneva B. I., Cherkezova-Zheleva Z. P., Mitov I. G., Mikhov M. T., *"Characterization of superparamagnetic $Mg_xZn_{1-x}Fe_2O_4$ powders",*Central European Journal of Chemistry, vol. 5, pp. 107-117, 2007.

[96] Patil S. N., Pawar A. M., Tilekar S. K., Ladgaonkar B .P., *"Investigation of magnesium substituted nano particle zinc ferrites for relative humidity sensors",* Sensors and Actuators A, vol. 244, pp. 35–43, June 2016.

[97] Mukherjee K., Majumder S. B., "*Synthesis of embedded and isolated $Mg_{0.5}Zn_{0.5}Fe_2O_4$ nano-tubes and investigation on their anomalous gas sensing characteristics",* Sensors and Actuators B: Chemical, vol. 177, pp.55-63, Feb. 2013.

[98] Skomski R., *"Nanomagnetics",* Journal of Physics: Condensed Matter, vol.15, pp. R841-R896, May 2003.

[99] Ansari M., Bigham A., Tabrizi S. A. H., Ahangar H. A., *"Copper-substituted spinel Zn-Mg ferrite nanoparticles as potential heating agents for hyperthermia"*, Jounral of the American Ceramic society, vol. 101, pp. 3649-3661, Feb.2018.

[100] Lodhi M. Y., Mahmood K., Mahmood A., Malik H., Warsi M. F., Shakir I., Asghar M., Khan M. A., *"New $Mg_{0.5}Co_xZn_{0.5-x}Fe_2O_4$ nano-ferrites: Structural elucidation and electromagnetic behavior evaluation"*, Current Applied Physics, vol. 14, pp. 716-720, May. 2014.

[101] Yadav A., Varshney D., *"Structural and temperature dependent dielectric behavior of Cr and Zn doped $MnFe_2O_4$ nano ferrites",* Superlattices and Microstructures, vol. 113, pp. 153-159, Jan. 2018.

[102] Abraham A.G., Manikandan A., Manikandan E., Vadivel S., Jaganathan S. K., Baykal A., Renganathan P. S., *"Enhanced magneto-optical and photo-catalytic properties of transition metal cobalt (Co^{2+} ions) doped spinel $MgFe_2O_4$ ferrite nanocomposites",* vol. 452, pp. 380-388, Apr. 2018.

[103] Ati A. A., *"Fast synthesis, structural, morphology with enhanced magnetic properties of cobalt doped nickel ferrite nanoscale"*, Journal of Materials Science: Materials in electronics, vol. 29, pp. 12010-12021, July 2018.

[104] Shahid M., Shafi S., Aboud M. F. A., Warsi M. F., Asghar M., Shakir I.*"Impacts of Co^{2+} and Gd^{3+} co-doping on structural, dielectric and magnetic properties of $MnFe_2O_4$ nanoparticles synthesized via micro-emulsion route"*, Ceramics International, vol. 43, pp. 14096-14100, Nov. 2014.

[105] Padmapriya G., Manikandan A., Krishnasamy V., Jaganathan S. K., Antony S. A., *"Spinel $Ni_xZn_{1-x}Fe_2O_4$ $(0.0\leq x\leq 1.0)$ nano-photocatalysts: Synthesis, characterization and photocatalytic degradation of methylene blue dye*", Journal of Molecular Structure, vol. 1119 pp. 39-47, Sept. 2016.

[106] Maalam K. E., Ali M. B., Moussaoui H. E., Mounkachi O., Hamedoun M., Masrour R., Hlil E. K., Benyoussef A., "*Magnetic properties of tin ferrites nanostructures doped with transition metal"*, Journal of Alloys and Compounds, vol. 622, pp. 761–764, Feb. 2015.

[107] Ali R., Khan M. A., Manzoor A., Shahid M., Warsi M .F., *"Structural and electromagnetic characterization of Co-Mn doped Ni-Sn ferrites fabricated via micro-emulsion route",* Journal of Magnetism and Magnetic Materials, vol. 441, pp. 578-584, Nov. 2017.

[108] Shikha P., Komal, Kang T. S., Randhawa B. S., *"Mn doping induced physico-chemical changes in La–Ce ferrite nanofabricated by ionic liquid assisted hydrothermal route"*, Journal of Alloys and Compounds, vol. 701, pp. 788-796, Apr. 2017.

[109] Ghodake U. R., Kamble R. C., Suryavanshi S. S., *"Effect of Mn^{2+} substitution on structural, electrical transport and dielectric properties of Mg-Zn ferrites"*, Ceramic International, vol. 43, pp. 1129-1134, Jan. 2017.

[110] Datt G., Abhyankar A. C., *"Dopant driven tunability of dielectric relaxation in $M_xCo(1-x)Fe_2O_4$ (M: Zn^{2+}, Mn^{2+}, Ni^{2+}) nano-ferrites"*, Journal of Applied Physics, vol. 122, pp. 034102, June 2017.

[111] Anjana V., John S., Prakash P., Nair A. M., Nair A. R., Sambhudevan S., Shankar B., *"Magnetic Properties of Copper Doped Nickel Ferrite Nanoparticles Synthesized by Co Precipitation Method",* IOP Conference Series: Materials Science and Engineering, vol. 310, pp. 012024, 2018.

[112] Yadav A., Varshney D., *"Structural and temperature dependent dielectric behavior of Cr and Zn doped $MnFe_2O_4$ nano ferrites",* Superlattices and Microstructures, vol. 113, pp. 153-159, Jan. 2018.

[113] Tatarchuk T. R., Bououdina M., Paliychuk N. D., Yaremiy I. P., Moklyak V. V., "Structural characterization and antistructure modeling of cobalt-substituted zinc ferrites", Journal of Alloys and Compounds, vol. 694, pp. 777-791, Feb. 2017.

[114] Lassoued A., Lassoued M. S., Dkhil B., Ammar S., Gadri A., *"Photocatalytic degradation of methyl orange dye by $NiFe_2O_4$ nanoparticles under visible irradiation: effect of varying the synthesis temperature",* Journal of Materials Science: Materials in Electronics, vol. 29, pp. 7057-7067, Jan. 2018.

[115] Gharibshahian M., Nourbakhsh M.S., Mirzaee O*., "Evaluation of the superparamagnetic and biological properties of microwave assisted synthesized Zn & Cd doped $CoFe_2O_4$ nanoparticles via Pechini sol–gel method",* Journal of Sol-gel Science and Technology, vol. 85, pp.684-692, Jan. 2018.

[116] Samavati A., Ismail A. F., *"Antibacterial properties of copper-substituted cobalt ferrite nanoparticles synthesized by co-precipitation method"*, Particuology, vol. 30, pp. 158-163, Feb. 2017.

[117] Hu W., Qin N., Wu G., Lin Y., Li S., Bao D., "*Opportunity of Spinel Ferrite Materials in Nonvolatile Memory Device Applications Based on Their Resistive Switching Performances"*, Journal of the American chemical society, vol. 134, pp. 14658-14661, Aug. 2012.

[118] Gilani Z. A., Shifa M.S., Khan A., Khan M. A., Anjum M. N., Usmani M. N., Ali R., Warsi M. F., "*New $LiCo_{0.5}Pr_xFe_{2-x}O_4$ nanoferrites: Prepared via low cost technique for high density storage application",* Ceramics International, vol. 44, pp. 1881-1885, Feb. 2018.

[119] Harris V. G., "*Modern microwave ferrites*", IEEE TRANSACTIONS ON MAGNETICS, vol. 48, pp.1075-1104, Mar. 2012.

[120] Ahmed M. A., Rady K. E., Shams M. S., "*Enhancement of electric and magnetic properties of Mn–Zn ferrite by Ni–Ti ions substitution",* Journal of Alloys and Compounds, vol. 622, pp. 269-275, Feb. 2015.

[121] Li Q. F., Du X., Chen S., Zhang S., *"Research on UV-cured composite films of epoxy with superparamagnetic, hollow nickel–zinc ferrite nano spheres and their microwave absorption",* Journal of Materials Science: Materials in Electronics, vol. 29, pp. 3286-3295, 2018

[122] Sutka A., Gross K. A., **"***Spinel ferrite oxide semiconductor gas sensors",* Sensors and Actuators B: Chemical, vol. 222, pp. 95-105, Jan.2016.

[123] Abu-Hani A. F. S., Mahmoud S. T., Awwad F., Ayesh A. I., *"Design, fabrication, and characterization of portable gas sensors based on spinel ferrite nanoparticles embedded in organic membranes",* Sensors and Actuators B: Chemical, vol. 241, pp. 1179-1187, Mar. 2017.

[124] Singh A., Singh A., Singh S., Tondon P., Yadav B. C., Yadav R. R., *"Synthesis, characterization and performance of zinc ferrite nanorods for room temperature sensing applications",* Journal of Alloys and Compounds, vol. 618, pp. 475-483, Jan. 2015.

[125] Mukherjee C., Mondal R., Dey S., Kumar S., Das J., *"Nanocrystalline Copper Nickel Zinc Ferrite: Efficient Sensing Materials for Ethanol and Acetone at Room Temperature",* IEEE sensors journal, vol. 17, pp. 2662-2669, Mar. 2017.

[126] Khandekar M. S., Tarwal N. L., Mulla I. S., Suryavanshi S. S., *"Nanocrystalline Ce doped CoFe2O4 as an acetone gas sensor"*, Ceramics International, vol. 40, pp. 447-452, Jan. 2014.

[127] Tatarchuk T., Bououdina M., Vijaya J. J., Kennedy L. J., "*Spinel Ferrite Nanoparticles: Synthesis, Crystal Structure, Properties, and Perspective Applications*", Springer International Publishing, Springer Proceedings in Physics, vol. 195, pp. 305-324, 2016.

[128] Sundararajan M., Sailaja V., Kennedy L. J., Vijaya J. J., *"Photocatalytic degradation of rhodamine B under visible light using nanostructured zinc doped cobalt ferrite: Kinetics and mechanism",* Ceramics International, vol. 43, pp. 540-548, Jan. 2017.

[129] Casbeer E., Sharma V. K., Li X. Z., *"Synthesis and photocatalytic activity of ferrites under visible light: A review"* Separation and Purification Technology, vol. 87, pp. 1-14, Mar. 2012.

[130] Sharma R., Bansal S., Singhal S., *"Tailoring the photo-Fenton activity of spinel ferrites (MFe_2O_4) by incorporating different cations (M=Cu, Zn, Ni and Co) in the structure"*, RSC Advances, vol. 5, pp. 6006-6018, 2015.

[131] Ghayour H., Abdellahi M., Ozada N., Jabbrzare S., Khandan A., *"Hyperthermia application of zinc doped nickel ferrite nanoparticles",* Journal of Physics and Chemistry of Solids, vol. 111, pp. 464-472, Dec. 2017.

[132] Jadhav S.V., Kim B. M., Lee H. Y., Im I. C., Rokade A. A., Park S. S., Patil M. P., Kim G. D., Yu Y. S., Lee S. H., *"Induction heating and in vitro cytotoxicity studies of MnZnFe2O4 nanoparticles for self-controlled magnetic particle hyperthermia",* Journal of Alloys and Compounds, vol. 745, pp. 282-291, May. 2018.

[133] Ahmad A., Bae H., Rhee I., *"Highly stable silica-coated manganese ferrite nanoparticles as high-efficacy T2 contrast agents for magnetic resonance imaging",* AIP Advances, vol. 8, pp. 055019, May 2018.

[134] Fan H., Li B., Shi Z., Zhao L., Wang K., Qiu D., *"A fibrous morphology silica-CoFe2O4 nanocarrier for anti-cancer drug delivery"*, Ceramics International, vol. 44, pp.2345-2350, Feb. 2018.

[135] Kefeni K., Msagati T., Mamba B., "*Ferrite nanoparticles: Synthesis, characterization and applications in electronic device*", Materials Science and Engineering B, vol. 215, pp.37-55, Jan. 2017.

CHAPTER 2

[1] Blanco-Gutierrez V., Saez-Puche R., Torralvo-Fernandez M., "*Superparamagnetism and interparticle interactions in $ZnFe_2O_4$ nanocrystals*", Journals of Materials Chemistry, vol.22, pp. 2992-3003, Jan. 2012.

[2] Babu K. C. B., Madhuri W., "*Microwave processed bulk and nano Ni Mg ferrites: A comparative study on X-band electromagnetic interference shielding properties*", Materials Chemistry and Physics, vol. 187, pp. 164-176, Feb. 2017.

[3] Fu L., Dravid V. P., Johnson D. L. "*Self-assembled (SA) bilayer molecular coating on magnetic nanoparticles*", Applied surface science, vol. 181, pp. 173-178, Sept. 2001.

[4] Zheng M., Wu X. C., Zou B. S., Wang Y. J., "*Magnetic properties of nanosized MnFe2O4 particles*", Journal of Magnetism and Magnetic materials, vol. 183, pp. 152-156, Mar. 1998.

[5] Cao X., Gu L., "*Spindly cobalt ferrite nanocrystals: preparation, characterization and magnetic properties*", Nanotechnology, vol. 16, pp.180–185, 2005.

[6] Sivakumar P., Ramesh R., Ramanand A., Ponnusamy S., Muthamizhchelvan C., "*Preparation and properties of nickel ferrite (NiFe2O4) nanoparticles via sol-gel auto-combustion method*", Materials Research Bulletin, vol. 46, pp. 2204‑2207, Dec. 2011.

[7] Reddy M., Shakoor R., Mohamed A., Gupta M., Huang Q., "*Effect of sintering temperature on the structural and magnetic properties of MgFe2O4 ceramics prepared by spark plasma sintering*", Ceramics International, vol. 42, pp. 4221-4227, Feb. 2016.

[8] Singh J., Roychoudhury A., Srivastava M., Chaudhary V., Prasanna R., Lee D., Lee S., Malhotra B., "*Highly Efficient Bienzyme Functionalized Biocompatible Nanostructured Nickel Ferrite−Chitosan Nanocomposite Platform for Biomedical Application*", The Journal of Physical Chemistry C, vol. 117, pp. 8491-8502, Apr. 2013.

[9] Mansour S. F., Elkestawy M. A., "*A comparative study of electric properties of nano-structured and bulk Mn–Mg spinel ferrite*", Ceramics International, vol. 37, pp. 1175-1180, May 2010.

[10] Sharma S., Choudhary N., Verma M. K., Sharma N. D., Singh D., "*Cation distribution and magnetic properties of nano and bulk CoCrFeO4 ferrite synthesized by glycine-nitrate combustion method*", Ceramics International, vol. 43, pp. 11083-11089, Oct. 2017.

[11] Bharti D., Mukherjee R., Majumder S., "*Wet chemical synthesis and gas sensing properties of magnesium zinc ferrite nano-particles*", Materials Chemistry and Physics, vol. 120, pp. 509-517, Apr. 2010

[12] Bid S., Pradhan S., "*Preparation of zinc ferrite by high-energy ball-milling and microstructure characterization by Rietveld's analysis*", Materials Chemistry and Physics, vol.82, pp. 27-37, Apr. 2004.

[13] Liang Y., Hsia H., "*Growth and crystallographic feature-dependent characterization of spinel zinc ferrite thin films by RF sputtering*", Nanoscale Research Letters, vol. 8, pp. 1-8, Dec. 2013.

[14] Xiong H. , Lai B., Johnson A., Ramanathan S., "*Low-temperature electrochemical characterization of dense ultra-thin lanthanum strontium cobalt ferrite (La0.6Sr0.4Co0.8Fe0.2O3) cathodes synthesized by RF-sputtering on nanoporous alumina-supported Y-doped zirconia membranes*", Journal of Power Sources, vol.193, pp.589-592, Sept. 2009.

[15] Matijevic´ E., "*Uniform colloidal barium ferrite nano-particles*", Journal of Colloid and Interface Science, vol.117, pp. 593-595, June 1987.

[16] Sharma R., Singhal S., "*Structural, magnetic and electrical properties of zinc doped nickel ferrite and their application in photo catalytic degradation of methylene blue*", Physica B, vol.414, pp. 83-90, Apr. 2013.

[17] Nasir S., Anis-ur Rehman M., "*Structural, electrical and magnetic studies of nickel–zinc nanoferrites prepared by simplified sol–gel and co-precipitation methods*", Physica Scripta, vol. 84, pp. 025603, Aug. 2011.

[18] Byrappa K., Adschiri T., "*Hydrothermal technology for nanotechnology*", Progress in Crystal Growth and Characterization of Materials, vol. 53, pp. 117-166, June 2007.

[19] Aziz H. S., Rasheed S., Khan R., Rahim A., Nisar J., Shah S., Iqbal F., Khan A., "*Evaluation of electrical, dielectric and magnetic characteristics of Al–La doped nickel spinel ferrites*", RSC Advances, vol. 6, pp. 6589-6597, Jan. 2016.

[20] Köseoğlu Y., Alan F., Tan M., Yilgin R., O¨ ztu¨rk M., "*Low temperature hydrothermal synthesis and characterization of Mn doped cobalt ferrite nanoparticles*", Ceramics International, vol. 38, pp.3625-3634, July 2012.

[21] Malale K., Ganjali M. R., Alizadeh T., Norouzi P., "Facile polyol synthesis of $CoFe_2O_4$ nanosphere clusters and investigation of their electrochemical behavior in different aqueous electrolytes", Applied Physics A, vol. 295, pp. 1-5, Mar. 2018.

[22] Ganguli A., Ganguly A., Vaidya S., "*Micro-emulsion-based synthesis of nanocrystalline materials*", Chemical Society Reviews, vol. 39, pp. 474-485, 2010.

[23] Kefeni K., Msagati T., Mamba B., "*Ferrite nanoparticles: Synthesis, characterization and applications in electronic device*", Materials Science and Engineering B, vol. 215, pp.37-55, Jan. 2017.

[24] Pulišová P., Kováč J., Voigt A., Raschman P., "*Structure and magnetic properties of Co and Ni nano-ferrites prepared by a two step direct microemulsions synthesis*", Journal of Magnetism and Magnetic Materials, vol. 341, pp.93–99, Sept.2013

[25] Zeng S., Duan S., Tang R., Li L., Liu C., Sun D., "*Magnetically separable Ni0.6Fe2.4O4 nanoparticles as an effective adsorbent for dye removal: Synthesis and study on the kinetic and thermodynamic behaviors for dye adsorption*", Chemical Engineering Journal, vol.258, pp.218-228, Dec. 2014.

[26] Vinosha P., Mely L., Jeronsia J., Krishnan S., Das S., "*Synthesis and properties of spinel $ZnFe_2O_4$ nanoparticles by facile co-precipitation route*", Optik - International Journal for Light and Electron Optics, vol. 134, pp. 99-108, Apr. 2017.

[27] Prabhakaran T., Mangalaraja R., Denardin J., Jimenez J., "*The effect of reaction temperature on the structural and magnetic properties of nano $CoFe_2O_4$*", Ceramics International, vol. 43, pp. 5599-5606, May 2017.

[28] Erfaninia N., Tayebee R., Foletto E.L, Amini M.M., Dusek M., Zonoz F.M., "*Preparation of magnetically recyclable ZnFe2O4 nanoparticles by easy single step co-precipitation method and their catalytic performance in the synthesis of 2-aminothiophenes*", Applied Organometallic Chemistry, DOI: 10.1002/aoc.4047, Sept. 2017.

[29] Ghandoor H. E., Zidan H. M., Khalil M.H. M., Ismail M. I. M., "*Synthesis and Some Physical Properties of Magnetite (Fe_3O_4) Nanoparticles*", International Journal of Electrochemical Science", vol. 2, pp. 5734-5745, Apr. 2012.

[30] Ebrahimi Y., Alvani A. A., Sarabi A. A., Sameie H., Salimi R., Alvani M. , Moosakhani S., "*A comprehensive study on the magnetic properties of nanocrystalline $SrCo_{0.2}Fe_{11.8}O_{19}$ ceramics synthesized via diverse routes*", Ceramics International, vol. 38, pp. 3885-3892, July 2012.

[31] Zaki H. M., Al-Heniti S., Elmosalami T. A., "*Structural, magnetic and dielectric studies of copper substituted nano-crystalline spinel magnesium zinc ferrite",* Journal of Alloys and compounds, vol. 633, pp. 104-114, June 2015.

[32] Cullity B. D., "*Elements of X-Ray Diffraction*", Addison-Wesley Publishing, 1956.

[33] Lorinczi A., "*Effect of Ultraviolet radiation on $Ge_{27}Sb_{13}Se_{60}$ amorphous films*", Journal of Optoelectronics and Advance Materials vol. 1, pp. 37-42, 1999.

[34] Ramgir N. S. , Hwang Y. K., Mulla I. S., Chang Jong-San, "*Effect of particle size and strain in nanocrystalline SnO_2 according to doping concentration of ruthenium*", Solid State Sciences, vol. 8, pp. 359–362, Mar. 2006.

[35] Borse P.H., Deshmukh N., Shinde R. F., Date S. K., Kulkarni S. K., "*Luminescence quenching in ZnS nanoparticles due to Fe and Ni doping*", Journal of materials science, vol. 34, pp. 6087-6093, Dec. 1999.

[36] Thankachan S., Jacob B. P., Xavier S., Mohammed E.M., "*Effect of neodymium substitution on structural and magnetic properties of magnesium ferrite nanoparticles*", Physica Scripta, vol. 87 pp. 025701, Jan. 2013.

CHAPTER 3

[1] Jadhav P., Patankar K., Mathe V., Tarwal N. L., Jang J-H. , Puri V., "*Structural and magnetic properties of $Ni_{0.8}Co_{0.2-2x}Cu_xMn_xFe_2O_4$ spinel ferrites prepared via solution combustion route*", Journal of Magnetism and Magnetic Materials, vol. 385, pp. 160-165, July 2015.

[2] Sugimoto M., "The *Past, Present, and Future of Ferrites*", Journal of the American Ceramic Society, vol. 82, pp. 269-280, Feb. 1999.

[3] Shaikh P. A., Kambale R. C., Rao A. V., Kolekar Y. D., "*Structural, magnetic and electrical properties of Co–Ni–Mn ferrites synthesized by co-precipitation method*", Journal of Alloys and Compounds, vol. 492, pp. 590-596, Mar. 2010.

[4] Rehman M., Malik M. A., Akram M., Khan K., Maqsood A., "*Proficient magnesium nanoferrites: synthesis and characterization"*, Physica Scripta, vol. 83, pp.015602, Jan. 2011.

[5] Joshi S., Kumar M., Chhoker S., Srivastava G., Jewariya M., Singh V. N., "*Structural, magnetic, dielectric and optical properties of nickel ferrite nanoparticles synthesized by co-precipitation method*", Journal of Molecular Structure, vol. 1076, pp. 55-62, Nov. 2014.

[6] Mathew D. S., Juang R-S, "*An overview of the structure and magnetism of spinel ferrite nanoparticles and their synthesis in microemulsions*", Chemical Engineering Journal, vol. 129, pp.51–65, May 2007.

[7] Blanco-Gutierrez V., Saez-Puche R., Torralvo-Fernandez M., "*Superparamagnetism and interparticle interactions in $ZnFe_2O_4$ nanocrystals*", Journals of Materials Chemistry, vol.22, pp. 2992-3003, Jan. 2012.

[8] Gharibshahian M., Nourbakhsh M. S., Mirzaee O., "*Evaluation of the superparamagnetic and biological properties of microwave assisted synthesized Zn & Cd doped $CoFe_2O_4$ nanoparticles via Pechini sol–gel method*", Journal of Sol Gel Science and Technology, https://doi.org/10.1007/s10971-017-4570-1, Jan. 2018.

[9] Chen D. G., Tang X. G., Liu Q. X., Jiang Y. P., Ma C. B., Li R., "*Impedance response and dielectric relaxation in co-precipitation derived ferrite (Ni, Zn) Fe_2O_4 ceramics*", Journal of Applied Physics, vol. 113, pp. 214110 June 2013**.**

[10] Yadav R., Kuřitka I., Vilcakova J., Urbánek P., Machovsky M., Masař M., Holek M., "*Structural, magnetic, optical, dielectric, electrical and modulus spectroscopic characteristics of $ZnFe_2O_4$ spinel ferrite nanoparticles synthesized via honey mediated sol-gel combustion method*", Journal of Physics and Chemistry of solids, vol. 110, pp. 87-99, Nov.2017.

[11] Loghman-Estarki M. R., Torkian S., Rastabi R. A., Ghasemi A., "*Effect of annealing temperature and copper mole ratio on the morphology, structure and magnetic properties of* $Mg_{0.5-x}Cu_xZn_{0.5}Fe_2O_4$ *nanoparticles prepared by the modified Pechini method*", Journal of Magnetism and Magnetic Materials, vol. 442, pp. 163-175, Nov. 2017.

[12] Mansour S. F., Abdoa M. A., El-Dek S. I., "*Improvement of physico-mechanical properties of Mg–Zn nanoferrites via* Cr^{3+} *doping*", Journal of Magnetism and Magnetic Materials, vol. 422, pp. 105–111, 2017.

[13] Verma S., Chand J., Singh M., "*Structural and electrical properties of* Al^{3+} *ions doped nanocrystalline* $Mg_{0.2}Mn_{0.5}Ni_{0.3}Al_yFe_{2-y}O_4$ *ferrites synthesized by citrate precursor method*", Journal of Alloys and Compounds, vol. 587, pp. 763–770, Feb. 2014.

[14] Ali R., Khan M. A., Manzoor A., Shahid M., Warsi M. F., *"Structural and electromagnetic characterization of Co-Mn doped Ni-Sn ferrites fabricated via micro-emulsion route",* Journal of Magnetism and Magnetic Materials, vol. 441, pp. 578-584, Nov. 2017.

[15] Hessien M. M., Rashad M. M., El-Barawy K., Ibrahim I. A., *"Influence of manganese substitution and annealing temperature on the formation, microstructure and magnetic properties of Mn–Zn ferrites",* Journal of Magnetism and Magnetic Materials, vol. 320, pp. 1615-1621, May 2008.

[16] Padmapriya G., Manikandan A., Krishnasamy V., Jaganathan S. K., Antony S. A., "*Spinel* $Ni_xZn_{1-x}Fe_2O_4$ $(0.0 \leq x \leq 1.0)$ *nano-photocatalysts: synthesis, characterization and photocatalytic degradation of methylene blue dye*", Journal of Molecular Structure, vol. 1119, pp. 39–47, Sept. 2016.

[17] Doaga A., Cojocariu A.M., Amin W., Heib F., Bender P., Hempelmann R., Caltun O. F., "*Synthesis and characterizations of manganese ferrites for hyperthermia applications*", Materials Chemistry and Physics, vol. 143, pp. 305–310, Dec. 2013.

[18] Abraham A. G., Manikandan A., Manikandan E., Vadivel S., Jaganathan S. K., Baykal A., Renganathan P. S., "*Enhanced magneto-optical and photo-catalytic properties of transition metal cobalt (*Co^{2+} *ions) doped spinel* $MgFe_2O_4$ *ferrite nanocomposites*", vol. 452, pp. 380-388, Apr. 2018.

[19] Prasad B. B. V. S., Ramesh K. V., Srinivas A., "*Structural and Soft Magnetic Properties of Nickel-Substituted Co-Zn Nanoferrites",* Journal of Superconductivity and Novel Magnetism, DOI https://doi.org/10.1007/s10948-018-4569-z, Jan. 2018.

[20] Dolla T. H., Pruessner K., Billing D. G., Sheppard C., Prinsloo A., Carleschi E., Doyle B., Ndungu P., "*Sol-gel synthesis of $Mn_xNi_{1-x}Co_2O_4$ spinel phase materials: Structural, electronic, and magnetic properties*", Journal of Alloys and Compounds, vol. 742, pp. 78-89, Apr. 2018.

[21] Rashmi S.K., Naik H.S. B., Jayadevappa H., Viswanath R., Patil S. B., Naik M. M., "*Solar light responsive Sm-Zn ferrite nanoparticle as efficient photocatalyst*", Materials Science & Engineering B, vol. 225, pp. 86-97, Nov. 2017.

[22] Gore S. K., Tumberphale U. B., Jadhav S. S., Kawale R. S., Naushad M., Mane R. S., "*Microwave-assisted synthesis and magneto-electrical properties of Mg-Zn ferrimagnetic oxide nanostructures*", Physica B : Condensed Matter, vol. 530, pp. 177-182, Feb. 2018.

[23] Raghuvanshi S., Mazaleyrat F., Kane S, N., "*Mg1-xZnxFe2O4 nanoparticles: Interplay between cation distribution and magnetic properties*", AIP Advances, vol. 8, pp. 047804, 2018.

[24] Mohammed K. A., Al-Rawas A. D., Gismelseed A. M., Sellai A., Widatallah H.M., Yousif A., Elzain M.E., Shongwe M., *"Infrared and structural studies of $Mg_{1-x}Zn_xFe_2O_4$ ferrites"* , Physica B: Condensed Matter, vol. 407, pp. 795-804, Feb. 2012

[25] Venkateswarlu K., Sandhyarani M., Nellaippan T. A., Rameshbabu N., *"Estimation of Crystallite Size, Lattice Strain and Dislocation Density of Nanocrystalline Carbonate Substituted Hydroxyapatite by X-ray Peak Variance Analysis"*, Procedia Materilas Science, vol. 5, pp. 212-221, 2014.

[26] Ponpandian N., Narayansamy A., *"Influence of grain size and structural changes on the electrical properties of nanocrystalline zinc ferrite",* Journal of Applied Physics, vol. 92, pp. 2770-2778, Aug. 2002.

[27] Lodhi M. Y., Mahmood K., Mahmood A., Malik H., Warsi M. F., Shakir I., Asghar M., Khan M. A., *"New $Mg_{0.5}Co_xZn_{0.5-x}Fe_2O_4$ nano-ferrites: Structural elucidation and electromagnetic behavior evaluation",* Current Applied Physics, vol. 14, pp. 716-720, May 2014.

[28] Iqbal M. A., Islam M., Ashiq M.N., Ali I., Hasan A. I., Khan H. M., *"Effect of Gd-substitution on physical and magnetic properties of $Li_{1.2}Mg_{0.4}Gd_xFe_{(2-x)}O_4$ ferrites",* Journal of Alloys and Compounds, vol. 579, pp. 181-186, Dec. 2013.

[29] Waldron R. D., *"Infrared spectra of ferrites"*, Physical Review, vol. 99, pp.1727–1735, Sept. 1955.

[30] Topkaya R., Gunguneş H., Eryiğit S., Shirsath S. E., Yıldız A., Baykal A., *"Effect of bimetallic (Ni and Co) substitution on magnetic properties of $MnFe_2O_4$ Nanoparticles"*, Ceramic International, vol.42, pp.13773–13782, Sept. 2016.

[31] JCPDS No-01-1114.

[32] JCPDS No-76-1363.

[33] Shand M. A., *"The Chemistry and Technology of Magnesia"*, John Wiley and Sons, pp. 200688.

[34] Manikandan A., Vijaya J. J., Sundararajan M., Meganathan C., Kennedy L. J., Bououdina M., "Optical and magnetic properties of Mg-doped Zn Fe_2O_4 nano-particles prepared by rapid microwave combustion method", Superlattices and Microstructures, vol. 64, pp. 118–131, Dec. 2013.

[35] Kumar E. R., Jayaprakash R., Seehra M. S., Prakash T., Kumar S., *"Effect of α-Fe_2O_3 phase on structural, magnetic and dielectric properties of Mn–Zn ferrite nano-particles"*, Journal of Physics and Chemistry of Solids, vol. 74, pp. 943–949, July 2013.

[36] Naseri M. G., Ara M. H., Saion E. B., Shaari A. H., *"Superparamagnetic magnesium ferrite nanoparticles fabricated by a simple, thermal-treatment method"*, Journal of Magnetism and Magnetic Materials, vol. 350, pp. 141–147, Jan. 2014.

[37] Zhang C. F., Zhong X. C., Yu H. Y., Liu Z. W., Zeng D. C., *"Effects of cobalt doping on the microstructure and magnetic properties of Mn-Zn ferrites prepared by the co-precipitation method"*, Physica B: Condensed Matter, vol. 404, pp. 2327–2331, Aug. 2009.

[38] Koseoglu Y., Alan F., Tan M., Yilgin R., Ozturk M., "*Low temperature hydrothermal synthesis and characterization of Mn doped cobalt ferrite nanoparticles*", Ceramics International, vol. 38, pp. 3625-3634, July 2012.

[39] Amer M. A., Hemeda O. M., "*57Fe Mössbauer and infrared studies of the system Co_{1-x} Cd_x Fe_2O_4*", Hyperfine Interactions, vol. 96, pp. 99–109, Dec. 1995.

CHAPTER 4

[1] Guijarro N., Bornoz P., Prévot M., Yu X., Zhu X., Johnson M., Jeanbourquin X., Formal F. L., Sivula K., "*Evaluating spinel ferrites MFe_2O_4 (M = Cu, Mg, Zn) as photoanodes for solar water oxidation: prospects and evaluation*", Sustainable Energy Fuels, vol. 2, pp. 109-117, 2018.

[2] Goldman A., "*Modern Ferrite Technology*", Springer Science & Business Media, 2006.

[3] Valenzuela R., "*Novel applications of ferrites*", Physics Research International, vol. 2012, pp. 1-9, 2012.

[4] Ponpandian N., Narayanasamy A., "*Influence of grain size and structural changes on the electrical properties of nano-crystalline zinc ferrite*", Journal of Applied Physics, vol. 92, pp. 2770, Aug. 2002.

[5] Verma S., Chand J., Singh M., "*Structural and electrical properties of Al3+ ions doped nanocrystalline $Mg_{0.2}Mn_{0.5}Ni_{0.3}Al_yFe_{2-y}O_4$ ferrites synthesized by citrate precursor method*", Journal of Alloys and Compounds, vol. 587, pp. 763-770, Feb. 2014.

[6] Kumar G., Kotnala R. K., Shah J., Kumar V., Kumar A., Dhiman P., Singh M., "*Cation distribution: a key to ascertain the magnetic interactions in a cobalt substituted Mg–Mn nanoferrite matrix",* Physical Chemistry Chemical Physics, vol. 19, pp. 16669-16680, June 2017.

[7] Patange S. M., Shirsath S. E., Toksha B. G., Jadhav S. S., Shukla S. J., Jadhav K. M., "*Cation distribution by Rietveld, spectral and magnetic studies of chromium-substituted nickel ferrites*", Applied Physics A : Materials Science and Processing, vol. 95, pp. 429-134, Sept. 2008.

[8] Lodhi M. Y., Mahmood K., Mahmood A., Malik H., Warsi M. F., Shakir I., Asghar M., Khan M. A., "*New $Mg_{0.5}Co_xZn_{0.5-x}Fe_2O_4$ nano-ferrites: Structural elucidation and electromagnetic behavior evaluation*", Current Applied Physics, vol. 14, pp. 716-720, May 2014.

[9] Haralkar S. J., Kadam R. H. , More S. S. , Shirsath S. E. , Mane M. L. , Patil S. , Mane D. R., "*Substitutional effect of Cr^{3+} ions on the properties of Mg–Zn ferrite nanoparticles*", Physica B, vol. 407, pp. 4338–4346, Nov. 2012.

[10] Bhukal S., Dhiman M., Bansal S., Tripathi M. K., Singhal S., "*Substituted Co–Cu–Zn nanoferrites: synthesis, fundamental and redox catalytic properties for the degradation of methyl orange",* RSC Advances, vol. 6, pp. 1360-1375, 2016.

[11] Zaki M., Al-Heniti S. H., Elmosalami T. A., "*Structural, magnetic and dielectric studies of copper substituted nano-crystalline spinel magnesium zinc ferrite*", Journal of Alloys and Compounds, vol. 633, pp. 104–114, June 2015.

[12] Mohammed K. A., Al-Rawas A. D., Gismelseed A. M., Sellai A., Widatallah H. M., Yousif A., Elzain M. E., Shongwe M., "*Infrared and structural studies of* $Mg_{1-x}Zn_xFe_2O_4$ *ferrites*", Physica B, vol. 407, pp. 795–804, Feb. 2012.

[13] Gabal M. A., Bayoumy W. A., "*Effect of composition on structural and magnetic properties of nanocrystalline* $Ni_{0.8-x}Zn_{0.2}Mg_xFe_2O_4$ *ferrite*", Polyhedron, vol. 29, pp. 2569–2573, Sept. 2010.

[14] Sharma R., Singhal S., "*Structural, magnetic and electrical properties of zinc doped nickel ferrite and their application in photo catalytic degradation of methylene blue*", Physica B, vol. 414, pp. 83–90 Apr. 2013.

[15] Hessien M. M., Rashad M. M., El-Barawy K., Ibrahim I. A., "*Influence of manganese substitution and annealing temperature on the formation, microstructure and magnetic properties of Mn–Zn ferrites"*, Journal of Magnetism and Magnetic Materials, vol. 320 pp. 1615-1621, May 2008.

CHAPTER 5

[1] Manohar A., Krishnamorthi C., "*Structural, Raman, magnetic and other properties of cosubstituted $ZnFe_2O_4$ nanocrystals synthesized by Solvothermal reflux method*", Journal of Materials Science: Materials in Electronics, vol. 29, pp.737-745, Jan. 2018.

[2] Babu K. V. , Kumar G. V. S., Jalaiah K., Shibeshi P. T., "*Effects of copper substitution on the microstructural, electrical and magnetic properties of $Ni_{0.7}Co_{0.3-x}Cu_xFe_2O_4$ ferrites*", Journal of Physics and Chemistry of Solids", vol. 118, pp.172-185, July 2018.

[3] Gabal M. A., Al-Zahrani N. H., Al Angari Y. M., Saaed A., "*Substitution Effect on the Structural, Magnetic, and Electrical Properties of Co1−xZnxFe2O4 Nanocrystalline Ferrites (x = 0–1) Prepared via Gelatin Auto-Combustion Method*", IEEE Transaction on Magnetics, vol. 54, pp 1-12, Jan. 2018.

[4] Choodamani C., Rudraswamy B., Chandrappa G. T., "*Structural, electrical, and magnetic properties of Zn substituted magnesium ferrite*", Ceramics International, vol. 42, pp. 10565-10571, July 2018.

[5] Pendyala S. K., Thyagarajan K., Kumar A. G. S., Obulapathi L., "*Effect of Mg doping on physical properties of Zn ferrite nanoparticles*", Journal of the Australian Ceramic Society, doi.org/10.1007/s41779-018-0173-8, Mar. 2018.

[6] Bhongale S. R., Ingawale H. R., Shinde T. J., Vasambekar P. N., "*Effect of Nd^{3+} Substitution on Structural and Magnetic Properties of Mg-Cd Ferrites Synthesized by Microwave Sintering Technique*", Journal of Rare Earths, vol. 36, pp. 390-397, Apr. 2018.

[7] Mansour S. F., Abdo M.A., Alwan S. M., "*The role of Cr^{3+} ions substitution on structural, magnetic and dielectric modulus of manganese zinc nanoferrites*", Ceramics International, vol. 44, pp. 8035-8042, May 2018.

[8] Mansour S. F., M.A. Abdoa M. A., El-Dek S. I., "*Improvement of physico-mechanical properties of Mg–Zn nanoferrites via Cr^{3+} doping*", Journal of Magnetism and Magnetic Materials, vol. 422, pp. 105-111, Jan. 2017.

[9] Mohseni H., Shokrollahi H., Sharifi I., Gheisari Kh., "*Magnetic and structural studies of the Mn-doped Mg–Zn ferrite nanoparticles synthesized by the glycine nitrate process",* Journal of Magnetism and Magnetic Materials, vol. 324, pp. 3741-3747, Nov. 2012.

[10] Reyes-Rodríguez P. Y., Cortés-Hernández D. A., Escobedo-Bocardo J. C., Almanza-Robles J. M., Sánchez-Fuentes H. J., Jasso-Terán A., De León-Prado L. E., Méndez-Nonell J., Hurtado-

López G. F., "*Structural and magnetic properties of Mg-Zn ferrites ($Mg_{1-x}Zn_xFe_2O_4$) prepared by sol-gel method",* Journal of Magnetism and Magnetic Materials, vol. 427, pp. 268-271, Apr. 2017.

[11] Patil S. N., Pawar A. M., Tilekar S. K., Ladgaonkar B. P., "*Investigation of magnesium substituted nano particle zinc ferrites for relative humidity sensors",* Sensors and Actuators A, vol. 244, pp. 35–43, Apr. 2016.

[12] Ichiyanagi Y., Kubota M., Moritake S., Kanazawa Y., Yamada T., Uehashi T., **"***Magnetic properties of Mg-ferrite nanoparticles***",** Journal of Magnetism and Magnetic Materials, vol. 310, pp. 2378-2380, Mar. 2007.

[13] Nadeem K., Rahman S., Mumtaz M., "*Effect of annealing on properties of Mg doped Zn ferrite nanoparticles*", Progress in Natural Science: Materials International, vol. 25, pp. 111-116, Apr. 2015.

[14] Goldman A., "*Modern Ferrite Technology*", Springer Science & Business Media, 2006.

[15] Li Q., Wang Y., Chang C., "*Study of Cu, Co, Mn and La doped Ni Zn ferrite nanorods synthesized by the coprecipitation method*", Journal of Alloys and Compounds, vol. 505, pp. 523-526, Sept. 2010.

[16] Mane D.R., Birajdar D.D., Patil S., Shirsath S. E., Kadam R. H., " *Redistribution of cations and enhancement in magnetic properties of sol–gel synthesized $Cu_{0.7-x}Co_xZn_{0.3}Fe_2O_4 (0 \leq x \leq 0.5)$",* Journal of Sol-Gel Science and Technology, vol. 58, pp. 70-79, Nov. 2010.

[17] Thorat L. M., Patil J. Y., Nadargi D. Y., Ghodake U. R., Kambale R. C., Suryavanshi S. S., "*Ni^{2+}*-substituted *Mg–Cu–Zn* ferrites: *a colloidal approach of tuning structural and electromagnetic properties*" Journal of Sol-Gel Science and Technology, vol. 86, pp. 731-742, June 2018.

[18] Lynda J. C., Durka M., Dinesh A., Manikandan A., Jaganathan S. K., Baykal A., Antony S. A., "*Enhanced magneto-optical and photocatalytic properties of ferromagnetic $Mg_{1-y}Ni_y Fe_2O_4$ $(0.0 \leq y \leq 1.0)$ spinel nano-ferrites*", Journal of Superconductivity and Novel Magnetism, doi.org/10.1007/s10948-018-4623-x, Mar. 2018.

[19] Sertkol M., Koseoğlu Y., Baykal A., Kavas H., Bozkurt A., Toprak M. S., "*Microwave synthesis and characterization of Zn-doped nickel ferrite nanoparticles*", Journal of Alloys and Compounds, vol. 486, pp. 325-329, Nov. 2009.

[20] Padmapriya G., Manikandan A., Krishnasamy V., Jaganathan S. K., Antony S. A., *"Spinel $Ni_xZn_{1-x}Fe_2O_4$ (0.0 ≤x ≤1.0) nano-photocatalysts: synthesis, characterization and photocatalytic degradation of methylene blue dye"*, Journal of Molecular Structure, vol. 1119, pp. 39-47, Sept. 2016.

[21] Jalaiah K., Babu K. V., "*Structural, magnetic and electrical properties of nickel doped Mn-Zn spinel ferrite synthesized by sol-gel method"*, Journal of Magnetism and Magnetic Materials, vol. 423, pp. 275–280, Feb. 2017.

[22] Topkaya R., Gunguneş H., Eryiğit S., Shirsath S. E., Yıldız A., Baykal A., "*Effect of bimetallic (Ni and Co) substitution on magnetic properties of MnFe2O4 Nanoparticles*", Ceramic International, vol. 42, pp. 13773–13782, Sept. 2016.

[23] Syue M. R., Wei F. J., Chou C. S., Fu C. M., "*Magnetic and electrical properties of Mn–Zn ferrites synthesized by combustion method without subsequent heat treatments",* Journal of Applied Physics, vol. 109, pp. 07A324, Mar. 2011.

[24] Ghodake U.R., Kambale R.C., Suryavanshi S.S., "*Effect of Mn2+ substitution on structural, electrical transport and dielectric properties of Mg-Zn ferrites"*, Ceramic International, vol. 43, pp. 1129-1134, Jan. 2017.

[25] Doaga A., Cojocariu A. M., Amin W., Heib F., Bender P., Hempelmann R., Caltun O. F., "*Synthesis and characterizations of manganese ferrites for hyperthermia Applications*", Materials Chemistry and Physics, vol. 143, pp. 305–310, Dec. 2013.

[26] Skumryev V., Stoyanov S., Zhang Y., Hadjipanayis G., Givord D., Nogue J., "Beating the superparamagnetic limit with exchange bias", Nature, vol. 423, pp. 850-853, June 2003.

[27] Zhang C. F., Zhong X. C., Yu H. Y., Liu Z. W., Zeng D.C., "*Effects of cobalt doping on the microstructure and magnetic properties of Mn–Zn ferrites prepared by the co-precipitation method*", Physica B: Condensed Matter, vol. 404, pp. 2327-2331, Aug. 2009.

[28] Kodama R.H., Berkowitz A.E., "*Atomic-scale magnetic modeling of oxide nanoparticles*", Physical Review B, vol. 59, pp. 6321-6336, Mar. 1999.

[29] Mathew D.S., Juang R.S., "*An overview of the structure and magnetism of spinel ferrite nanoparticles and their synthesis in microemulsions*", Chemical Engineering Journal, vol. 129, pp. 51-56, May 2007.

[30] Lodhi M Y., Mahmood K., Mahmood A., Malik H., Warsi M. F., Shakir I., Asghar M., Khan M. H., "*New $Mg_{0.5}Co_xZn_{0.5-x}$ nano ferrites : Structural elucidation and electromagnetic behaviour evaluation*", Current Applied Physics, vol. 14, pp. 716-720, May 2014.

[31] Nair S. S., Mathews M., Joy P.A., Kulkarni S. D., Anantharaman M.R., "*Effect of cobalt doping on the magnetic properties of superparamagnetic γ-Fe_2O_3-polystyrene nanocomposites*", Journal of Magnetism and Magnetic Materials, vol. 283, pp. 344-352, Dec. 2004.

[32] Liou S. H., Huang S., Klimek E., Kirby R. D., "*Enhancement of coercivity in nanometer size CoPt crystallites*" Journal of Applied Physics, vol. 85, pp. 4334–4336, Apr. 1999.

[33] Thankachan S., Jacob B. P., Xavier S., Mohammed E. M., "*Effect of neodymium substitution on structural and magnetic properties of magnesium ferrite nanoparticles*", Physica Scripta, vol. 87, pp. 1-7, Jan. 2013.

[34] Haralkar S. J., Kadam R. H., More S. S., Shirsath S. E., Mane M. L., Patil S., Mane D. R., "*Substitutional effect of Cr^{3+} ions on the properties of Mg–Zn ferrite nanoparticles*", Physics B : Condensed Matter, vol. 407, pp. 4338–4346, Nov. 2012.

[35] Zaki H. M., Al-Heniti S. H., Elmosalami T. A., "Structural, magnetic and dielectric studies of copper substituted nano-crystalline spinel magnesium zinc ferrite", Journal of Alloys and Compounds, vol. 633, pp. 104-114, June 2015.

[36] V.K. Lakhani, T.K. Pathak, N.H. Vasoya, K.B. Modi, "*Structural parameters and X-ray Debye temperature determination study on copper-ferrite-aluminates*", Solid State Sciences, vol.13, pp. 539–547, Mar. 2011.

[37] Kumar G., Shah J., Kotnala R. K., Singh V. P., Sarveena, Garg G., S.E. Shirsath S. E., Batoo K. M., Singh M., "*Superparamagnetic behaviour and evidence of weakening in super-exchange interactions with the substitution of Gd^{3+}ions in the Mg–Mn nanoferrite matrix*", Materials Research Bulletin, vol.63, pp.216–225, Mar. 2015.

[38] Topkaya R., Baykal A., Demir A., "*Yafet–Kittel-type magnetic order in Zn-substituted cobalt ferrite nanoparticles with uniaxial anisotropy"*, Journal of Nanoparticle Research, vol. 15 pp. 1–18, 2013.

[39] Hao L., Zhao Y., Jiao Q., Chen P., "*Synthesis of zinc–nickel ferrite nanorods and their magnetic properties*", RSC Advances, vol. 4, pp. 15650-15654, Mar. 2014.

[40] Zhang H.E., Zhang B.F., Wang G.F., Dong X.H., Gao Y., "*The structure and magnetic properties of $Zn_{1-x}Ni_xFe_2O_4$ ferrite nanoparticles prepared by sol–gel auto-combustion*", Journal of Magnetism and Magnetic Materials, vol. 312, pp. 126–130, May. 2017.

[41] Pong W.F., Chang Y.K., Su M.H., Tseng P.K., "*Magnetic orientation of Ni in Zn-Ni ferrites studied by soft-x-ray magnetic circular dichroism*", Physical Review B, vol. 55, pp. 11409–11413, May 1997.

[42] Nikam D.S., Jadhav S.V., Khot V. M, Bohara R.A., Hong C.K., Mali S.S., Pawar S.H., "Cation distribution, structural, morphological and magnetic properties of $Co_{1-x}Zn_xFe_2O_4$ (x = 0–1) nanoparticles", RSC Advances, vol. 5, pp. 2338–2345, 2015.